

2011

# Fracture Analysis Using Enriched Finite Elements for Three-Dimensional Welded Structures

Zhiye LI  
*Lehigh University*

Follow this and additional works at: <http://preserve.lehigh.edu/etd>

---

## Recommended Citation

LI, Zhiye, "Fracture Analysis Using Enriched Finite Elements for Three-Dimensional Welded Structures" (2011). *Theses and Dissertations*. Paper 1202.

This Thesis is brought to you for free and open access by Lehigh Preserve. It has been accepted for inclusion in Theses and Dissertations by an authorized administrator of Lehigh Preserve. For more information, please contact [preserve@lehigh.edu](mailto:preserve@lehigh.edu).

**FRACTURE ANALYSIS USING ENRICHED  
FINITE ELEMENTS for THREE-DIMENSIONAL  
WELDED STRUCTURES**

by

Zhiye Li

Presented to the Graduate and Research Committee

of Lehigh University

in Candidacy for the Degree of

Master of Science

in

Mechanical Engineering

Lehigh University

2011

Approved and recommended for acceptance as a dissertation in partial fulfillment of the requirements for the Degree of Master of Science.

---

Date

---

Thesis Advisor

---

Chairperson of Department

# Acknowledgments

I gratefully thank my advisor Prof. Herman F. Nied for his constructive comments on my research and this thesis. Without his support and knowledge, it would be hard to complete this thesis.

Also, I express my love to my parents.

# Table of Contents

<b>Table of Contents</b>	<b>iv</b>
<b>List of Figures</b>	<b>vi</b>
<b>List of tables</b>	<b>xi</b>
<b>Abstract</b>	<b>1</b>
<b>Chapter 1. Introduction</b>	<b>3</b>
1.1 <i>Finite element analysis of crack problems</i>	3
1.2 <i>Welding simulation</i>	8
1.3 <i>Finite element analysis of 3D welding/ fracture Problem</i>	11
<b>Chapter 2. Numerical Analysis</b>	<b>16</b>
2.1 <i>Numerical Method</i>	16
2.2 <i>Welding Geometry</i>	21
2.3 <i>Mesh Generation</i>	24
2.4 <i>HYPERMESH®/SYSWELD® Interface</i>	28
<b>Chapter 3. Fusion Welding Simulation</b>	<b>31</b>
3.1 <i>Material Properties and Fusion Welding Simulation</i>	31
3.2 <i>Initial Clamping Condition</i>	35
3.3 <i>Heat Source Modeling</i>	36
3.4 <i>Heat Transfer Modeling</i>	40
3.5 <i>Thermal Analysis</i>	42

<i>3.6 Mechanical Analysis</i>	45
<b>Chapter 4. Fracture Mechanics Analysis</b>	<b>46</b>
<i>4.1 Finite Element code FRAC_3D</i>	46
<i>4.2 SYSWELD/FRAC3D Interface</i>	51
<i>4.3 Superposition Results</i>	54
<b>Chapter 5. Conclusions and Furture Work</b>	<b>57</b>
<i>5.1 Finite element analysis of crack problems</i>	57
<i>5.2 Future Works</i>	85
<b>References</b>	<b>87</b>
<b>Appendix</b>	<b>91</b>
<b>VITA</b>	<b>117</b>

# List of Figures

Figure 1.1 Running FRAC3D	4
Figure 1.2 Graphical User Interface FCPAS based on Frac3D and ANSYS	5
Figure 2.1 Schematic flow chart for the file transfer process	17
Figure 2.2 geometry of Longitudinal-Bead-Weld Notch-Bend test specimen	21
Figure 2.3 Longitudinal-Bead-Weld Notch-Bend test specimen in Fracture analysis	22
Figure 2.4 1/4 welding bead model	23
Figure 2.5 cross section of 1/4 welding bead model	23
Figure 2.6 3D mesh generation of Longitudinal-Bead-Weld Notch-Bend model	24
Figure 2.7 2D mesh and 1D mesh of Longitudinal-Bead-Weld Notch-Bend model	25
Figure 2.8 2D mesh and 1D mesh of Longitudinal-Bead-Weld Notch-Bend model	25
Figure 2.9 Cross section	26
Figure 2.10 (a) Hex20, 3D (2nd order)quadrilateral hexahedra element with 20 nodes in HYPERMESH.(b)Quad8, 2D (2nd order)quadrilateral elements with 8 nodes ordered in HYPERMESH	28
Figure 2.11 Element definition and nodal number order in SYSWELD	29
Figure 3.1 Trajectory line and reference line for fusion welding	34
Figure 3.2 Initial boundary condition	35
Figure 3.3 Double ellipsoid source and display of possible trajectories	36
Figure 3.4 Weld pool	38
Figure 3.5 Calibrating heat sources	38

Figure 3.6 Moving heat source	42
Figure 3.7 (a) Temperature distribution of plate-bead. (b) Temperature distribution of z-direction symmetry plane	43
Figure 4.1 20-Node three-dimensional enriched crack tip element	47
Figure 4.2 General flow of FRAC_3D analysis	49
Figure 4.3 Surface Loads Pressures format, face 1: (J-I-L-K), face 2: (I-J-N-M), face 3 (J-K-O-N), face 4: K-L-P-O), face 5: (L-I-M-P), face 6 (M-N-O-P)	52
Figure 5.1 Model description	57
Figure 5.2 Temperature distribution after fusion welding (time=2000second)	59
Figure 5.3 Residual stress distribution after fusion welding (time=2000second)	59
Figure 5.4 Temperature distributions during welding process. (1) t=5; (2) t=10; (3) t=20; (4) t=30; (5) t=40; (6) t=50.	60
Figure 5.5 Temperature distributions after welding(time=50s)	61
Figure 5.6 $\sigma_{33}$ configurations. (1) $\sigma_{33}$ of the whole welding plate (2) Residual stress $\sigma_{33}$ in crack surface after fusion welding (3) Cross view of $\sigma_{33}$ in plane of crack surface (4) $\sigma_{33}$ along the crack front.	61
Figure 5.7 Von Mises stress distributions during welding process. (1) t=5; (2) t=10; (3) t=20; (4) t=30; (5) t=40; (6) t=50.	62
Figure 5.8 Von Mises stress distributions during cooling process. (1) t=75; (2) t=257; (3) t=542; (4) t=1183; (5) t=1788; (6) t=2000.	63



Figure 5.9 Residual stress $\sigma_{33}$ distributions during welding process. (1) t=5; (2) t=10; (3) t=20; (4) t=30; (5) t=40; (6) t=50.	64
Figure 5.10 Residual stress $\sigma_{33}$ distributions during cooling process. (1) t=75; (2) t=257; (3) t=542; (4) t=1183; (5) t=1788; (6) t=2000.	65
Figure 5.11 Displacements Magnitude after crack	66
Figure 5.12 Total stress configurations in direction of zz axial	66
Figure 5.13 Stress Intensity factor (Mpa/m)	67
Figure 5.14 Temperature distributions during welding process. (1) t=5; (2) t=10; (3) t=20; (4) t=30; (5) t=40; (6) t=50.	68
Figure 5.15 Temperature distributions after welding(time=50s)	69
Figure 5.16 Residual stresses distribution after fusion welding for finer mesh case	69
Figure 5.17 Von Mises stress distributions during welding process. (1) t=5; (2) t=10; (3) t=20; (4) t=30; (5) t=40; (6) t=50.	70
Figure 5.18 Von Mises stress distributions during cooling process. (1) t=75; (2) t=257; (3) t=542; (4) t=1183; (5) t=1788; (6) t=3000.	71
Figure 5.19 Residual stress $\sigma_{33}$ distributions during welding process. (1) t=5; (2) t=10; (3) t=20; (4) t=30; (5) t=40; (6) t=50.	72
Figure 5.20 Residual stress $\sigma_{33}$ distributions during cooling process. (1) t=75; (2) t=257; (3) t=542; (4) t=1183; (5) t=1788; (6) t=3000.	73

Figure 5.21 $\sigma_{33}$ configuration for finer mesh case. (1) $\sigma_{33}$ of the whole welding plate. (2) Residual stress $\sigma_{33}$ in crack surface after fusion welding (3) Cross view of $\sigma_{33}$ in plane of crack surface. (4) $\sigma_{33}$ along the crack front.	74
Figure 5.22 Stress intensity factor $k_1$ (Mpa/m)	74
Figure 5.23 Residual stresses distribution after fusion welding for coarser mesh case	75
Figure 5.24 $\sigma_{33}$ configuration for coarser mesh case. (1) $\sigma_{33}$ of the whole welding plate. (2) Residual stress $\sigma_{33}$ in crack surface after fusion welding. (3) Cross view of $\sigma_{33}$ in plane of crack surface. (4) $\sigma_{33}$ along the crack front.	75
Figure 5.25 Stress intensity factor $k_1$ (Mpa/m).	76
Figure 5. 26 Temperature distributions during welding process. (1) $t=5$ ; (2) $t=10$ ; (3) $t=20$ ; (4) $t=30$ ; (5) $t=40$ ; (6) $t=50$ .	77
Figure 5.27 Temperature distributions after welding( $t=50s$ )	78
Figure 5.28 Residual stresses distribution after cooling for smaller front ( $t=3000s$ )	78
Figure 5.29 Von Mises stress distributions during welding process. (1) $t=5$ ; (2) $t=10$ ; (3) $t=20$ ; (4) $t=30$ ; (5) $t=40$ ; (6) $t=50$ .	79
Figure 5.30 Von Mises stress distributions during cooling process. (1) $t=75$ ; (2) $t=257$ ; (3) $t=542$ ; (4) $t=1183$ ; (5) $t=1788$ ; (6) $t=3000$ .	80
Figure 5.31 Residual stress $\sigma_{33}$ distributions during welding process. (1) $t=5$ ; (2) $t=10$ ; (3) $t=20$ ; (4) $t=30$ ; (5) $t=40$ ; (6) $t=50$ .	81

Figure 5.32 Residual stress $\sigma_{33}$ distributions during cooling process. (1) $t=75$ ; (2) $t=257$ ; (3) $t=542$ ; (4) $t=1183$ ; (5) $t=1788$ ; (6) $t=3000$ .	82
Figure 5.33 $\sigma_{33}$ configuration after cooling for smaller front case. (1) $\sigma_{33}$ of the whole welding plate after cooling. (2) Residual stress $\sigma_{33}$ in crack surface after cooling. (3) Cross view of $\sigma_{33}$ in plane of crack surface after cooling. (4) $\sigma_{33}$ along the crack front after cooling.	83
Figure 5.34 Stress intensity factor $k_1$ (Mpa/m).	83
Figure 5.35 Total stress $\sigma_{33}$ configurations in direction of zz axial	84
Figure 5.36 Current model and model for future work.	85

# List of tables

Table3.1 Chemical composition of the consumable materials (in wt%)	32
Table3.2 Typical mechanical properties	32

# Abstract

The objective of this investigation is to evaluate the effect of residual stresses that arise during welding processes, on localized fracture behavior. The primary fracture parameters of interest are the Stress Intensity Factors (SIFs) associated with cracks that develop around the welded area. The simulation of the welding process is accomplished through the finite element code SYSWELD® and the computation of fracture behavior uses a finite element user-defined enriched crack tip element code, FRAC3D, developed at Lehigh University. In this study, quadratic 3D finite element models which are generated in HYPERMESH®, are first introduced into SYSWELD® to perform the thermo-mechanical transient analysis needed to predict the welding residual stresses, global stresses, strain and displacement. Residual stresses from the welding simulation and the original quadratic 3D finite element HYPERMESH® model are combined, modified and transferred into the ANSYS/FRAC3D code to obtain the final Stress Intensity Factor (SIF) for 3D cracks, and the stresses, strains and displacements in the cracked configuration. In order to verify the accuracy of the welding simulation residual stress, different mesh densities were examined in detail. In addition, different welding model meshes were applied to test the sensitivity of the SIF results to different meshes and geometries. Finally, refined weld/crack models with a progression of crack shapes that follow the contours of the highest stresses around the weld zone were generated to simulate the behavior

of a crack emerging from a weld defect The effect that different welding parameters have on the fracture parameters represent an important result from this study.

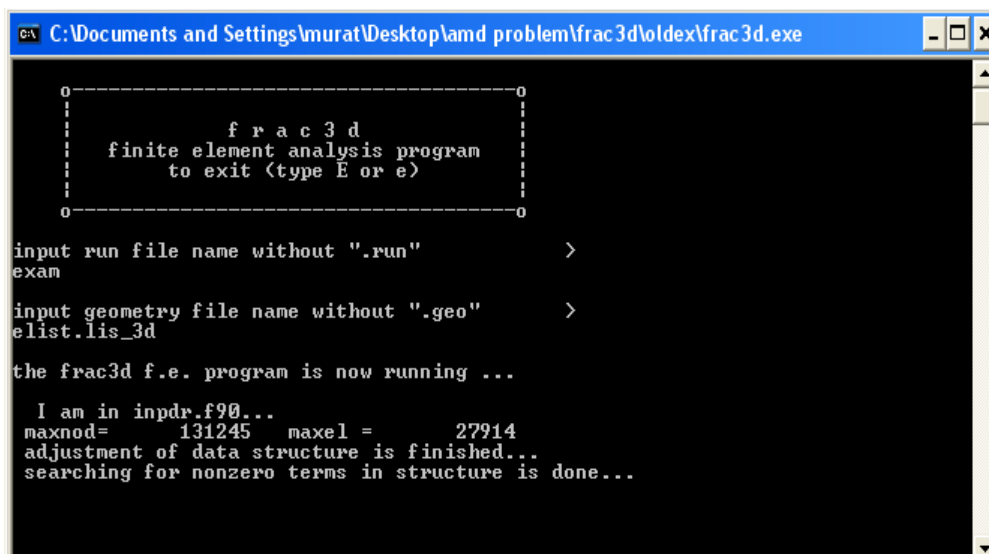
# Chapter 1. Introduction

## 1.1 Finite element analysis of crack problems

Finite element analysis of three-dimensional fracture problems based on linear elastic fracture mechanics is an important tool for design analysis in industry. Meaningful 3-D fracture computations should include such quantities as mixed mode stress intensity factors, strain energy release rate, and phase angles to be considered as an appropriate engineer tool with broad applications. Fracture analysis of structures fabricated using welding also require careful consideration of the welding residual stresses that often result in localized cracking in the neighborhood of the weld. Such a fracture analysis requires a systematic technique to link the results from the welding simulation with secondary computations needed to extract the relevant fracture parameters, e.g. stress intensity factors. One problem when using the finite element methodology to analyze crack problems is the difficulty in adequately capturing the mathematical singularity that occurs at the hypothetical crack tip in linear elastic bodies. The usual polynomial based elements available in most commercially available finite element codes converge very slowly to a suitably accurate solution when the finite element model contains a sharp crack that does not incorporate the correct asymptotic solution with the appropriate  $1/\sqrt{r}$  singular stress terms. Enriched finite elements are very convenient for representation of singularities in

fracture analysis. In this study, a specialized finite element program [1], which uses enriched crack tip elements, developed at Lehigh University, is utilized to perform the fracture analysis for this research.

In 2002, Ayhan and Nied[2] implemented asymptotic terms into enriched elements for six different types of 3-D elements and developed an efficient finite element code, which could perform fracture mechanics analysis for three dimensional fracture problems using enriched crack tip elements. This code (FRAC3D, Figure1.1) also has the ability to solve general plane strain fracture problem and certain classes of non-linear problems, e.g., (small strain plasticity) [1]. One important advantage of the enriched finite element method is that the fracture parameters of interest, i.e., the stress intensity factors, are defined as additional unknowns in the formulation. Thus, the stress intensity factors are computed simultaneously with other regular displacement degrees of freedom. In the enriched element approach, no additional post-processing is required to obtain the relevant fracture parameters.



```
C:\Documents and Settings\murat\Desktop\lamd problem\frac3d\oldex\frac3d.exe
-----0
      f r a c 3 d
    finite element analysis program
      to exit (type E or e)
    -----0

input run file name without ".run"      >
exam

input geometry file name without ".geo"  >
elist.lis_3d

the frac3d f.e. program is now running ...

I am in inpdr.f90...
maxnod= 131245 maxel = 27914
adjustment of data structure is finished...
searching for nonzero terms in structure is done...
```

**Figure 1.1** Running FRAC3D



One aspect of the enriched element formulation is the need for transition elements to rigorously satisfy displacement compatibility. Displacement compatibility is satisfied exactly on all element surfaces between the enriched crack tip elements and the surrounding isoperimetric finite elements in this methodology. The formulation for 3-D interfacial crack problems was updated in FRAC3D by Ayhan, Kaya and Nied[3]. Further development of this research code continues, e.g., in 2010, Ayhan developed a Graphical User Interface FCPAS (Figure 1.2) based on Frac3D and ANSYS.

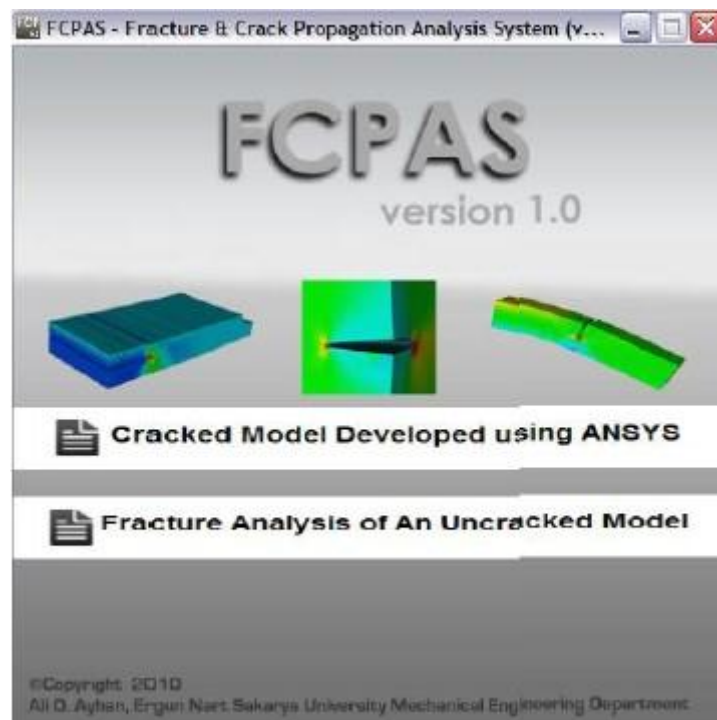


**Figure 1.2** Graphical User Interface FCPAS based on Frac3D and ANSYS

Most commercially available finite element codes have some capacity for fracture analysis. For example, ANSYS [4] can be used to compute stress intensity factors using the virtual crack extension technique. However, this requires the

generation of a specialized “tunnel” crack tip mesh that completely surrounds the crack front, which greatly complicates the generation of a mesh for a general 3-D problem. The main benefit of using FRAC3D in this study, is that the finite element meshes used for fracture analyses of the welded geometry do not require specialized crack tip meshes, and thus automatic meshing from HYPERMESH® can be routinely used to generate a mesh for the cracked structure.

In the paper by Ayhan and Nied [1], it was demonstrated that even for coarse finite element meshes, the direct calculation of the stress intensity factors using enriched elements, results in rapid convergence to the correct stress intensity factor solution. Currently, enrichment capabilities of FRAC3D include asymptotic crack tip elements for: interface cracks, anisotropic materials, poroelastic materials, dynamic loading and crack surface contact.

However, fracture analysis for welded structures is somewhat different than the type of fracture problems that are routinely addressed in most engineering fracture problems. First, the highly nonlinear nature of the welding physics requires a separate type of finite element formulation to take into account the melting and resolidification that occurs during welding. The welding simulation can be completely separate from the fracture analysis. However, the residual stresses are an important driving force (in conjunction with additional external loads) for subsequent crack growth when a welded structure is in actual use. This combination of welding simulation and fracture

analysis is of considerable importance, since weld joints are considered to be the portion of the structure most susceptible to cracking.

## 1.2 Welding simulation

Cracking behavior is strongly influenced by the residual stresses which arise during the fusion welding process. Computation of heat transfer and welding induced residual stress invariably involves a complex nonlinear numerical simulation of the fusion weld process, starting with the heat source description, and its moving path definition. Since the thermo-mechanical properties depend on temperature in a highly nonlinear manner, analysis of welding requires highly computationally intensive simulation. In order to meet this need, specialized finite element codes have been developed that can model and simulate a variety of fusion welding processes. In addition, many of the larger commercial finite element packages, e.g., ANSYS, ABAQUS, can be made to simulate welding processes by using appropriate user-defined moving heat sources and nonlinear material property models. SYSWELD [5] is a specialized commercial code specifically designed to handle complex welding simulations and contains built in welding heat source models and the necessary material property behavior to accurately simulate a wide variety of welding behavior.

The paper of Suraj Joshi, Cumali Semetay, John WH Price and Herman F. Nied [6] presents the simulation of welding-induced residual stresses in a CHS T-Joint, which would form the first of the four lacings welded on to the main chord of a typical mining dragline cluster. In this paper, computed temperature distributions during fusion welding and relevant welding distortion for CHS T-joint are presented.

The paper compares numerically generated residual stresses during the welding process in a single weld pass, and the observation that residual stresses in the fused area at some points can be higher than the uniaxial yield stress. The moving heat source defined in these fusion welding simulations, utilized double-ellipsoid power density distribution functions, which adequately describe the heat transfer behavior for various metal arc welding processes.

After the transient temperature distribution during welding has been determined, the residual stresses can be calculated by performing a nonlinear thermal stress analysis of the structure as the weld cools from above its melting temperature, down to the normal environmental temperature. The residual stress components in the weld region often can become greater than the temperature dependent uniaxial yield strength of the filler metal as the welded part cools. This is due to localized triaxial constraint that causes relatively high hydrostatic stresses during cooling solidification in the neighborhood of the weld. Long longitudinal welds are generally subjected to longitudinal tensile residual stress approximately equal to the metal's uniform axial yield stress, unless post-weld heat treatment or some other residual stress reduction treatment is performed. In order to compute residual stress correctly, the stresses that result from solid phase transformation also should be considered in the residual stress computation.

Solid phase transformations during cooling are known to cause local material dilatation and contribute to additional strains similar to thermal strains. [6] This effect

can be substantial and can even reverse the sign of the residual stresses in determined solely from a thermo-mechanical simulation.

## 1.3 Finite element analysis of 3D welding/ fracture

### Problem

The fracture behavior of welded structures is of considerable importance, since fusion welding is the most commonly used technique for joining metal structures. Numerous descriptions of catastrophic failures attributed to fracture of a welded joint appear in highly constrained welded plate girders [7]. A specific example of a historic bridge failures is the Hoan Bridge in Milwaukee, WI.[8]



**Figure 1.3** Fracture in highly constrained welded plate girders. [8]

Thus, a better understanding of the relationship between welding processing parameters and post-weld fracture behavior is of great importance for improving the ultimate load carrying capacity and fatigue life of load bearing structures. Numerous experimental studies have indicated that the weld induced residual stress can significantly affect the subsequent fracture behavior of a fusion welded structure [9]. It is well known that fusion welding processes introduce high residual stresses. Unfortunately determination of welding residual stresses to a high degree of accuracy

is not easy. In addition, most welding processes are known to introduce crack-like defects due to many reasons. For example, the heat affected zone around a weld experiences metallurgical changes that can seriously degrade the fracture resistance of the base metal. Besides, inadequate gas shielding will cause the formation of oxides that are inherently brittle and will result in initiation of weld defects. Incomplete fusion can embed crack-like defects underneath the weld, etc. Generally, it is almost impossible to create a perfect weld with zero defects. Thus, when failure occurs in a welded structural component, the welded part is most likely to be identified as the initial location of fracture. Consequently, an accurate and efficient technique for the determination of the weld residual stress distribution is the required starting point for an accurate fracture prediction methodology for welded structures.

In Michaleris P [10], a finite element methodology is presented to assess the effect of residual stresses on fracture analysis. Residual stress calculated from welding simulation, after interpolation, was transferred onto fine meshes for succeeding computation of fracture mechanical parameters.

In V.Robin and T.Pyttel[11], a calculation methodology for failure analysis of jointing system such as weld line submitted to dynamic crash loading was presented. In this research, the advantage of the built in interface between SYSWELD® [5] and PAM-CRASH® was used. For example, the results from a SYSWELD® welding simulation is loaded into the rupture modeling of a weld line made of solid elements.



The damage parameters are identified through an inverse method based on comparisons between numerical and experimental results.

Z.Barsoum [12] investigated the residual stresses near the weld root and the weld toe of multi-pass welded tube-to plate structures. In this paper, a 2-D axi-symmetric finite element model was developed to calculate the welding solution and the fracture analysis was accomplished by using the LEFM code FRANC2D [12].

In an ATLSS report by H. F. Nied, S. Marugan, M. Ozturk, E. Nart, A. Mengel, and E. Citirik. [9], a fundamental understanding of the transient nature of residual stress evolution during various metal fusion welding processes was developed. This work determined the effectiveness of simplified fusion welding finite element models, such as two dimensional plane strain and generalized plane strain models, to simulate the cracking progress a 3-D crack model was developed in which there is a crack front in planes perpendicular to the axial residual stress that arise from welding.

In E.Citirik, U. Ozkan, H. F. Nied [13], prediction of welding residual stress was performed by using two finite element codes (HEAT2D and FRAC2D\_WELD), which are developed at Lehigh University. The fracture mechanics parameter calculation part was computed by FRAC3D, which is the algorithm methodology used in this study.

To accurately analyze crack behavior in fusion welded components, Cumali Senetay, H. Mahmoud, H. F. Nied [7] developed a nonlinear transient welding simulation using commercial SYSWELD code. They superposed the residual stress

and external load from an ABAQUS finite element simulation and used these results to perform a fracture analysis.

The paper by Labeas, Tsirkas, Diamantakos, and Kermanidis [14] introduces an effective method to study the effect of residual stresses due to laser welding on the Stress Intensity Factors (SIFs) of cracks developing nearby the welded area. The simulation of the welding process and the calculation of SIFs on the cracked structure are performed using an explicit and an implicit Finite Element code, respectively. The developed residual stresses due to the welding of two flat plates by laser welding are calculated first, using a thermo-mechanical transient analysis. Subsequently, a linear elastic analysis is applied for the calculation of SIFs at the crack tips. For the entire finite element calculation, linear solid elements ‘SOLID45’ in the ANSYS code are used. SOLID45 is a brick element and is defined by eight nodes, having three displacement degrees of freedom at each element node. The calculated results of the welding simulation are verified by comparing the computed angular distortions to the corresponding experimental values. The verification of the important fracture mechanics parameter SIF is performed through comparisons between computed and experimental crack opening displacement (COD) values.

In this study the residual stresses that arise during the weld process are a function of the welding parameters, e.g., material phase, temperature, displacement, etc. Thus, the influence of different weld parameters on the fracture behavior -is an important result in this study.

In this work, 3-D welding simulations were carried out in order to determine the residual stresses which are transported to the three-dimensional fracture analyses. Application of both software built-in interfaces and transformed ASCII files are necessary. Various types of loading and meshes are applied to check the accuracy of simulation. Another objective was to investigate the sensitivity of the SIFs to the various controllable welding parameters. In this application, which requires the superposing of two numerical algorithms, fundamental data need to be specified common to both the welding model and the fracture model. This includes the geometry of the welded plate and the dimensions of the fusion weld. The results from the SYSWELD welding simulation include: (i) time dependent temperature distribution ;(ii) stress tensor, strain tensor and nodal displacement ;(iii) residual stress and strains; and (iv) final stress, strain and displacements everywhere in the model

# Chapter 2. Numerical Analysis

## 2.1 Numerical Method

The focus of this numerical study will be on the thermo-mechanical and fracture behavior of a long longitudinal bead weld (Figure 2.1). This very common weld geometry contains important features observed in most weld geometries and represents a generic baseline for developing a systematic numerical methodology for analyzing weld fracture behavior.

Generally, two types of numerical analyses (welding simulation and fracture simulation) are required for the fracture mechanics design of longitudinal-bead weld Crack test specimens with center crack underneath weld bead. The principle goal of this study is to investigate the residual stresses that arise during the welding process and their influence on the fracture behavior. Therefore, determination of the residual stress field that evolves during the fusion welding process is required prior to computing stress intensity factors for the cracks that may develop along the crack front near the weld bead.

Simulation of the fusion welding process was performed using the explicit finite element code SYSWELD [11]. The residual stress field around the welded area depends on a detailed heat transfer analysis that is exported to the mechanical phase

of the simulation. Once the complete thermo-mechanical solution for the residual stresses has been obtained, the implicit finite element codes ANSYS [4] and FRAC3D can be used to perform the fracture analysis.

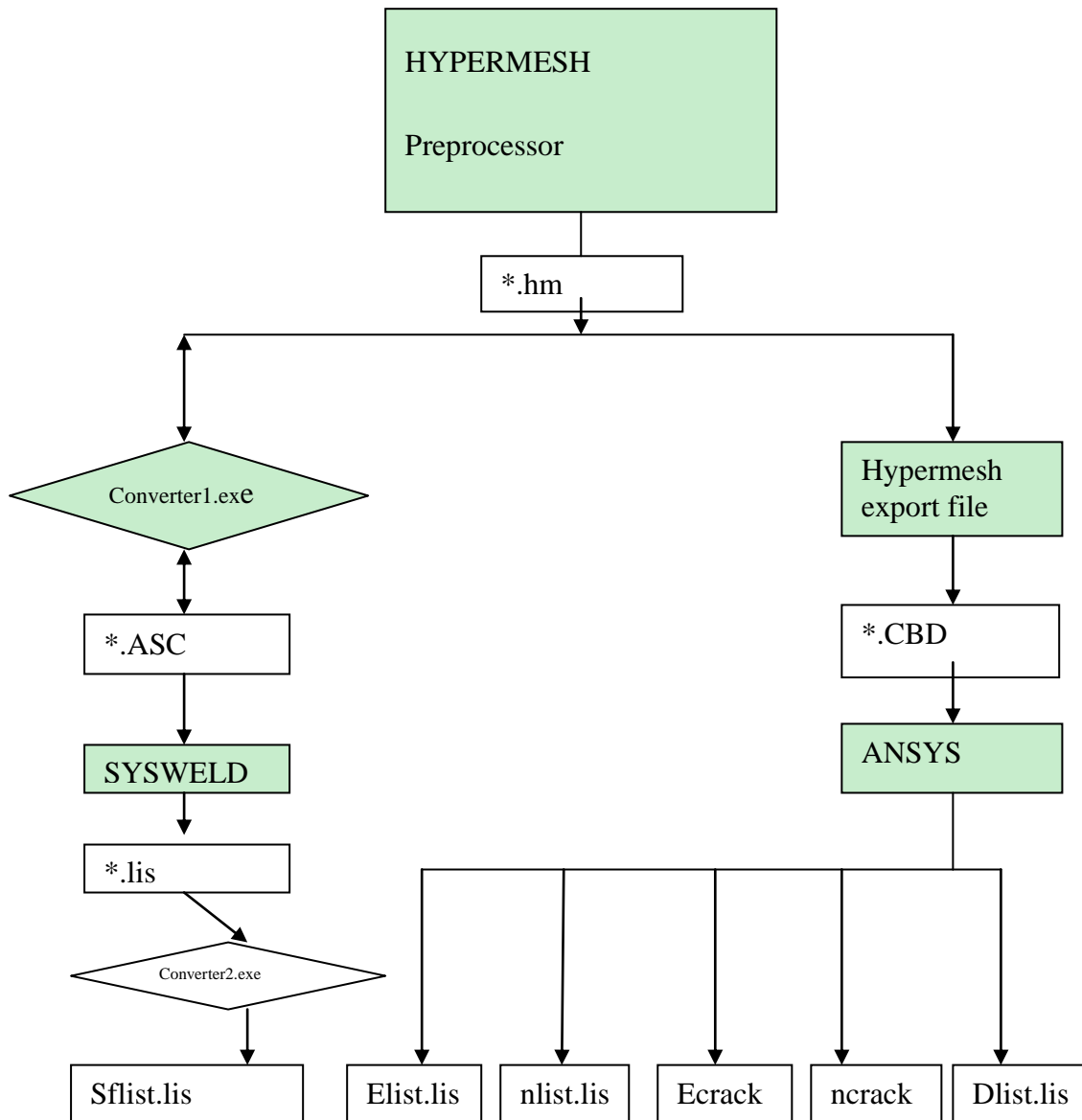


**Figure 2.1** Schematic flow chart for the file transfer process

The main problem in this study is that if all the stress results on the final time from SYSWELD are transferred to ANSYS as an initial stress file, then essentially the

same results in ANSYS will be obtained as which is obtained in SYSWELD, for the same geometry parameter, element and node information, and boundary conditions. However, the SYSWELD model in fact is not completely identical to ANSYS model, since the SYSWELD model doesn't have a stress-free crack surface, while the ANSYS model does. Basically in the superposition procedure shown in Figure 2.1, the residual stresses for the un-cracked configuration are obtained using SYSWELD and then these stresses are applied as crack surface pressure for the fracture mechanics calculation. The superposition of the two solutions gives the complete solution for the final state of stress in the cracked configuration. If the crack is in the problem before welding occurs, then the heat transfer conditions will simply be different and at the same time a preexisting flaw may decrease the accuracy of residual stress results from SYSWELD, i.e., the crack faces should be insulated to prevent heat from flowing across the crack face surfaces. Admittedly simulation of model with a crack is an interesting problem in and of itself, but is more representative of a weld repair problem. On the other hand, the model of interest in this study represents the case where the crack appears (nucleates) after welding. In this circumstance, heat transfer is not impeded by any pre-existing crack faces.

The approach that is used in this study relies on a superposition method (figure 2.1), i.e., SYSWELD stress output files are generated to characterize the state of stress only for the zone where the crack surface will be in the subsequent ANSYS/FRAC3D model. Thus the residual stress data from SYSWELD is used as an applied crack

surface pressure on the hypothetical crack surface area. There should be no other loads acting on the FRAC3D model (refer to a schematic of the superposition procedure in Figure 2.1) with all other boundary conditions the same. In this approach, the initial stresses are applied as a pressure on surface element. When this pressure is applied to a surface, the finite element program will compute the correct consistent nodal forces that are work equivalent to the pressure distribution, i.e., the FEM software will determine the proper nodal forces according to pressure information applied on the crack surface elements. This approach will yield the correct stress intensity factors in FRAC3D.

After running the FRAC3D program, the initial stresses obtained from SYSWELD can be added to the FRAC3D results, to determine the complete stress field, strain field displacement and nodal reaction forces. Clearly, this will result in cancellation of the stresses on the crack surfaces, providing the correct stresses throughout the cracked geometry. However, in most instances the full stress field is not of great interest and only the stress intensity factors are desired. Thus, the actual superposition of stresses is not generally required.

In this study, the FE model is initially developed using geometry and meshing tools in the HYPERMESH preprocessor. The finite element entities needed for the model are transferred to or from the SYSWELD code by way of modified ASCII files between \*.ASC file from SYSWELD and \*.CDB HYPERMESH file, which contains the topology of the model (nodes, elements and sets/groups/components). At the same

time, the finite element entities of the model are also transferred to ANSYS by way of transformed ASCII files from \*.HM file from HYPERMESH to \*.CDB ANSYS file, which contains the same topology of the model. After simulation of the fusion welding process in SYSWELD is completed, the computed residual stresses are exported from the SYSWELD postprocessor as a \*.lis file and are imported as pressure into the ANSYS/FRAC\_3D model through a FORTRAN program. The methodology described, uses the same topology for both of the models required for the numerical analyses, with the exception of the boundary conditions on the crack surface. This procedure ensures excellent integration between the two models. One benefit of this technique, is that it does not require separate meshes for the welding simulation and the fracture mechanics problem, i.e., both are solved using the same FE mesh..



## 2.2 Welding Geometry

In this study, the modeling and simulation effort focuses on generating solutions for a simple welded configuration that can easily be tested in experimental facilities. The test configuration that is modeled in this study is based on the so-called Longitudinal-Bead-Weld Notch-Bend test specimen [15].

Figure 2.2 shows a schematic drawing of the proposed test specimen configuration. In this model, a weld bead is deposited onto a pre-cracked specimen. The crack length extends beyond the edges of the weld bead and the crack shape is depicted in blue as shown in Figure 2.2. This test configuration approximates the type of cracking often observed in welded structures fabricated using longitudinal welds.

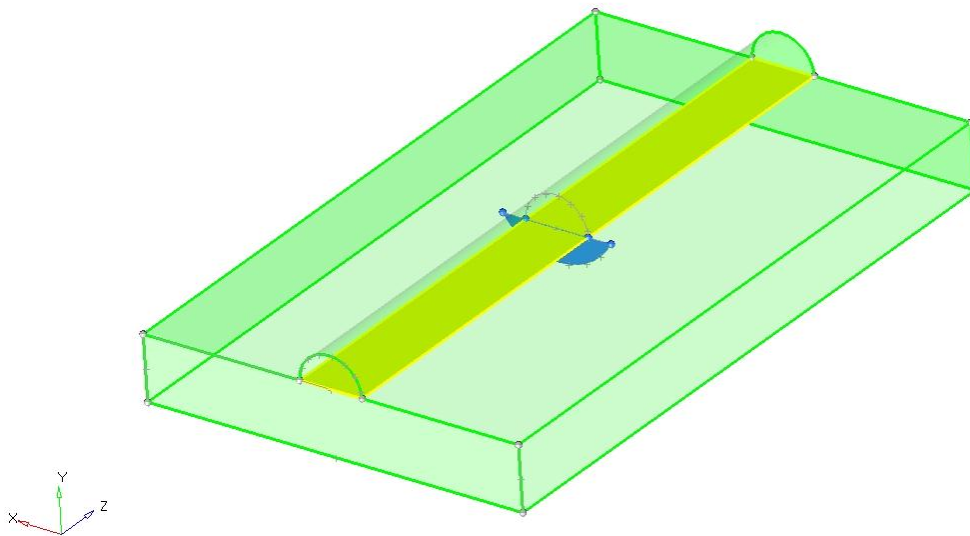


**Figure 2.2** geometry of Longitudinal-Bead-Weld Notch-Bend test specimen

After simulation of diffusion welding is accomplished, the SYSWELD stresses output files will be transferred only for the zone where the crack surface will be in the

ANSYS/FRAC3D model. The hypothetical crack surface is shown in blue in Figure 2.3. Thus the residual stress data for the hypothetical crack surface area to the crack surface as a un-uniform pressure distribution. There should be no other loads acting on the FRAC3D model with all other boundary conditions the same (figure 2.1).

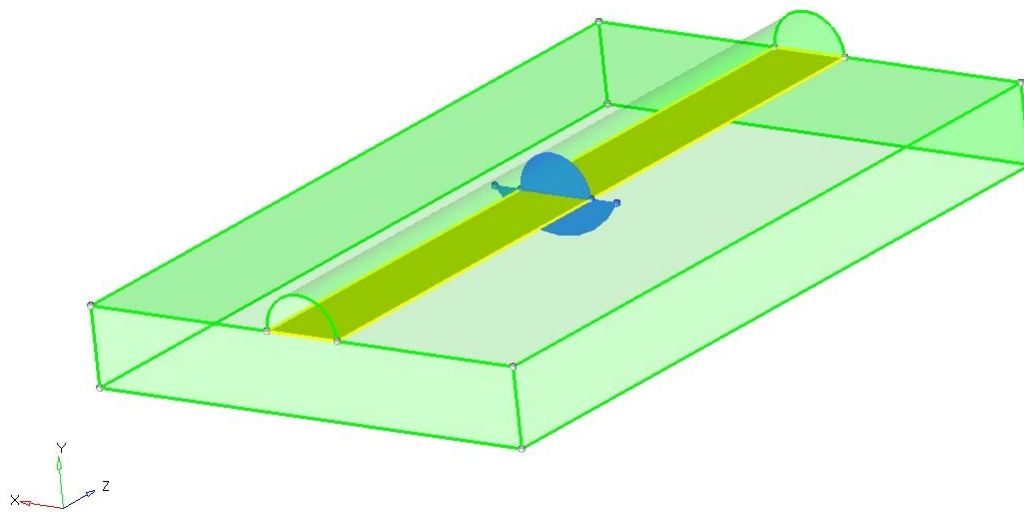


**Figure 2.3** Longitudinal-Bead-Weld Notch-Bend test specimen in Fracture analysis

Since the welding simulation process and fracture analysis share the same finite element model information set (nodes, elements, and element sets/groups/components), a fine mesh along the crack front is required. Considering that the file containing the fundamental finite element information is generally very large for these 3-D problems, this study will take the advantage of symmetry boundary conditions and use a one-quarter model as shown in Figure 2.4 for the fracture mechanics portion of the calculations. As before, the crack surface is marked

in blue in the figure. In the welding simulation, half-symmetry along the length of the longitudinal weld bead is appropriate.

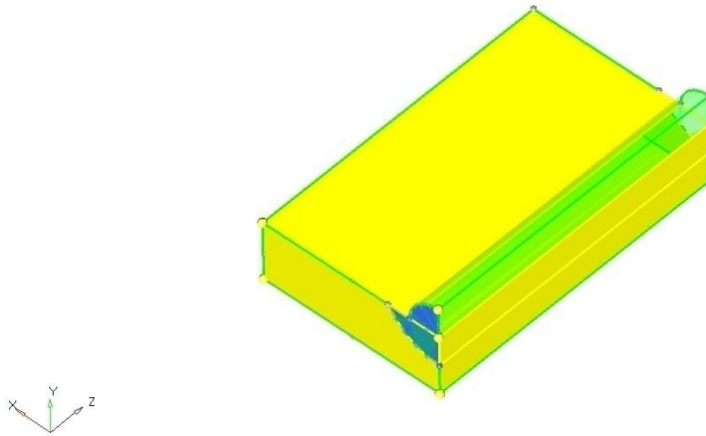


**Figure 2.4** 1/4 welding bead model

The length of the specimen is 100mm, which means the length for the one-quarter symmetry model is 50mm. The parameter of the geometry is: the width of the plate  $a$  equal to 30mm, the height of the plate which is  $b$  in the figure is 10mm. The radius of the weld cross-section (designated as  $R1$  in Fig. 2.5) is equal to 5mm and the crack front is modeled as a circular arc with a radius of 10mm.

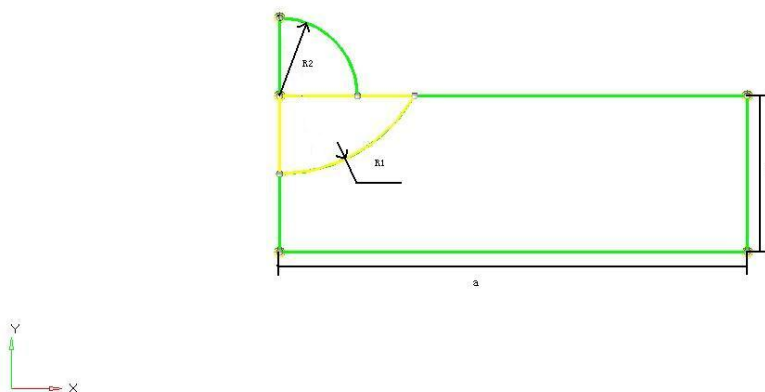


**Figure 2.5** cross section of 1/4 welding bead model

## 2.3 Mesh Generation

For volumetric 3-D simulation, three different meshing techniques are employed to construct the entire mesh for the Longitudinal-Bead-Weld Notch-Bend model using 1) the HYPERMESH mesh generator for SYSWELD solver, 2) WELD ADVISER, and 3) mesh techniques are applied for ANSYS/FRAC\_3D model.

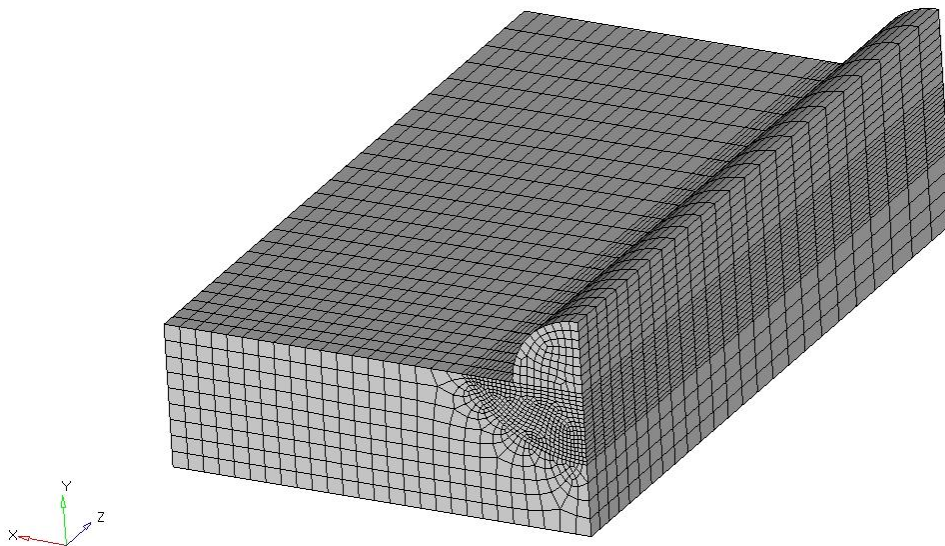


**Figure 2.6** 3D mesh generation of Longitudinal-Bead-Weld Notch-Bend model

First, Hex20 elements were generated in HYPERMESH as shown in figure2.6. These are 3-D (2nd order) hexahedra elements, with 20-nodes. These elements were used to compute volumetric heat conduction using the SYSWELD code. Quadratic hexahedral elements are preferable for HYPERMESH to generate complex mesh. In order to obtain reliability for reaching convergence in the thermal and mechanical results, it is necessary to generate a finer mesh along the crack front and in crack surface, but to keep elements in other part of the mesh comparatively coarser. Heat

transfer convection to the surroundings occurs on the surface at a constant room temperature. Figure 2.7 shows a model of a 20°C room temperature air is showed. The elements are quadratic 8nodes plane elements.

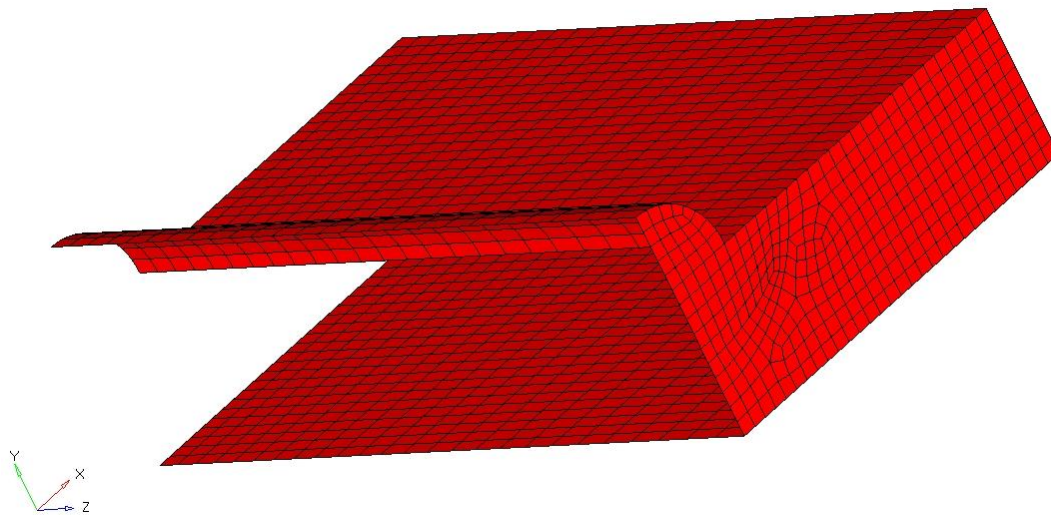


**Figure 2.7** 2D mesh and 1D mesh of Longitudinal-Bead-Weld Notch-Bend model

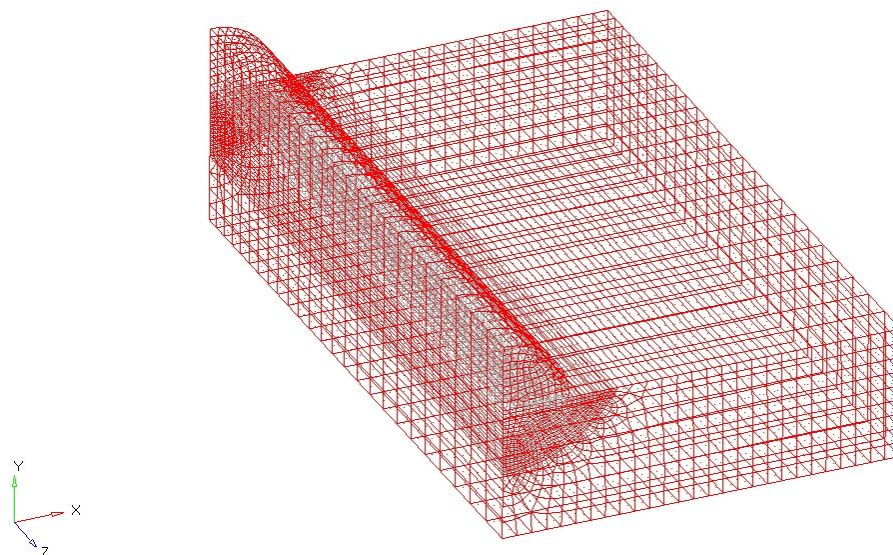


**Figure 2.8** 2D mesh and 1D mesh of Longitudinal-Bead-Weld Notch-Bend model

To compute the heat transfer behavior of the longitudinal-bead-weld notch-bend

model, a two-dimensional quadrilateral element with 8 nodes, QUAD8 in HYPERMESH is required to impose natural convection boundary conditions on the surface. Radiation on the model surface is also numerically calculated using the QUAD8 elements as well. As a matter of practice, once a mesh is generated in the 2-D cross-sectional plane, the 2-D plane mesh can be extruded in the welding direction (Z axial direction), meshing the entire volume. The generated meshes are shown in Figure2.6 and Figure2.8.

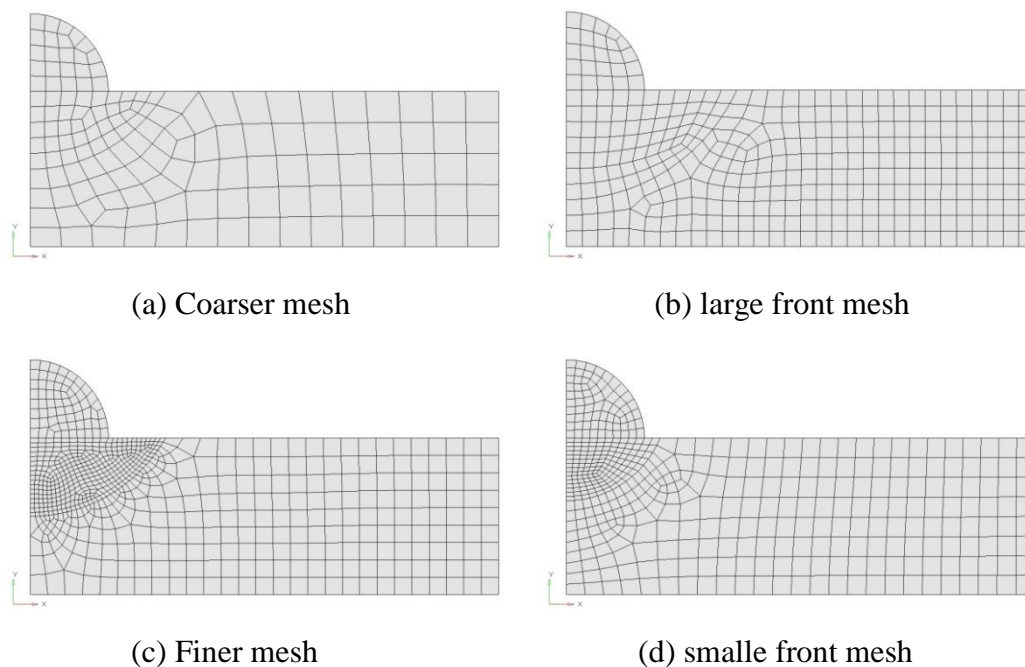


**Figure 2.9** Cross section

The deposition of the welding metal in the weld bead is simulated by using an element activation-deactivation technique [5, 16]. The activation-deactivation procedure gives the time dependent material properties for the weld bead only when the heat source passes across the surface of the plate. The material properties of the

weld bead and the gap are not given in this study; however, the properties are activated when the heat source passes through the corresponding nodes.

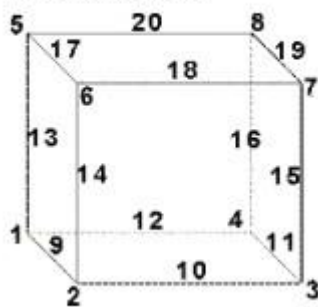
Since the computational results in SYSWELD and FRAC3D may depend on the element mesh density, the model described above was meshed using both a large (the crack front is a part of a circle with a radius of 12mm) front mesh as well as a coarser mesh and a finer mesh. After comparison of the result e.g. stresses, displacements and stress intensity factor, a modified model with a progression of crack shapes that follow the contours of the highest stresses around the weld zone was studied. This represents a sequence of separate crack configurations



## 2.4 HYPERMESH®/SYSWELD® Interface

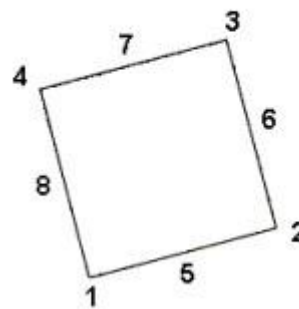
The Geometry/Meshing module, which is an integral part of SYSWELD software, is a sophisticated tool for the creation of model geometry and finite element mesh preprocessor. However, it is more expedient to create a finite element mesh which can be used in different programs in HYPERMESH. For further possibilities for the creation of complex geometry and mesh and for computation the same model in different environment, this study develops a HYPERMESH®/SYSWELD® Interface. Thus it is possible to convert HYPERMESH standard file to SYSWELD standard file. Also, it can convert SYSWELD standard file to HYPERMESH standard file (refer to figure 2.1).

Element Configuration 220  
20-noded hexa



(a) Hex20

Element Configuration 108  
8-noded quad



(b) Quad8

**Figure 2.10** (a) Hex20, 3D (2nd order)quadrilateral hexahedra element with 20 nodes in HYPERMESH.(b)Quad8, 2D (2nd order)quadrilateral elements with 8 nodes ordered in HYPERMESH



Although, the FORTRAN code can export/import most of elements in SYSWELD, there are only three types of element that are used in this study. These elements are depicted in Fig. 2.10. The third type is an two point line element of 1<sup>st</sup> order.

The element name and order of the nodal numbering in the elements from HYPERMESH and SYSWELD are shown in Figures 2.10 and 2.11, respectively. More information concerning these elements is given in Appendix 1.

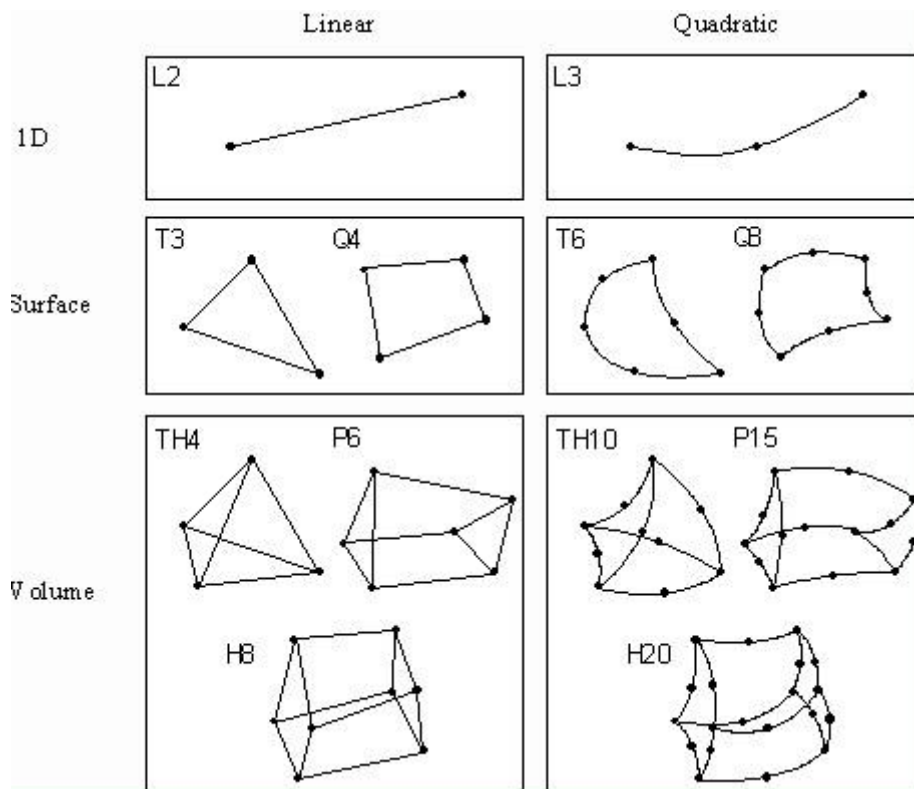


**Figure 2.11** Element definition and nodal number order in SYSWELD

The code allows creation of the SYSWELD data file or HYPERMESH-ANSYS standard format data file in ASCII format, which contains the FE mesh (nodes and

elements) and definition of Groups/Sets. The code does not permit exporting other pre-processing data, e.g., material properties, constraints, loads, etc.); these are defined directly in SYSWELD using SYSWELD's standard pre-processing capabilities or advisors or in ANSYS/FRAC\_3D using ANSYS preprocessor.

# Chapter 3. Fusion Welding Simulation

## 3.1 Material Properties and Fusion Welding Simulation

There has been an increasing interest in the effect of fusion welding residual stresses on mechanical properties, as the design of engineering components has become less conservative. The effects of residual stresses introduced by fusion welding are known to play a large role in structural failure mechanisms. Residual stresses are formed in welded structures primarily as the result of differential contractions which occur as the weld metal solidifies and cools to the ambient temperature. These stresses can have important consequences on the performance of the structure and its fracture behavior.

The material used in this study is a low-carbon steel [15]. The chemical composition of the parent material and weld metal are given in Table 3.1. The dimension of the plate is  $100 \times 60 \times 10 \text{ mm}^3$ ; the bead-on-plate welds were produced along the center line of the plate. The width of the weld beads is 10 mm. Typical mechanical properties of the parent and weld metal are given in Table 3.2. In the welding simulations, the sample was fully restrained when it is clamped. There was no pre- or post-weld heat treatment.

The objective of the welding simulation is to perform three-dimensional, finite-elements modeling of the one-quarter bead-on-plate experiment to export the

residual stress data, nodal stresses, nodal strain and displacement information. The parent and the weld material were assumed to have the same mechanical and thermal properties, as was provided in the SYSWELD database for the material S355J2 with chemical composition as follows: C:0.20%, Mn:1.60%, Si:0.55%; S:0.035% and P:0.035%. The solidus temperature was 1400°C, the liquidus is 1505 °C and the latent heat of fusion was 270,000 J/kg [5, 15]. The temperature dependent properties supplied with SYSWELD are measured values obtained by extensive experimentation. Three-dimensional meshes of the substrate plate and the weld bead were constructed as illustrated in Chapter 2, Figure 2.6.

**Table 3.1** Chemical composition of the consumable materials (in wt%)

Composition material	C	Mn	Si	S	P	Ni	Cr	Mo	Cu	V
Parent metal	0.12	0.63	0.13	0.01	0.02	0.02	0.01	0.01	0.01	<0.01
Weld metal	0.10	1.7	0.68	0.02	0.02	0.05	0.03	0.04	–	0.04

**Table 3.2** Typical mechanical properties (20°C)

Mechanical properties	Yield stress (MPa)	Tensile strength (MPa)	Elongation (%)
Parent metal (experimental measurements according to AS 1391:1991)	285	429	38
Weld metal ('as manufactured' using Argosshield 52 shielding gas)	445	550	29

The volume of the bead was modeled, for the sake of geometric convenience, as a one-quarter circular solid with the front and the back faces of the bead also one-quarter circle. Care should be taken to ensure that the mesh size control

specified at different lines and edges, especially, at the juncture of the supposed crack front line, the bead surface and the substrate plate, are such that the nodes lay on top of each other. The volume mesh was created with quadratic elements in 2-D and 3-D. Three differential element sizes are used in mesh; the mesh in the zone of the bead was built with a higher mesh density than that on the plate. Similarly, the mesh density is higher near the crack front line where the crack is placed, and progressively reduced towards the edges of the substrate plate.

In order to generate the convection and radiation boundary conditions, skin elements (two-dimensional quadratic plane mesh) were constructed on all the exposed domains of the model. As before, the mesh density of the surface mesh was specified such that the skin element nodes were coincident with the volume element nodes lying underneath them. A combined convective and radioactive heat transfer coefficient of  $25 \text{ W/m}^2 \cdot \text{K}$  was assumed. The initial temperature was assumed to be  $20^\circ\text{C}$  (ambient temperature).

The program required that the welding heat source trajectory be explicitly specified along the direction and position of the moving heat source using linear, one-dimensional elements. The trajectory was chosen to be along the center line of the whole substrate plate, with mesh size control of the weld line to ensure that the nodes coalesced with those on the skin and volume elements. The simulation was run for fully restrained, i.e., clamped boundary conditions.

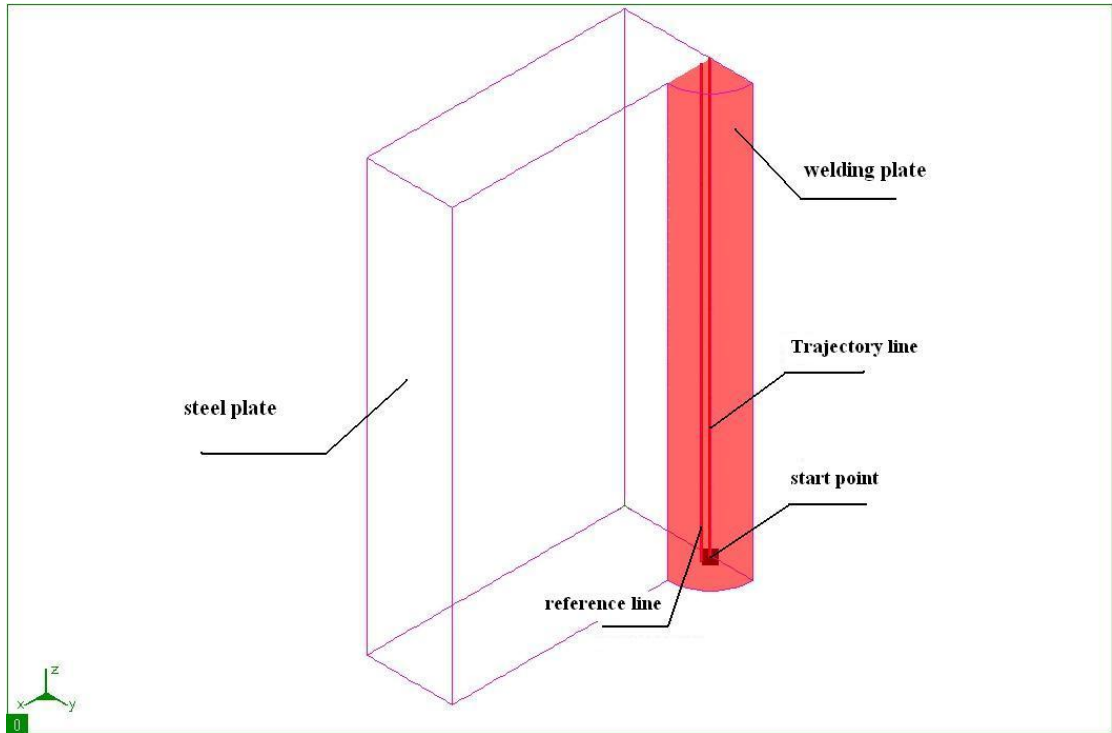
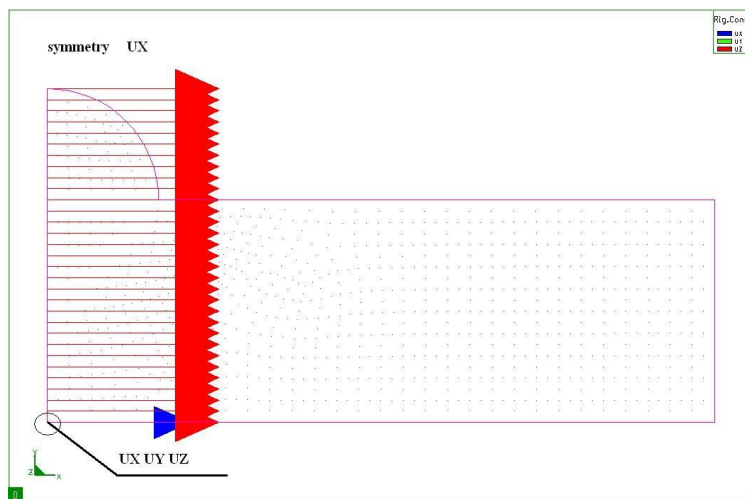


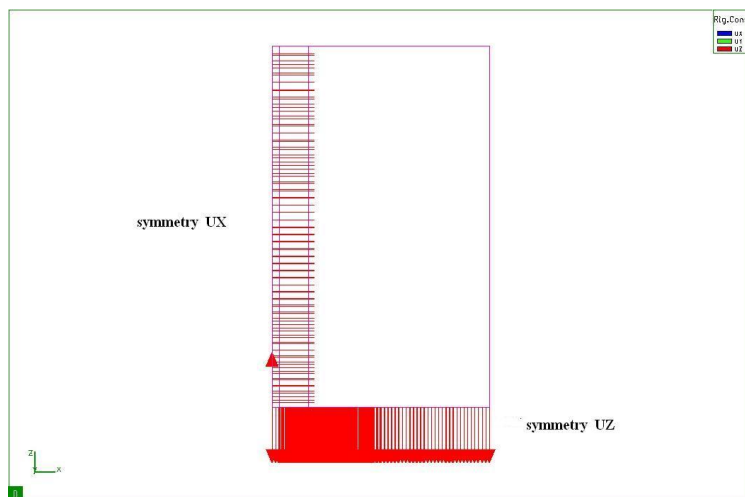
**Figure 3.1** Trajectory line and reference line for fusion welding

### 3.2 Initial Clamping Condition

Welding simulation results depend on the nature of the clamping condition. In this study the model is fully constrained. As shown in Figure 3.2( a) and Figure 3.2 (b) ,all nodes on the symmetric UX plane and symmetric UZ plane are fixed in a direction normal to X and Z planes, respectively. In addition to these, a bottom-front node is restrained in all degrees of freedoms ( $U_{x,y,z}=0$ ).



(a) X-Y view



(b) X-Z view

**Figure 3.2** Initial boundary condition

### 3.3 Heat Source Modeling

The welding heat source used in this study is an arc plasma radiating intense heat outwards with decreasing temperature. For accurate simulation of the welding heat source, a 3-D double ellipsoidal heat source developed by Goldak [5] is usually used in arc welding simulation. Considering a Gaussian distribution, this heat source model has been found to be considerably more accurate than a point or a line heat source model, especially when simulating metal gas arc welding processes [5]. The total heat rate ( $q$ , power) from the arc welding gun is simply expressed as Eq. (3.1), with  $\eta$  being the efficiency and  $V$  and  $I$  being the arc voltage and current, respectively:

$$q = \eta VI [w] \quad (3.1)$$

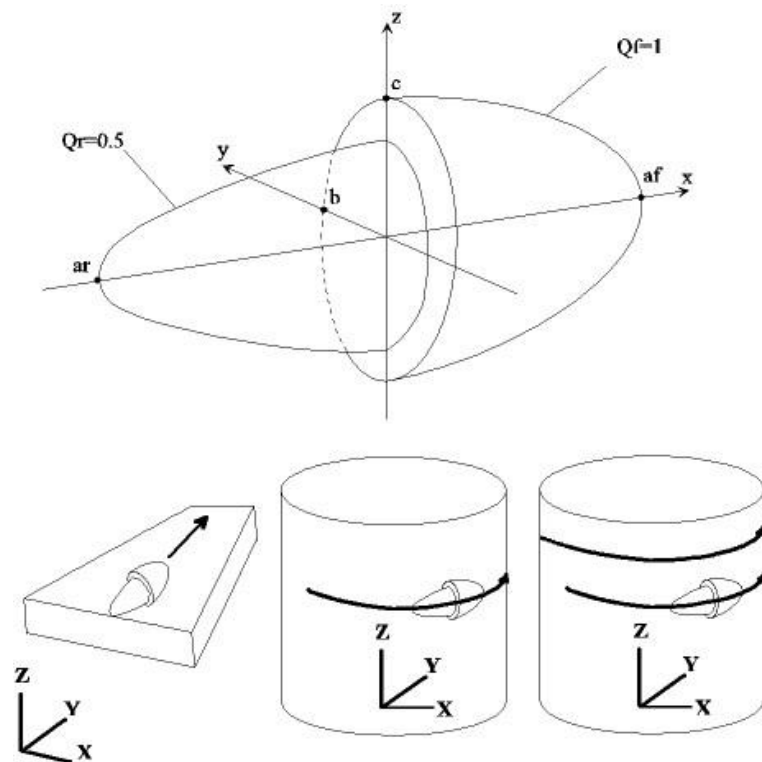


**Figure 3.3** Double ellipsoid source and display of possible trajectories



According to Nguyen et al. [15], the most appropriate model for the heat source for TIG and MIG welding procedures is the double ellipsoidal heat source. A double ellipsoidal heat source consists of two different single ellipsoids as shown in Figure 3.3, and is properly considered to be a more sophisticated heat source compare to a single ellipsoidal on account of its better flexibility in modeling realistic shapes of the moving heat source. The heat density  $Q(x, y, z)$  at an arbitrary point within the front half ellipsoid and rear half ellipsoid is described by the following equation [5], respectively:

$$Q(x, y, z) = \frac{6\sqrt{3}r_f Q}{a_h b_h c_{hf} \pi \sqrt{\pi}} e^{-3(x^2/c_{hf}^2 + y^2/a_h^2 + z^2/b_h^2)}, \quad (3.2)$$

$$Q(x, y, z) = \frac{6\sqrt{3}r_b Q}{a_h b_h c_{hb} \pi \sqrt{\pi}} e^{-3(x^2/c_{hb}^2 + y^2/a_h^2 + z^2/b_h^2)}, \quad (3.3)$$

Where,  $a_h$ ;  $b_h$ ;  $c_{hf}$ ;  $c_{hb}$  are the ellipsoidal heat source parameters,  $Q$  is arc heat input defined in Eq.3.2., and  $r_f$ ,  $r_b$  are the proportional coefficients at the front and the back of the heat source, respectively, such that ( $r_f + r_b = 2$ ).

An expedient method of calibrating the coefficients is built into the SYSWELD program to achieve the correct heat energy density in ( $W/mm^3$ ) of each one-half ellipsoid. The heat input fitting tool of the SYSWELD welding adviser allows the user to enter the basic value of the geometric parameters with accurate arc energy input to give the values of  $Q_f$  (heat energy density in the front half) and  $Q_r$  (heat energy

density in the rear half) iteratively. A simple Fortran code provides an efficient way to iterate several time steps to calibrate the heat source with the known dimensions of thermal image of the molten weld pool, as well as distortions of the edges or even temperatures at specified points. In this study, the heat source was calibrated using the image of the weld pool as shown in Figure 3.4.

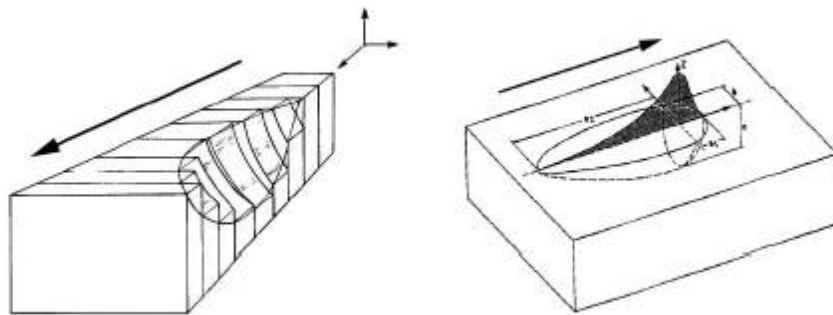


**Figure 3.4** Weld pool

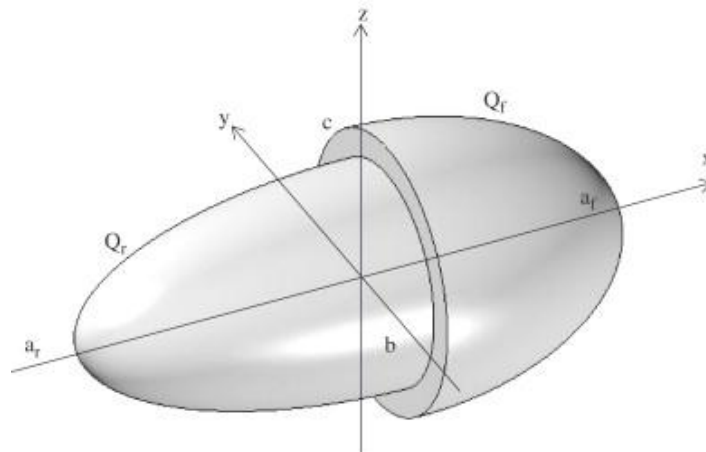


**Figure 3.5** Calibrating heat sources

The geometry dimension showed in Figure 3.5 of the heat source in this study is:  $a_f = 4$ ;  $a_r = 8$ ;  $b = 7$ ;  $c = 0:8$  and velocity of the weld torch along the weld trajectory line  $V_y = 6\text{mm/s}$ . The energy input is  $15000\text{W}$ , with an assumed arc efficiency of  $0.8$

and the density of energy source for front and rear ellipsoids are  $Q_f = 268 \text{ W/mm}^3$  and  $Q_r = 138 \text{ W/mm}^3$ , respectively. The parameters mentioned here are used in the definition of the double ellipsoidal model as provided in the documentation of SYSWELD in Figure. 3.5. At  $t=0$ , the heat source will move from the start point to the end of trajectory line as shown in Figure 3.1 in velocity of  $1 \text{ mm/s}$

### 3.4 Heat Transfer Modeling

Radiation, convection, and conduction are considered as the main factors during the transient heat transfer associated with welding. SYSWELD offers numerical compute result to analysis heat transfer rates including radiation, convection and conduction.

For radiation evaluation, the surrounding environment is specified at an ideal temperature of 20°C. In SYSWELD, the surrounding environment is created as a group of elements as shown in Figure 2. 7 (the name of the group is skin). The “skin” elements are used to apply the radiation boundary condition. In fundamental heat transfer, radiation heat transfer is generally given as an expression in Equation (3.4) where  $\sigma$  is the Stefan-Boltzmann constant,  $5.67 \times 10^{-8}[\text{W}/\text{m}^2 \cdot \text{K}^4]$ , and  $\epsilon$  is the emissivity, and  $T_0$  is an ambient temperature, 20°C.  $h_{\text{rad}}$  is defined as the radiation heat transfer coefficient.

$$\begin{aligned} q''_{\text{rad}} &= \sigma\epsilon(T^2 - T_0^4) = \sigma\epsilon(T^2 + T_0^2)(T + T_0)(T - T_0) \\ &= h_{\text{rad}}(T - T_0)[\text{W}/\text{mm}^2] \end{aligned} \quad (3.4)$$

In Equation (3.4), the surface emissivity is assumed be 70% for molten stainless steel although the emissivity is temperature-dependent. [17]. The equation is simplify Newtonian convection:

$$q''_{\text{conv}} = h(T - T_0)[\text{W}/\text{mm}^2] \quad (3.5)$$

$h$  [ $\text{W}/\text{m}^2\text{K}$ ] is the convective heat transfer coefficient.

Conduction heat energy flux from the weld, which is influenced by both of the

energy balance and the welding heat source and the heat transfer, is expressed in the linear equation of the temperature gradient  $\nabla T$ . In Equation (3.5),  $h$  [ $W/m^2 \cdot K$ ] is a function of time (thermal conductivity) and  $\nabla$  is defined as tensor symbol  $(\frac{\partial}{\partial x}, \frac{\partial}{\partial y}, \frac{\partial}{\partial z})$  in Cartesian coordination.

$$q''_{cond} = k \nabla T [W/mm^2] \quad (3.6)$$

The initial boundary condition for the weld surface area is expressed as Equation (3.7), associate with radiation and convection terms [17, 18, 19]. In the Equation (3.7),

$$k \nabla T + (h + h_{rad})(T - T_0) = k \nabla T + q'' = 0 \quad (3.7)$$

$q''$  is the assumed constant represent summation of the convective and radioactive heat losses. [17]. Equation (3.7) with the heat input can be deduced as following equation in the Cartesian coordinates, as long as heat  $C_p$  is determined. [20, 24]

$$\frac{\partial}{\partial x} \left( k \frac{\partial T}{\partial x} \right) + \frac{\partial}{\partial y} \left( k \frac{\partial T}{\partial y} \right) + \frac{\partial}{\partial z} \left( k \frac{\partial T}{\partial z} \right) + \dot{q} = \rho c_p \frac{\partial T}{\partial t} \quad (3.8)$$

In equation (3.8),  $\rho$  [ $kg/mm^3$ ] and  $C_p$  [ $J/kg \cdot ^\circ C$ ] are the density and the specific heat, respectively. Term  $\dot{q}$  is the thermal energy generation term and it may be related with applied volumetric heat source or power density  $q'''$  [ $W/mm^3$ ]. Equation can be simplified as equation (3.9).

$$\rho c \dot{T} - \nabla(k \nabla T) - q''' = 0 \quad (3.9)$$

The homogeneous equations, involving heat transfer, phase transformation and linear plasticity, are contained in SYSWELD numerical program depended on time. SYSWELD contains the finite element formulation of the nonlinear transient heat transfer equations.

### 3.5 Thermal Analysis

Figure 3.6 shows the temperature distribution contour when a moving heat source passes long the trajectory line from start node to end node. The color in red represent the center of heat source and the green, yellow and red zone represent the liquid part, which has its temperature higher than, or equal to the melting temperature. The solidus temperature was 1440°C, the liquids are 1505°C and the latent heat of fusion was 270,000 J/kg [5, 15].

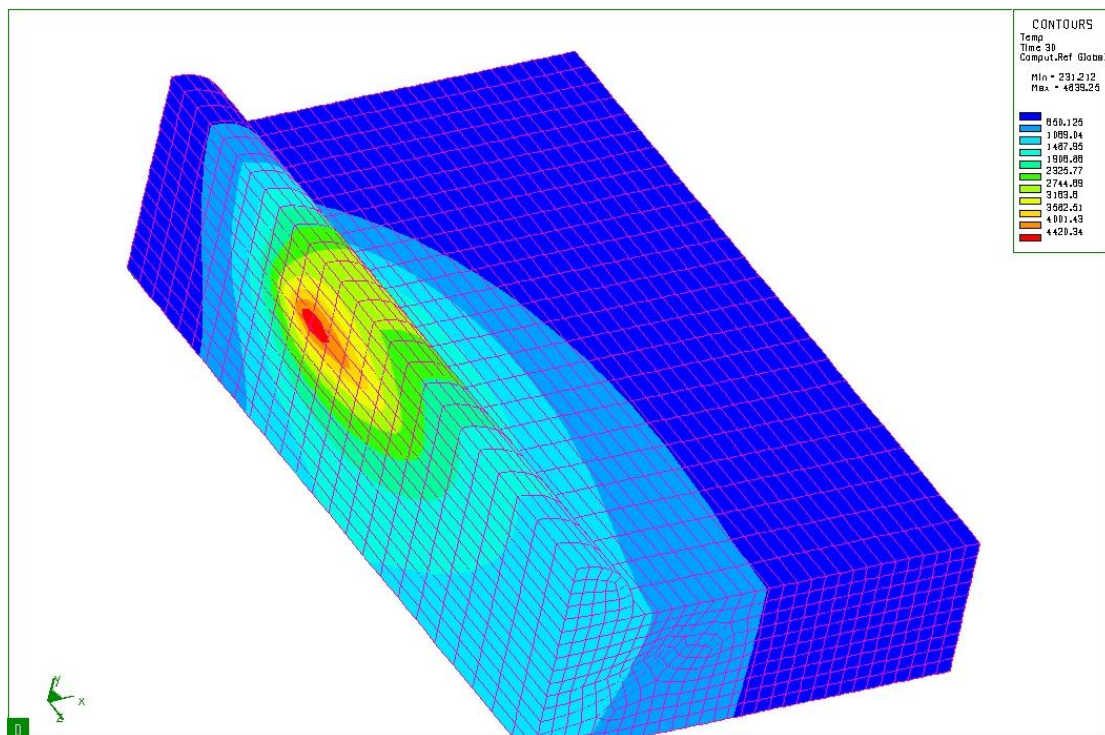
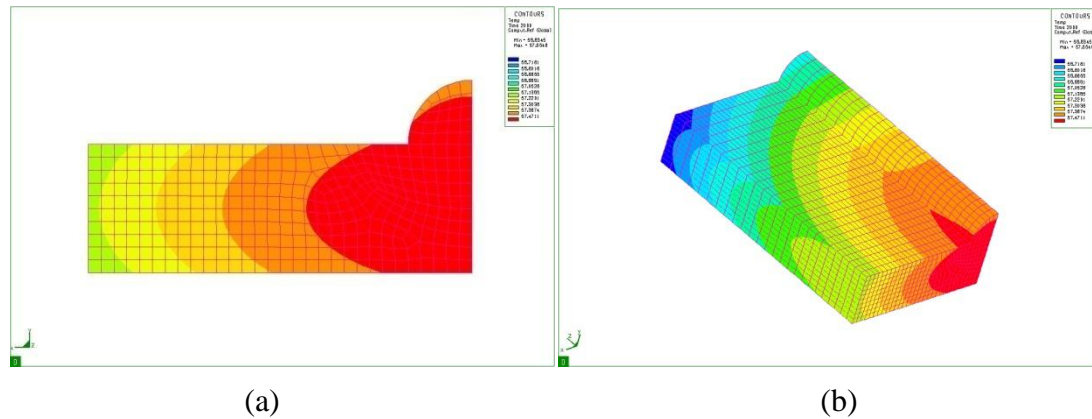


Figure 3.6 Moving heat source

The contours of temperature distribution are plotted on the Longitudinal-Bead-Weld Notch-Bend model in Figures 3.7(a) and 3.7(b). Figure 3.7(a) shows

temperature distribution on cross section of plane  $z = 0$ . Figure 3.7(b) shows temperature distribution of the whole Longitudinal-Bead-Weld Notch-Bend model. The welding parameters are described in Chapter 3.3, e.g., the velocity, efficiency, heat input, etc.



**Figure 3.7** (a) Temperature distribution of plate-bead. (b) Temperature distribution of z-direction symmetry plane

Through the given temperature profile at the symmetry z-direction plane cross section in Figure 3.7(b), the contour of the fusion zone can be estimated using material properties mentioned in Chapter 3, section1. It should be also to be noted when calibrating the heat source that the dimension of the melted zone should cover the entire one-quarter circle weld bead, thus the simulation models a deep weld penetration for fabrication of a satisfactory weld. In order to analyze the residual stresses, Von Mises stresses are usually plotted with units given in Mega-Pascal [MPa]. The distribution of residual stresses in the direction of the trajectory line will be printed in an ASCII file to evaluate the change of stresses after each welding process. Figure 7.8 shows the temperature configuration as a function of time.

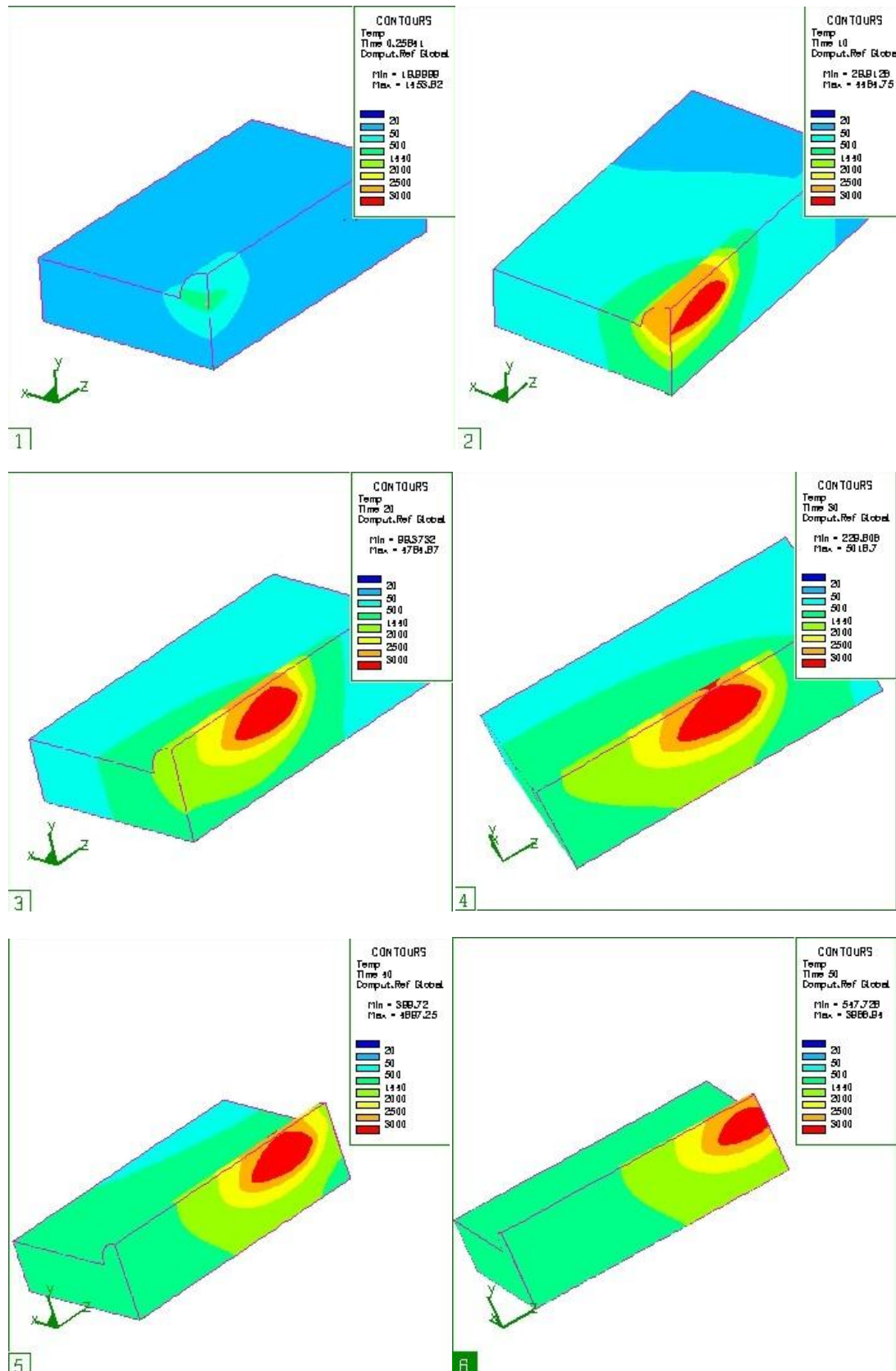


**Figure 3.8** Temperature distributions during welding process. (1)  $t=5$ ; (2)  $t=10$ ; (3)  $t=20$ ; (4)  $t=30$ ; (5)  $t=40$ ; (6)  $t=50$ .



## **3.6 Mechanical Analysis**

In SYSWELD, the mechanical analysis is based on results obtained from the thermal analysis and is generally much more computationally intensive. The original output data included stresses in elements, integration points and element nodes. Stress and strain in nodes, integration points, reaction forces at nodes and other forms of computed results can be exported by the convert and extrapolate tool that is built into the SYSWELD ADVISOR

# Chapter 4. Fracture Mechanics Analysis

## 4.1 Finite Element code FRAC\_3D

After simulation of the welding process, the computed residual stresses in the zone of crack surface (blue zone in Figure 2.2) are exported from SYSWELD and are imported as initial stresses into ANSYS/FRAC3D, through the HYPERMESH/SYSWELD interface described in Chapter2, Section 4. The methodology followed utilizes the same FE mesh for both numerical analyses in order to simplify the transfer of data between the two simulations.

The finite element program FRAC3D is specifically designed to treat crack problems in fracture mechanics with a stress singularity at the tip of the crack. The enriched crack tip element formulation for 2-D problem begins from Benzley's work [20], and is generalized such that any singularity may be represented by including the proper near field terms. FRAC3D contains 6 different types of crack tip element, in this study, a 20-noded three-dimensional crack tip element shown in Figure.4.1 is used, where the crack tip has 4 nodes.

For the enriched crack tip elements in 3-D problems, the asymptotic displacement field is given by the following [20].

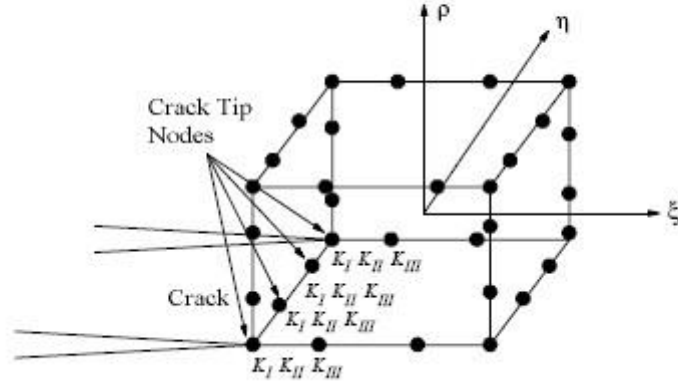


**Figure 4.1** 20-Node three-dimensional enriched crack tip element

$$\begin{aligned}
u(\xi, \eta, \rho) &= \sum_{j=1}^{32} N_j(\xi, \eta, \rho) u_j \\
&+ Z_0(\xi, \eta, \rho) \left( \sum_{i=1}^4 N_i(\xi, \eta, \rho) K_I^i \right) \left\{ f_1(\xi, \eta, \rho) - \sum_{j=1}^{32} N_j(\xi, \eta, \rho) f_{1j} \right\} \\
&+ Z_0(\xi, \eta, \rho) \left( \sum_{i=1}^4 N_i(\xi, \eta, \rho) K_{II}^i \right) \left\{ g_1(\xi, \eta, \rho) - \sum_{j=1}^{32} N_j(\xi, \eta, \rho) g_{1j} \right\} \quad (4.1)
\end{aligned}$$

$$\begin{aligned}
v(\xi, \eta, \rho) &= \sum_{j=1}^{32} N_j(\xi, \eta, \rho) v_j \\
&+ Z_0(\xi, \eta, \rho) \left( \sum_{i=1}^4 N_i(\xi, \eta, \rho) K_I^i \right) \left\{ f_2(\xi, \eta, \rho) - \sum_{j=1}^{32} N_j(\xi, \eta, \rho) f_{2j} \right\} \\
&+ Z_0(\xi, \eta, \rho) \left( \sum_{i=1}^4 N_i(\xi, \eta, \rho) K_{II}^i \right) \left\{ g_2(\xi, \eta, \rho) - \sum_{j=1}^{32} N_j(\xi, \eta, \rho) g_{2j} \right\} \quad (4.2)
\end{aligned}$$

$$\begin{aligned}
w(\xi, \eta, \rho) &= \sum_{j=1}^{32} N_j(\xi, \eta, \rho) w_j \\
&+ Z_0(\xi, \eta, \rho) \left( \sum_{i=1}^4 N_i(\xi, \eta, \rho) K_{III}^i \right) \left\{ h(\xi, \eta, \rho) - \sum_{j=1}^{32} N_j(\xi, \eta, \rho) h_j \right\} \quad (4.3)
\end{aligned}$$

In the equation (4.1), (4.2), (4.3), stress intensity factors are included, i.e., for a 32-node three dimensional element, there are 3 more stress intensity factors for each of four crack tip nodes, which means 12 additional degrees of freedom in total. The

contributions from these 12 stress intensity factors, as well as nodal displacements are then assembled into the global matrix as unknowns in the same way it is done for the regular elements. In each equation above, the first summation terms refer to the normal part of the displacement field, i.e., they have the same field approximation used in regular isoperimetric elements. [20]

Since an analytic singular field is defined in the enriched crack tip elements, displacement incompatibility will arise between elements along the crack tip if not properly adjusted. Thus  $Z_0(\xi, \eta, \rho)$  is defined as the “zeroing function” which enforces compatibility between the crack tip elements and the surrounding regular iso-parametric elements. In the enriched crack tip elements  $Z_0$  equal to one; in the transition elements the  $Z_0$  function is one for nodal points where the transition element is adjacent to any of the crack tip elements, or it is zero if the transition elements is adjacent to regular iso-parametric elements.

$K_I^i$ ,  $K_{II}^i$  and  $K_{III}^i$  represent the stress intensity factors, for mode I, mode II, and mode III, respectively. From Figure 4.1, there are four crack tip nodes on one element which are associated with the corresponding interpolation function of each node. For example, the variation of stress intensity factors in the "z" direction,  $K_{III}^i$ , is relative to the shape function values of the crack tip nodes. To evaluate the mode I, mode II and mode III stress intensity factors,  $K_I^i$ ,  $K_{II}^i$  and  $K_{III}^i$ , five asymptotic displacement coefficients  $f_1$ ,  $f_2$ ,  $g_1$ ,  $g_2$  and  $h$  for each node should be determined. Therefore, in the enriched element shown in the Figure 4.1, there will be 108 unknowns (96

displacement unknowns and 12 stress intensity factor unknowns). [20]

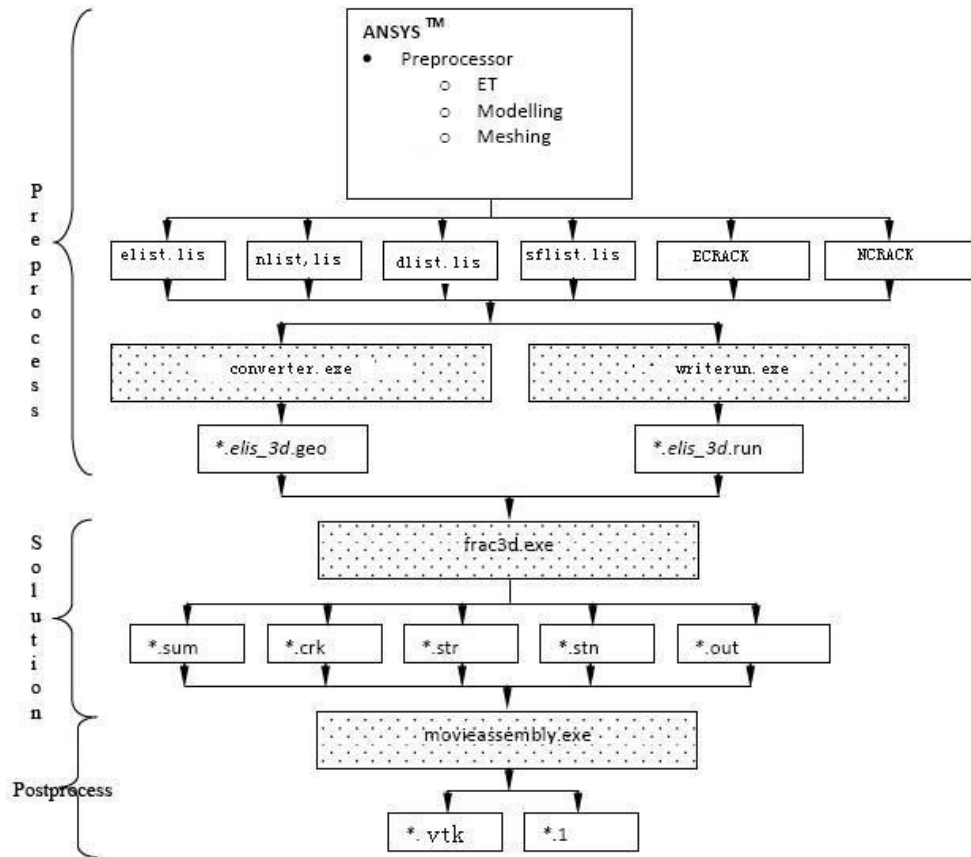


**Figure 4.2** General flow of FRAC\_3D analysis

The general flow of FRAC3D analysis is shown in Figure 4.2. In order to import the required finite element information into FRAC3D, all the data should be converted to ANSYS standard format ASCII \*.lis file by applying either the ANSYS preprocessor [21] or self-developed program(?).

In this study, finite element information for nodes, elements, sets/components and material properties are exported from HYPERMESH and loaded into the ANSYS

preprocessor directly by utilizing the built in HYPERMESH interface with ANSYS program. As shown in Figure 4.2, six files are required to prepare for analysis in FRAC\_3D. In this thesis, five files are exported from ANSYS and one is created using a FORTRAN program that will be described in Chapter 4 Section 2 from stress data generated by SYSWELD. For the five files, elist.lis file provides the finite element connectivity information; nlist.lis contains nodal coordinate data; dlist.lis contains boundary conditions; and ECRACK and NCRACK represent crack element file and crack tip element file (what's the difference between these two files?), respectively. The file sflist.lis is a pressure file generated by a FORTRAN program and contains the pressure on the crack surface from fusion welding simulation. In the process of creating a \*.elsit\_3d.goe file, it was necessary to constrain  $K_{II}^I$  and  $K_{III}^I$  to zero along the whole crack front, since the problem should be symmetric by definition. Another assumption is that there shouldn't be any shear stresses on the cross-section, since in this study only mode I loading is permitted.

## 4.2 SYSWELD/FRAC3D Interface

The SYSWELD/FRAC3D Interface generates a file contains pressures on the crack surface. This file is used in the superposition methodology which is the most expedient approach to solve problem of Longitudinal-Bead-Weld plate with a notch. The purpose of this step is to use the SYSWELD stresses that are transferred only for the zone where the crack surface will be in the ANSYS/FRAC3D model. Then these stresses will be applied to the crack surface as pressure. There should be no other loads acting on the FRAC3D model with all other boundary conditions the same. In this approach the initial stresses normal to the weld cross-section are applied as a pressure on the crack surface. When applying pressure to a surface, the finite element program will compute the correct consistent nodal forces that are work equivalent to the pressure distribution. It should be noted that this Interface does not determine these forces directly; i.e., the FEM software determines these nodal forces. This approach will give the correct stress intensity factors in FRAC3D.

Typically most finite element programs provide two sets of stress output. The element by element output gives the stress components at the nodes, which is extrapolated from the integration points within that particular element. These stresses are fairly accurate, but the nodal stresses are not the same for nodes shared by the different elements, i.e., the stresses between elements are averaged at the nodes. The second stress information that's usually output is the averaged nodal stresses. This results in a stress smoothing that gives a reasonably good representation of the state of

stress at the nodes. The only time that average nodal stresses are not accurate, is when the node is shared by two adjacent elements that have different material properties. In this special case, there is a stress discontinuity in the component of stress parallel to the element boundary. Of course, this is not an issue in the problems that this study is dealing with. Thus, for the superposition calculations in this study, the averaged stresses that are given for the nodes, instead of the nodal stresses that are given by the individual elements are used for fusion welding residual stress transfer.

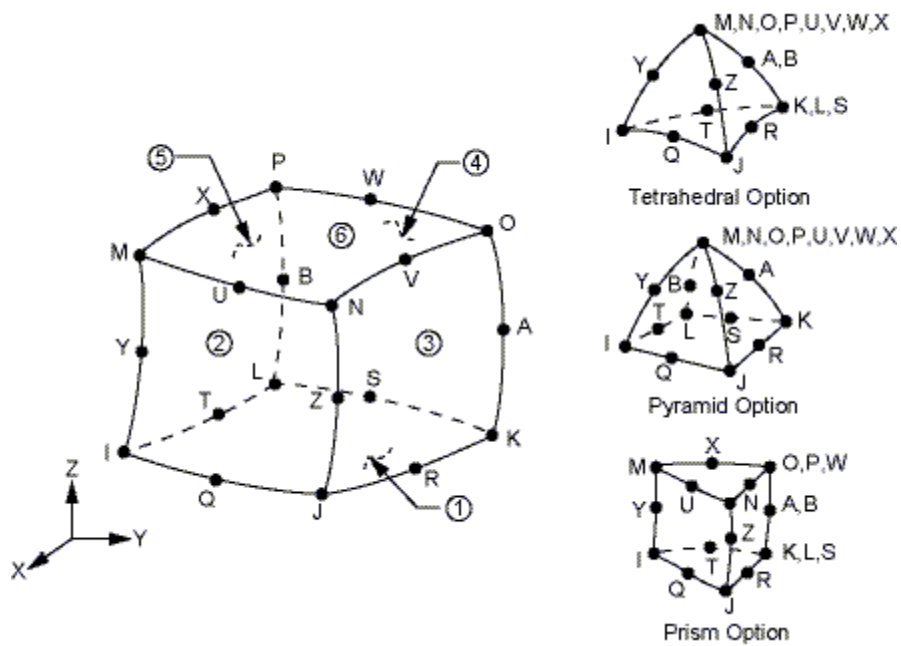


**Figure 4.3** Surface Loads Pressures format, face 1: (J-I-L-K), face 2: (I-J-N-M), face 3 (J-K-O-N), face 4: K-L-P-O), face 5: (L-I-M-P), face 6 (M-N-O-P)

When applying residual stress as pressure, ANSYS file require four nodal stresses for each quadratic HEAX20/3020/SOLID95 element on the crack surface. The point and the number are shown in Figure 4.3. For example, in



SYSWELD/FRAC3D Interface, the program automatically picks four corner nodes J, I, L, K in face 1 which is shown in Figure 4.3.

### 4.3 Superposition Results

The purpose of this section is to describe the process of superimposing the stresses from the un-cracked configuration obtained from SYSWELD to the cracked configuration in FRAC3D to obtain the correct stress intensity factors. The superposition process can be used to obtain the stress result for the whole configuration, if the stresses obtained from both configurations are added together. However, since the most important result from a fracture mechanics point of view is the stress intensity factor values obtained from FRAC3D, it is usually unnecessary to generate the entire stress state. In this study, the main purpose of merging the two stress states is to provide an overall sense of the state of stress in the cracked configuration.

From the flow chart shown in Figure 4.2, the FRAC3D output information is saved in six ASCII files. Among the six files, the \*.crk file gives the computed stress intensity factor along the crack front tip..

When applying pressure to the crack surface, the crack surface will not be stress free, though this will give the correct stress intensity factors. To obtain the actual stresses in the cracked structure, it is necessary to add the FRAC3D nodal stresses to the initial stresses from SYSWELD. For example, if the initial stresses from SYSWELD on the plane where the crack surface is located are tensile stresses, when these stresses are applied as pressure on the crack surface in FRAC3D, the result will be compressive stresses at the nodes on the crack surface. Thus, if the positive initial

stresses from SYSWELD are added to the compressive stresses on the crack surface from FRAC3D, they cancel out and will yield a stress-free crack surface. The stresses everywhere else in the model can be obtained by superposing the stresses from the two calculations.

The \*.str file provides stress tensor information for each element in Cartesian coordinates. In the stress output for each element, there is the effective stress  $\sigma_{\text{eff}}$ , the normal stress component in the x direction  $\sigma_1$ , stress in y direction  $\sigma_2$ , stress in z direction  $\sigma_3$ , and shear stress component xy  $\sigma_4$ , shear stress yz  $\sigma_5$ , shear stress xz  $\sigma_6$  for each node in the element. When superposing components of the stress tensor in a specific direction, the FORTRAN program first adds the two sets of  $\sigma_1, \sigma_2, \sigma_3, \sigma_4, \sigma_5$  and  $\sigma_6$  from fusion welding simulation and fracture mechanics analysis together; then new effective stresses are recalculated use equation. This will provide a stress free crack surface.

$$\sigma_{\text{eff}} = \sqrt{3} \cdot \sqrt{(\sigma_4)^2 + (\sigma_5)^2 + (\sigma_6)^2 + 0.5 \cdot (\sigma_1 - \sigma_{\text{mean}})^2 + (\sigma_2 - \sigma_{\text{mean}})^2 + (\sigma_3 - \sigma_{\text{mean}})^2}$$
(4.4)

$$\sigma_{\text{mean}} = \frac{1}{3} \times (\sigma_1 + \sigma_2 + \sigma_3)$$
(4.5)

The \*.stn file provides strain tensor information for each element in Cartesian coordinate. In the strain tensor for each element, there is the effective strain  $\tau_{\text{eff}}$ , strain in xx direction  $\tau_1$ , strain in yy direction  $\tau_2$ , strain in zz direction  $\tau_3$ , strain in

xy direction  $\tau_4$ , strain in yz direction  $\tau_5$ , strain in xz direction  $\tau_6$  for each node in the element. When superposed strain tensors, the FORTRAN program first recalculated  $\tau_1, \tau_2, \tau_3, \tau_4, \tau_5$  and  $\tau_6$  uses the same procedure for computing stresses. New effective strains are equal to zero, because this is not a general plane stress problem. The result will provide the total strain configuration.

The \*.out file from FRAC3D contains three sections of data output in Cartesian coordinates. Firstly, it provides displacement in x, y, z direction for each node, which provides a total displacement configuration. Secondly, it lists average stress tensor in xx, yy, zz, xy, yz, xz direction for each node. Last is the nodal reaction forces in x, y, z direction for each node. And they will be added together directly.

After all results in these three files are superposed, they are written by a FORTRAN program to a Python standard format file. As shown in Figure 4.2, ultimately two files, \*.1 file and \*.vtk file, are created to generate visible stress, strain, and displacement contour plots in the PARAVIEW program.

# Chapter 5. Conclusions and Future Work

## 5.1 Finite element analysis of crack problems

In this chapter, the results of fusion welding simulation and fracture mechanics analysis are summarized in terms of residual stress and stress intensity factor at the crack front.

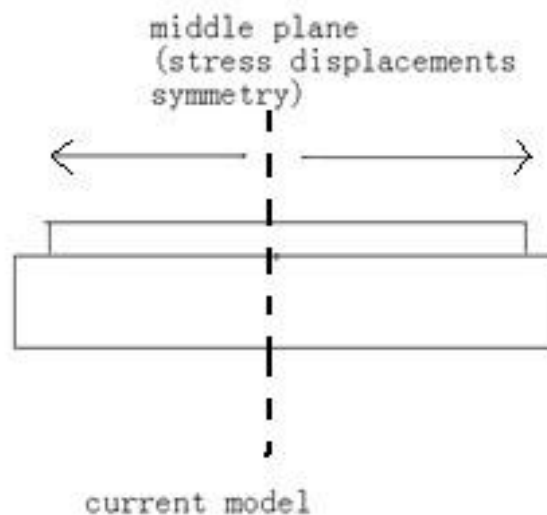


**Figure 5.1** Model description

The model which is currently used in this study is using two same heat sources moving from the center point and reaching the to two ends of the block at the same time. The model is shown in Figure 5.1.

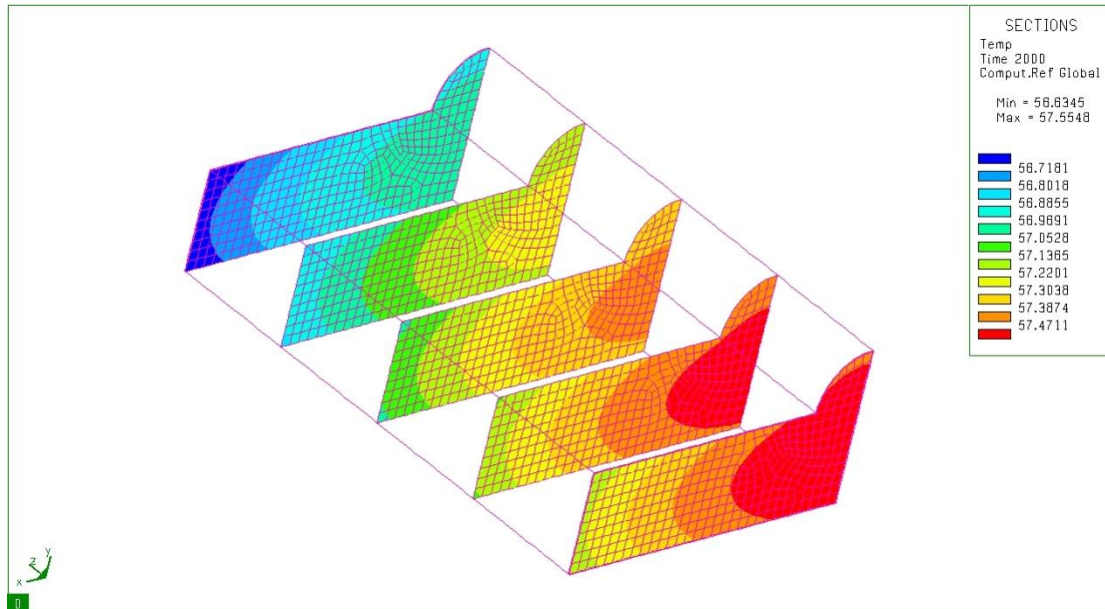
Currently the middle plane should be the symmetry plane because the movement of heat sources and heat transfer process should be symmetry on middle plane. Thus, stresses, strains displacements and other results of the right part and the left part will be symmetry.

The result generally includes: 1) temperature distribution as a function of time; 2) temperature shortly after welding process; 3) temperature distribution after cooling; 4) Von Mises stress configuration as a function of time; 4) residual stress as a function of time; 5) stress intensity factor along the crack front; 5) total stress configuration; 6) displacement configuration.

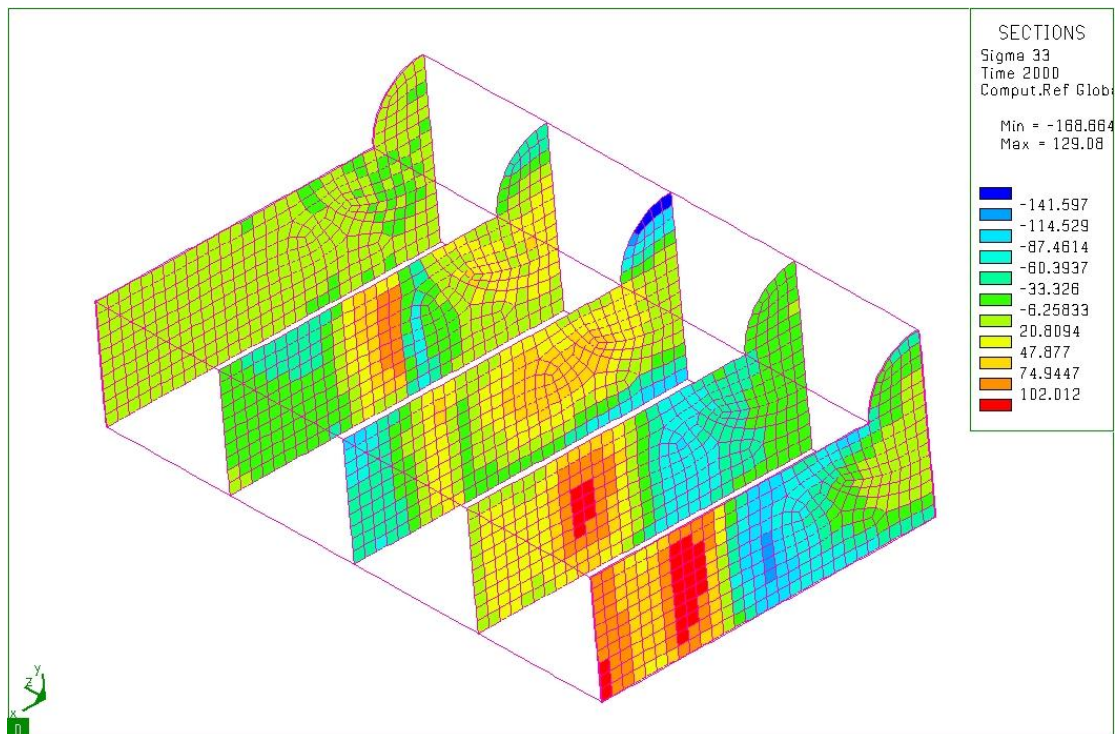
### **1. General mesh for large front case**

Figure 5.1 shows the temperature distribution in five cross-section views perpendicular to the welding direction. The geometry is described in chapter 2.2. In this model the crack front is represented by a part of a  $60^\circ$  arc whose radius is 12 mm. The welding parameters are described in Chapter 3.1, 3.2 and 3.3. Temperatures on elements along the crack front after cooling are compared in Figure 5.3. Residual stress distributions can be found in Figure 5.4, where five cross-section views are selected along the fusion welding direction to represent the global  $\sigma_{33}$  configuration results from the fusion welding process after the part has cooled down. It should be noted that the part is still full clamped in these images. Figure 5.5(1) shows the total  $\sigma_{33}$  configuration after superposition of welding stress output and FRAC3D analysis.

In Figure 5.12 and Figure 5.13, the final stress  $\sigma_{33}$  in zz direction is comparatively higher along the crack front line in the zone between  $15^\circ < \theta < 48^\circ$ .



**Figure 5.2** Temperature distribution after fusion welding (time=2000second)



**Figure 5.3** Residual stress distribution after fusion welding (time=2000second)

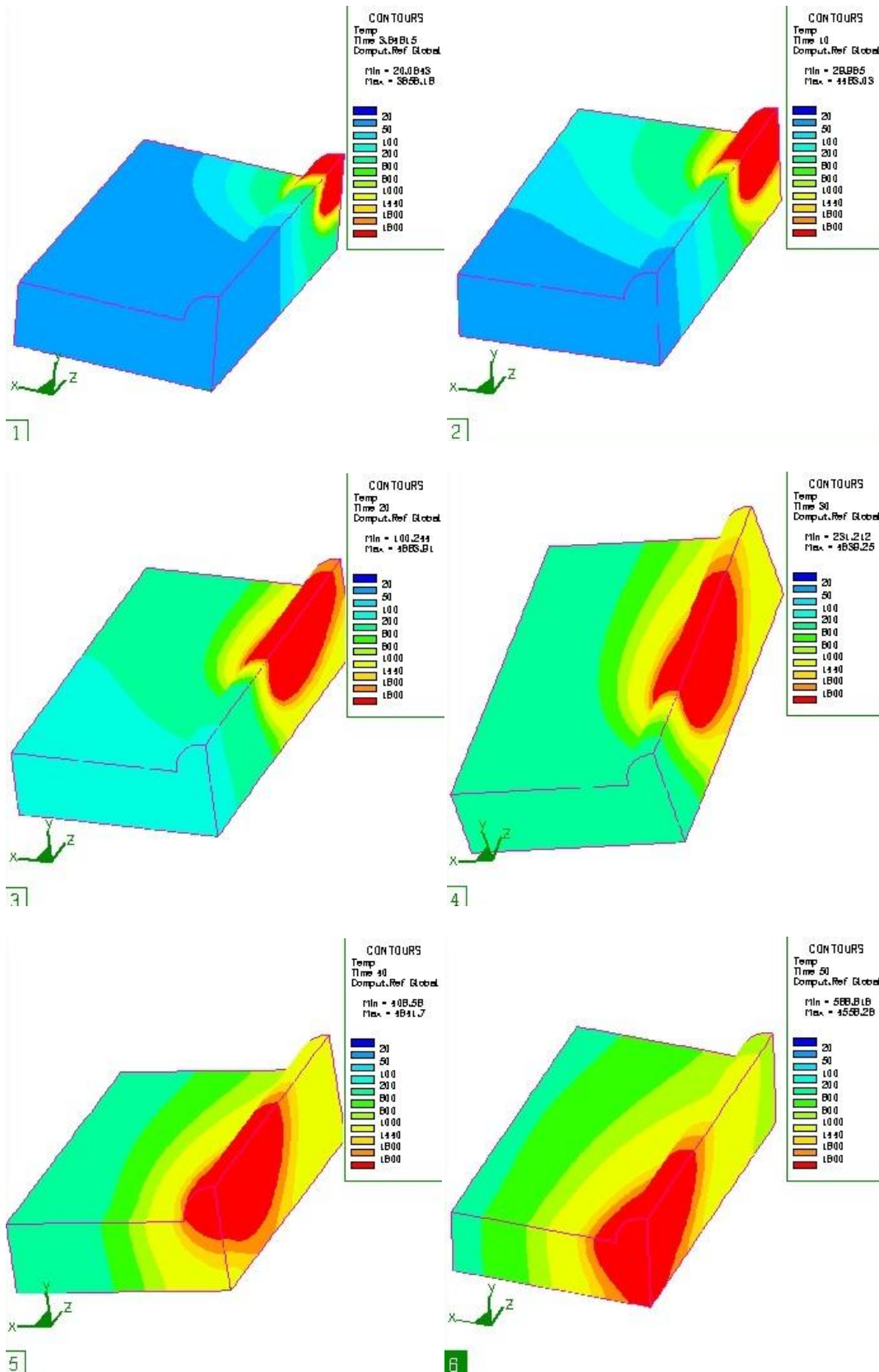


**Figure 5.4** Temperature distributions during welding process. (1)  $t=5$ ; (2)  $t=10$ ; (3)  $t=20$ ; (4)  $t=30$ ; (5)  $t=40$ ; (6)  $t=50$ .



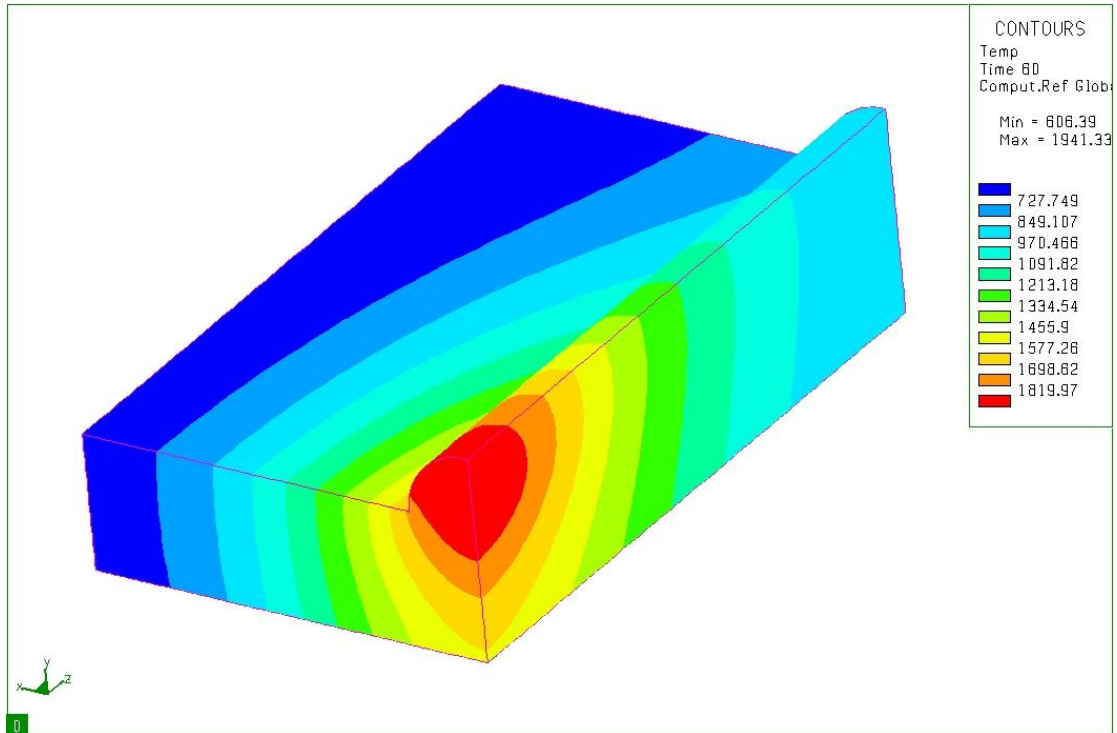


Figure 5.5 Temperature distributions after welding(time=50s)

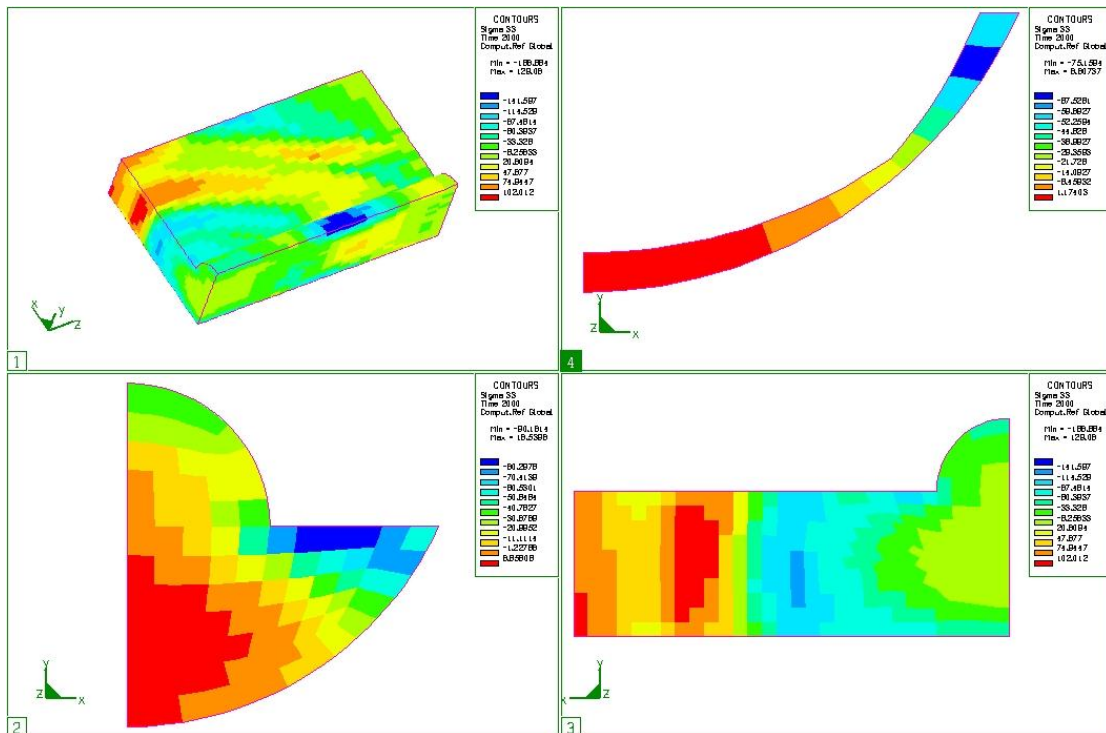
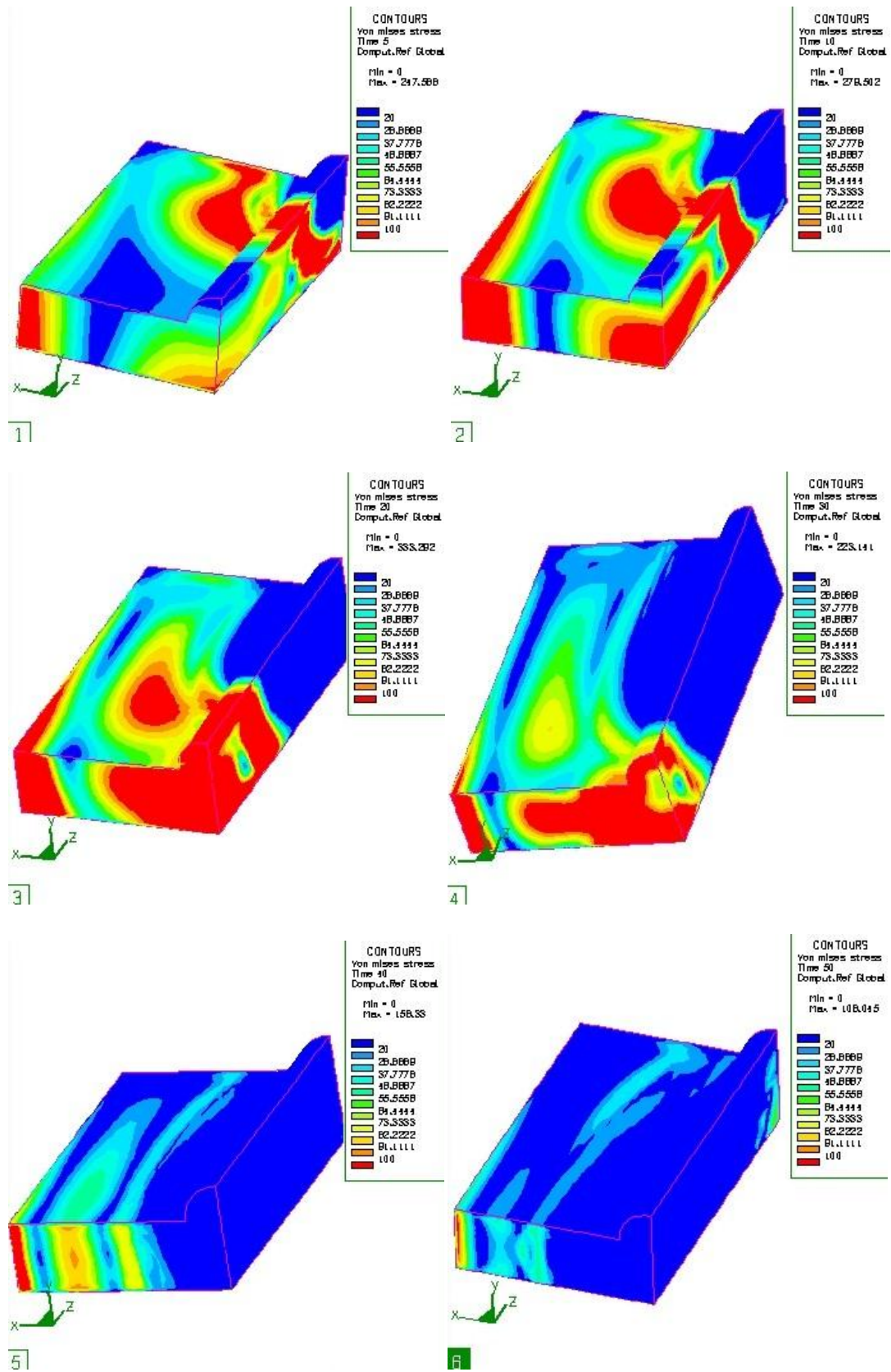


Figure 5.6  $\sigma_{33}$  configurations. (1)  $\sigma_{33}$  of the whole welding plate (2) Residual stress

$\sigma_{33}$  in crack surface after fusion welding (3) Cross view of  $\sigma_{33}$  in plane of crack

surface (4)  $\sigma_{33}$  along the crack front.



**Figure 5.7** Von Mises stress distributions during welding process. (1)  $t=5$ ; (2)  $t=10$ ; (3)  $t=20$ ; (4)  $t=30$ ; (5)  $t=40$ ; (6)  $t=50$ .

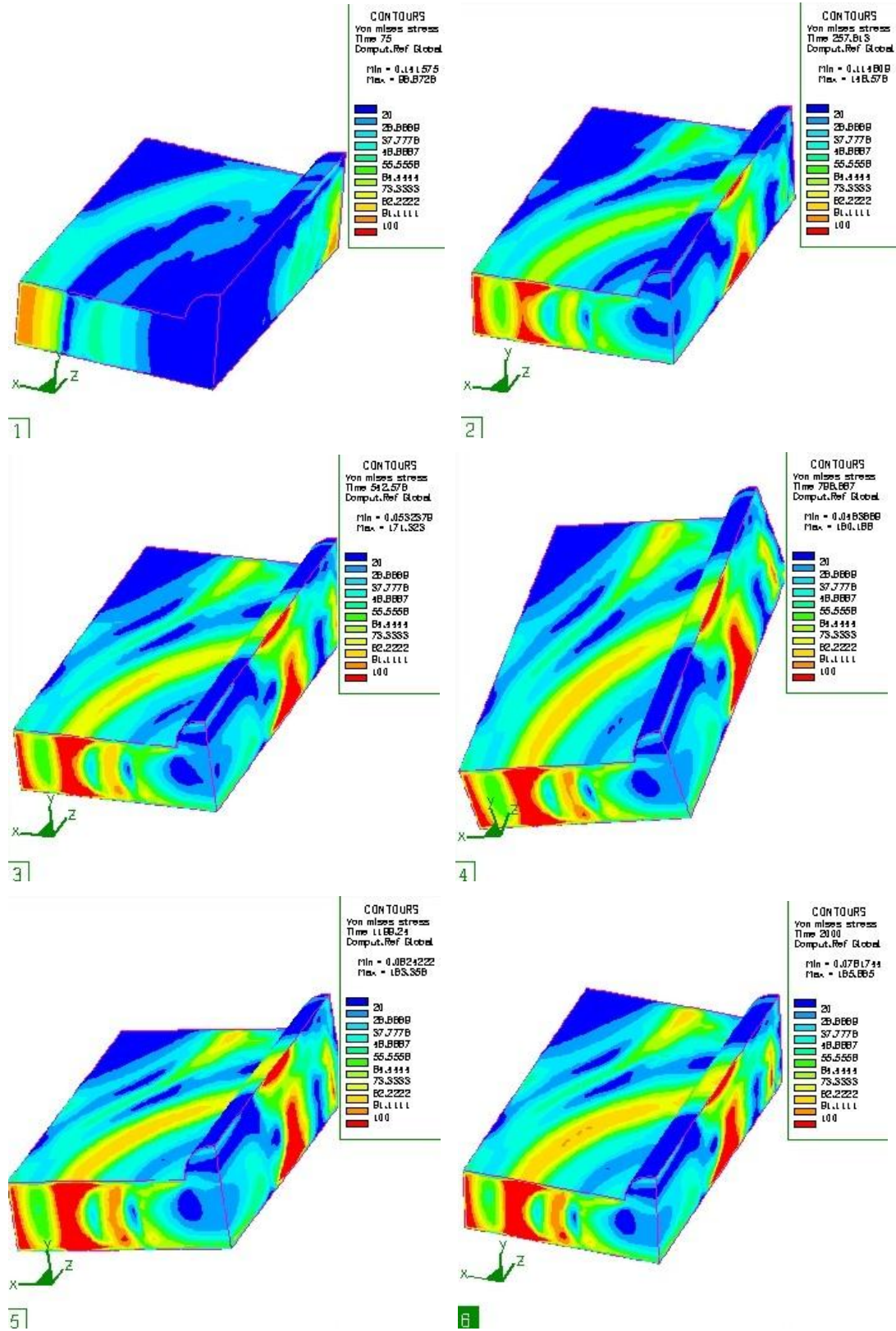


**Figure 5.8** Von Mises stress distributions during cooling process. (1)  $t=75$ ; (2)  $t=257$ ; (3)  $t=542$ ; (4)  $t=1183$ ; (5)  $t=1788$ ; (6)  $t=2000$ .



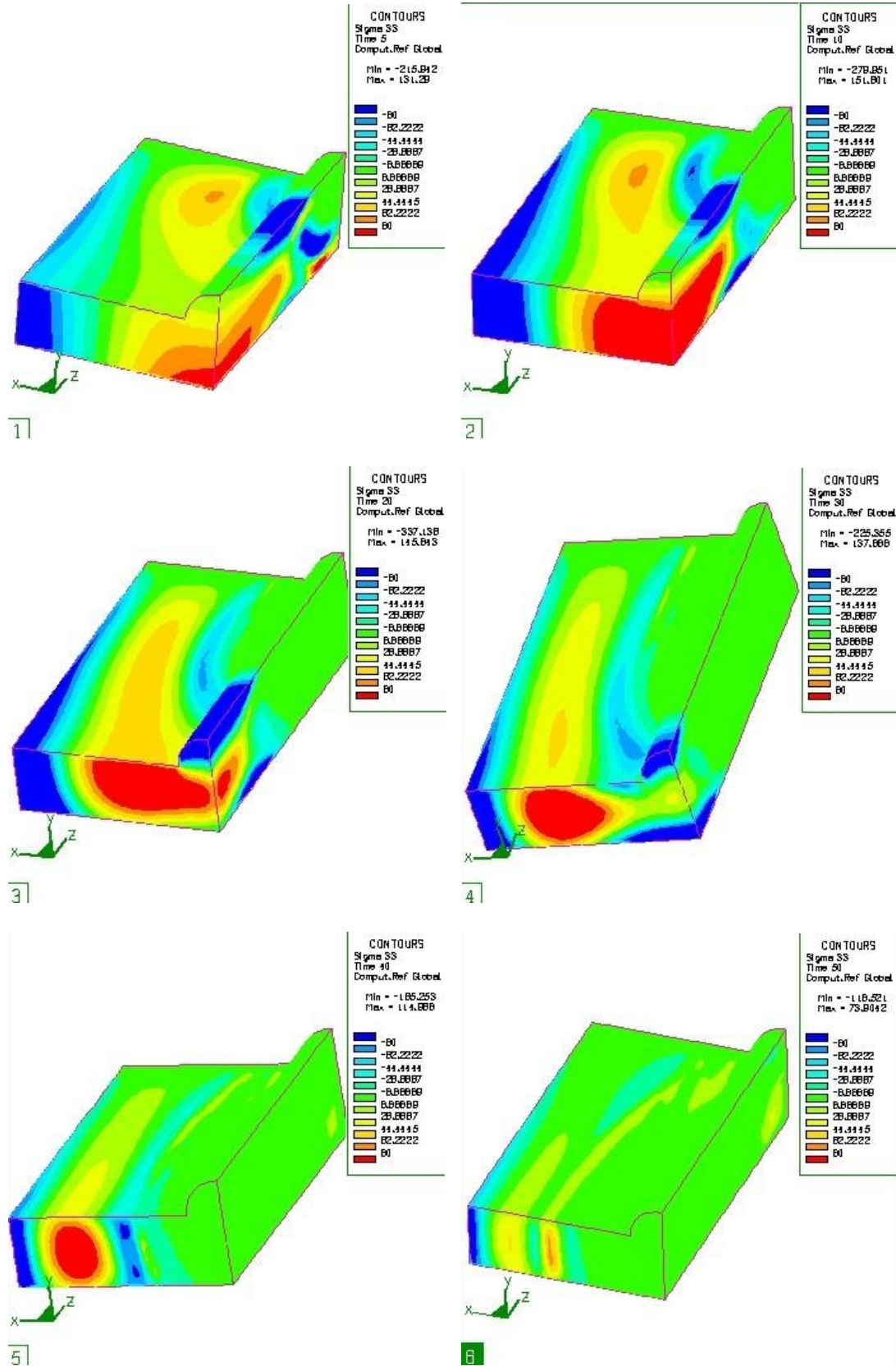


**Figure 5.9** Residual stress  $\sigma_{33}$  distributions during welding process. (1) t=5; (2) t=10;

(3) t=20; (4) t=30; (5) t=40; (6) t=50.

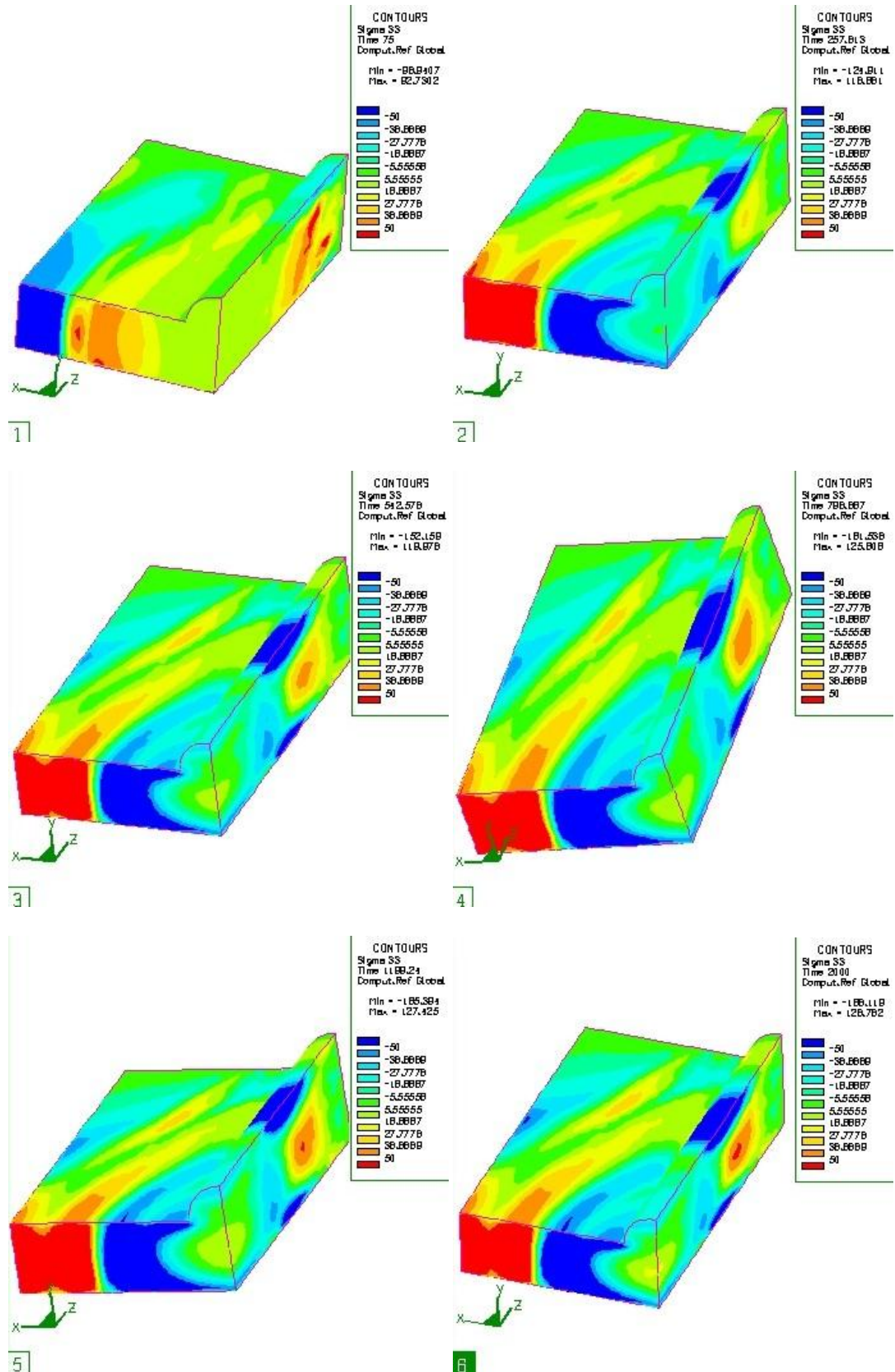


**Figure 5.10** Residual stress  $\sigma_{33}$  distributions during cooling process. (1)  $t=75$ ; (2)

$t=257$ ; (3)  $t=542$ ; (4)  $t=1183$ ; (5)  $t=1788$ ; (6)  $t=2000$ .

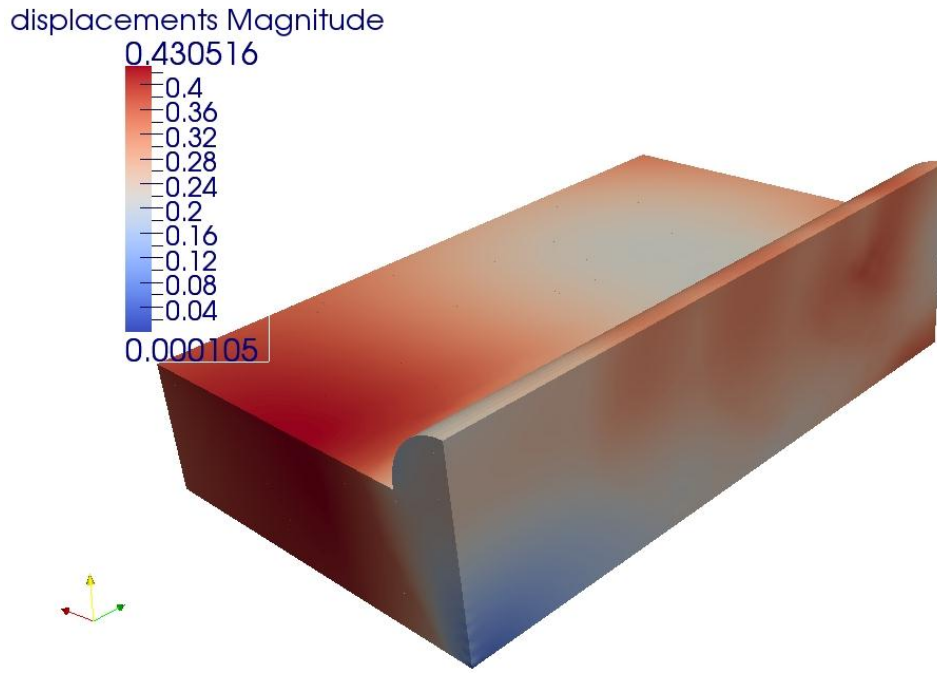


**Figure 5.11** Displacements Magnitude

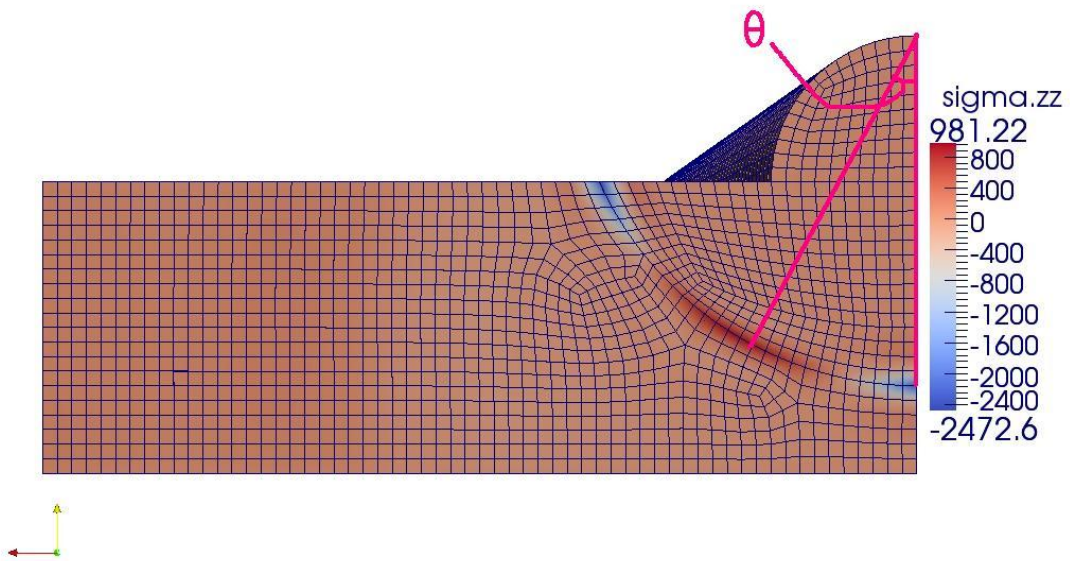


**Figure 5.12** Total stress configurations in direction of zz axial

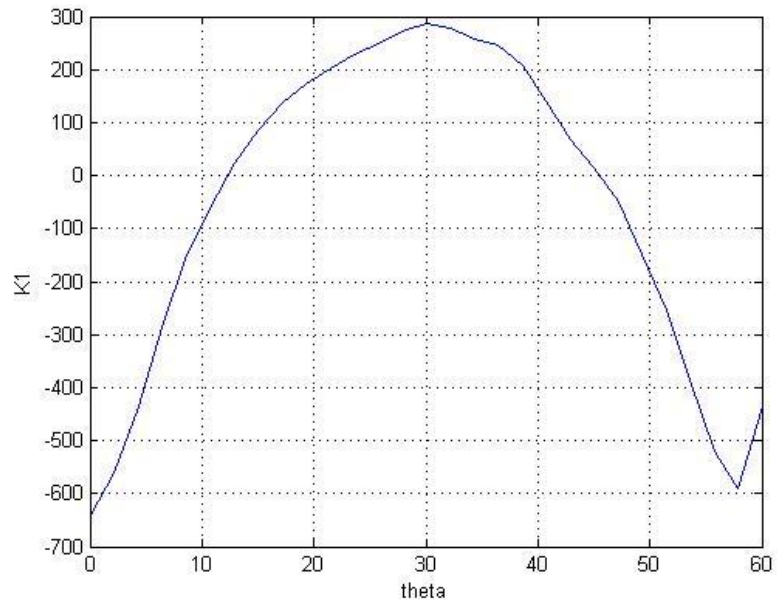


**Figure 5.13** Stress Intensity factor ( $\text{Mpa}/\sqrt{\text{m}}$ )



## 2 finer mesh case

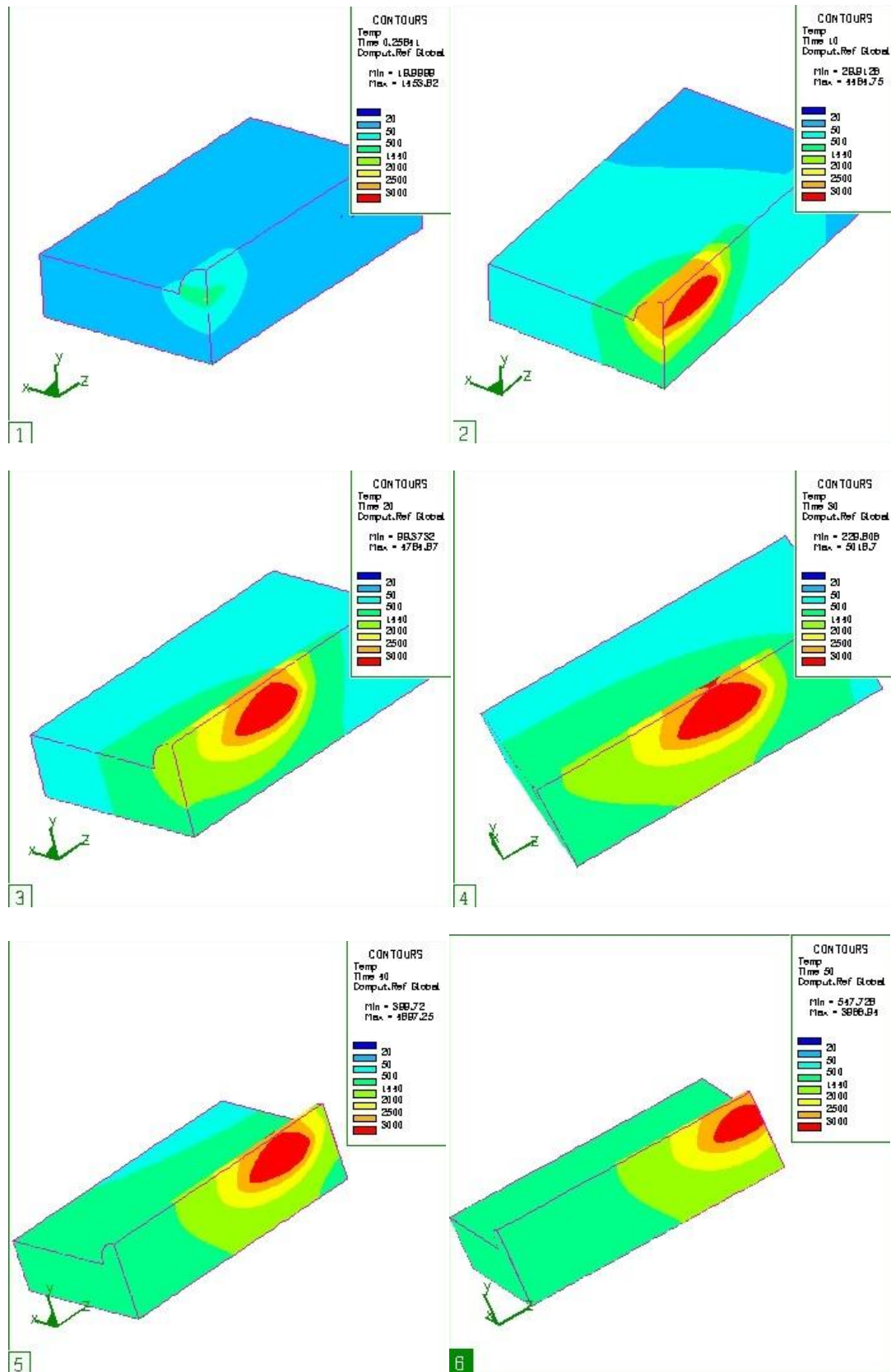


**Figure 5.14** Temperature distributions during welding process. (1)  $t=5$ ; (2)  $t=10$ ; (3)  $t=20$ ; (4)  $t=30$ ; (5)  $t=40$ ; (6)  $t=50$ .



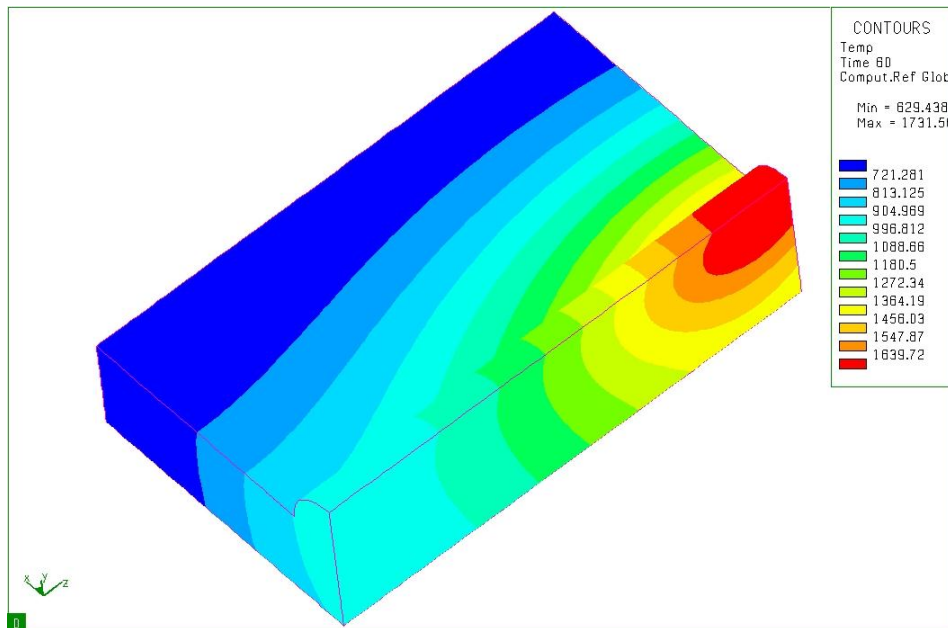


**Figure 5.15** Temperature distributions after welding(time=50s)

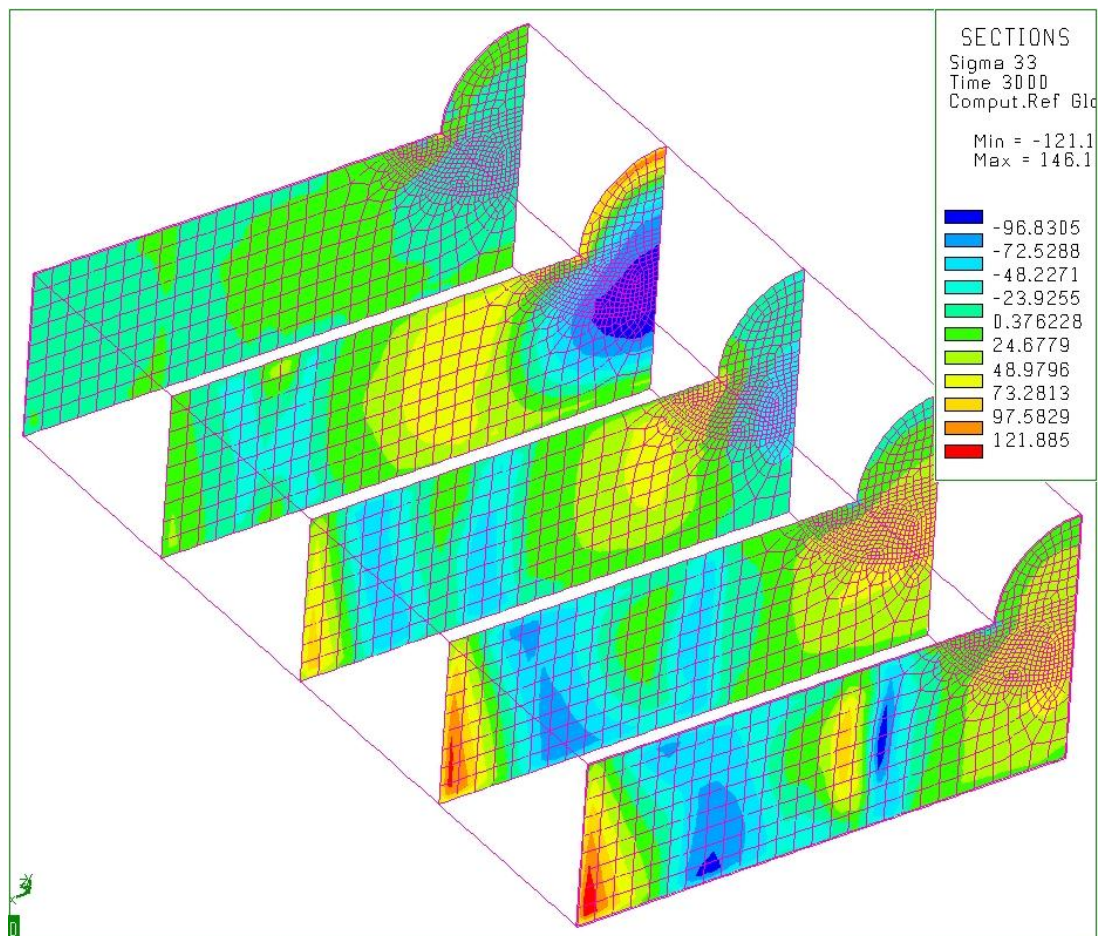


**Figure 5.16** Residual stresses distribution after fusion welding for finer mesh case

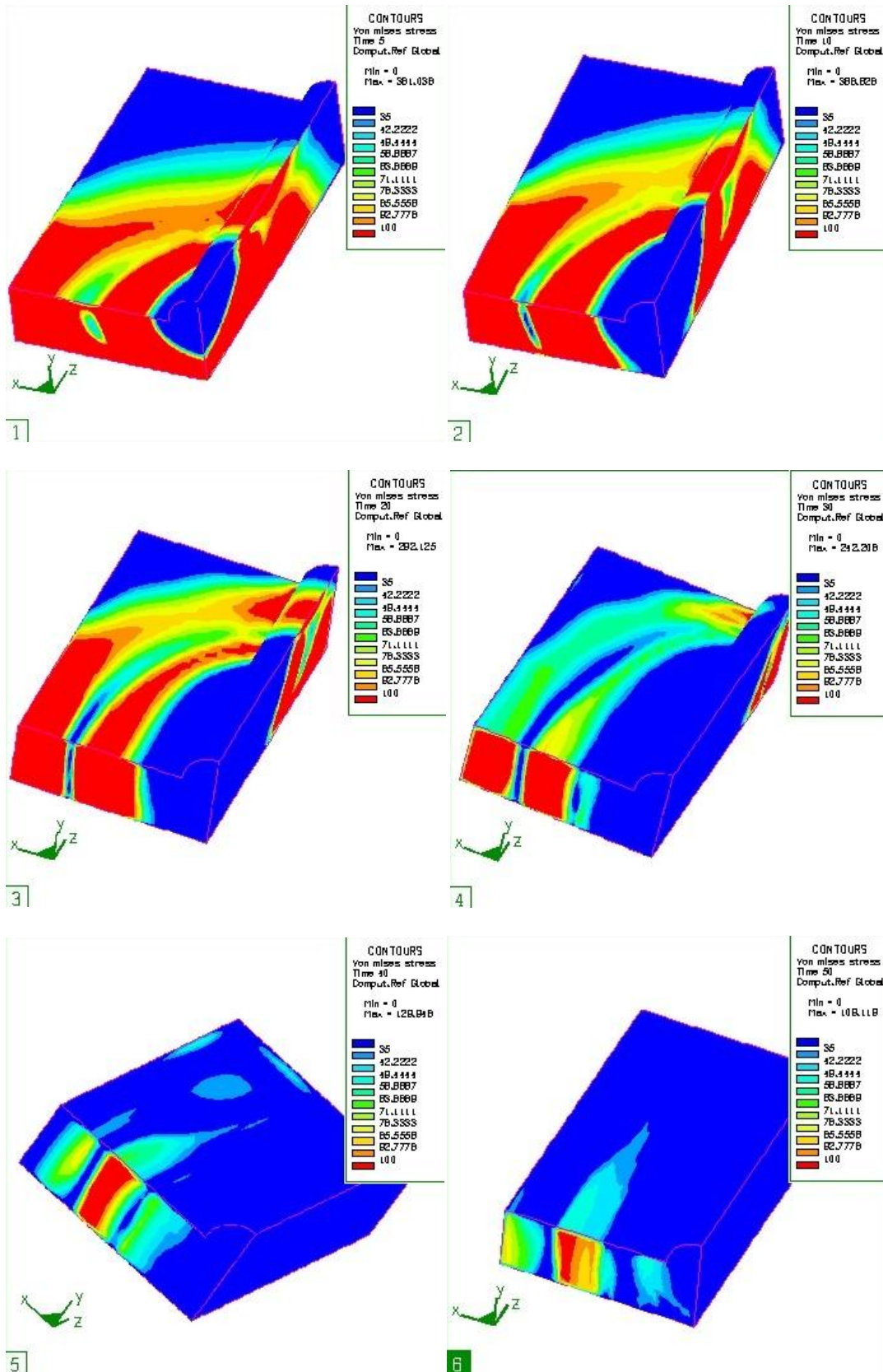


**Figure 5.17** Von Mises stress distributions during welding process. (1)  $t=5$ ; (2)  $t=10$ ;

(3)  $t=20$ ; (4)  $t=30$ ; (5)  $t=40$ ; (6)  $t=50$ .

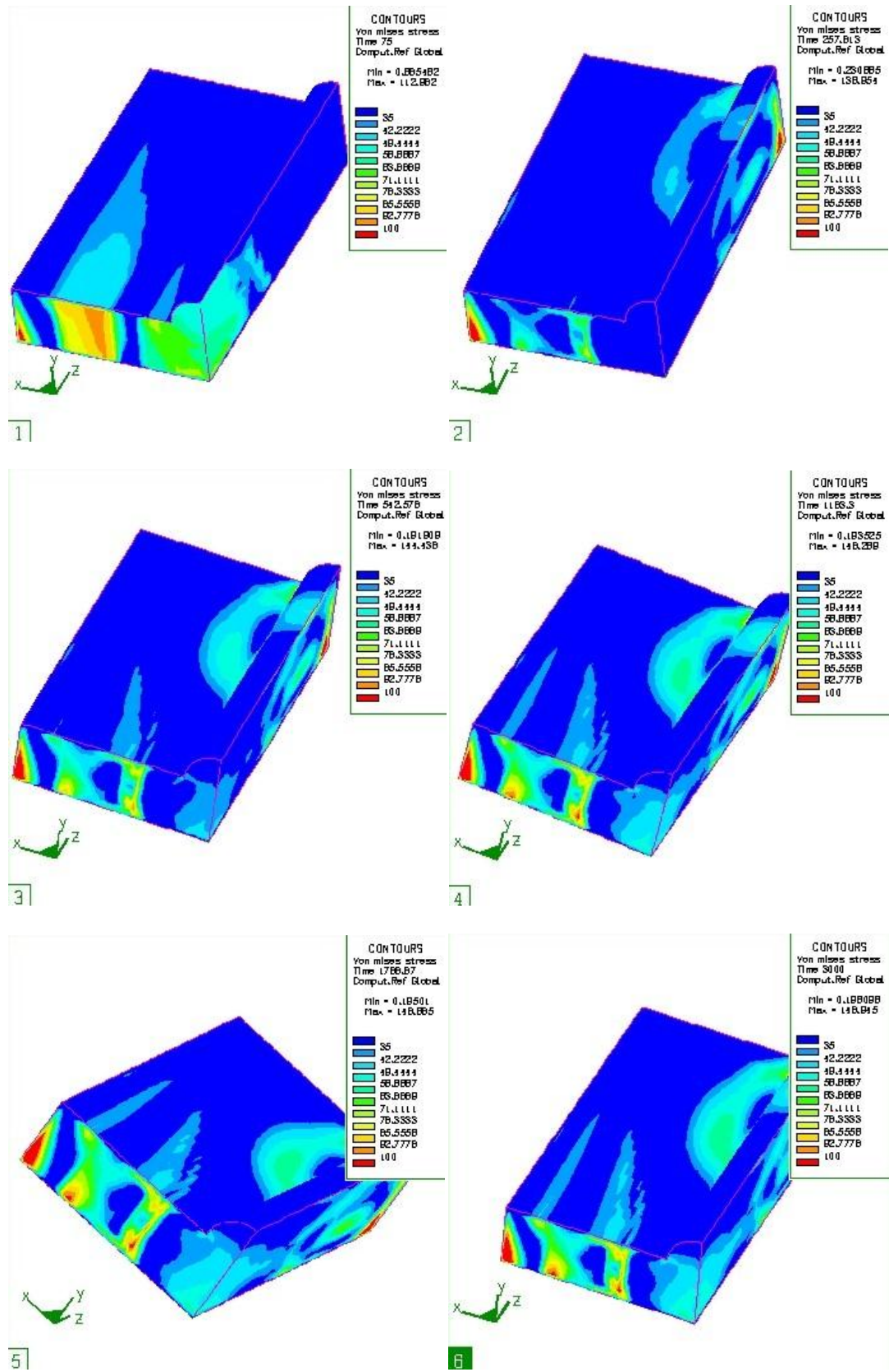


**Figure 5.18** Von Mises stress distributions during cooling process. (1)  $t=75$ ; (2)  $t=257$ ;

(3)  $t=542$ ; (4)  $t=1183$ ; (5)  $t=1788$ ; (6)  $t=3000$ .



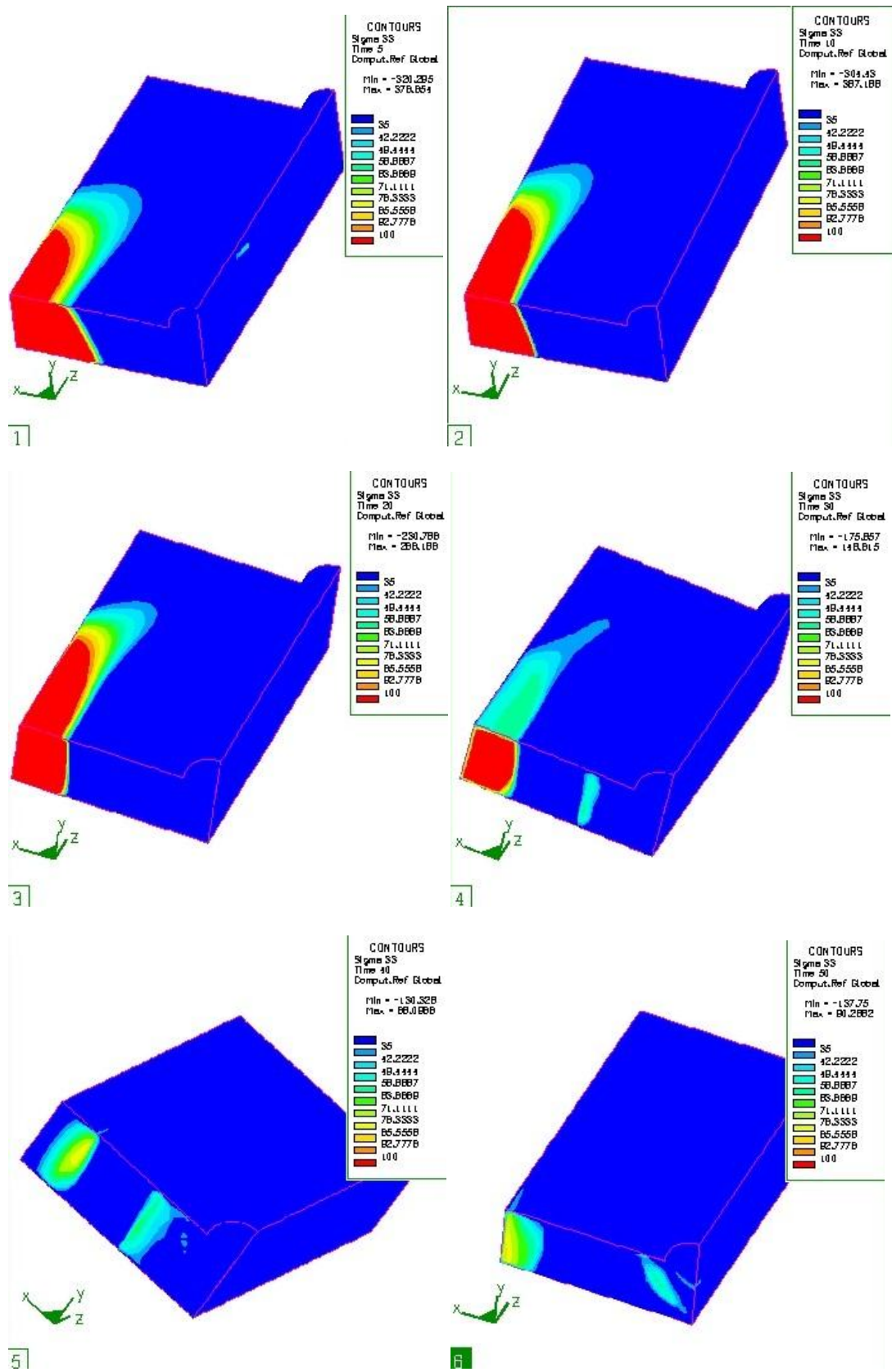


**Figure 5.19** Residual stress  $\sigma_{33}$  distributions during welding process. (1) t=5; (2)

t=10; (3) t=20; (4) t=30; (5) t=40; (6) t=50.

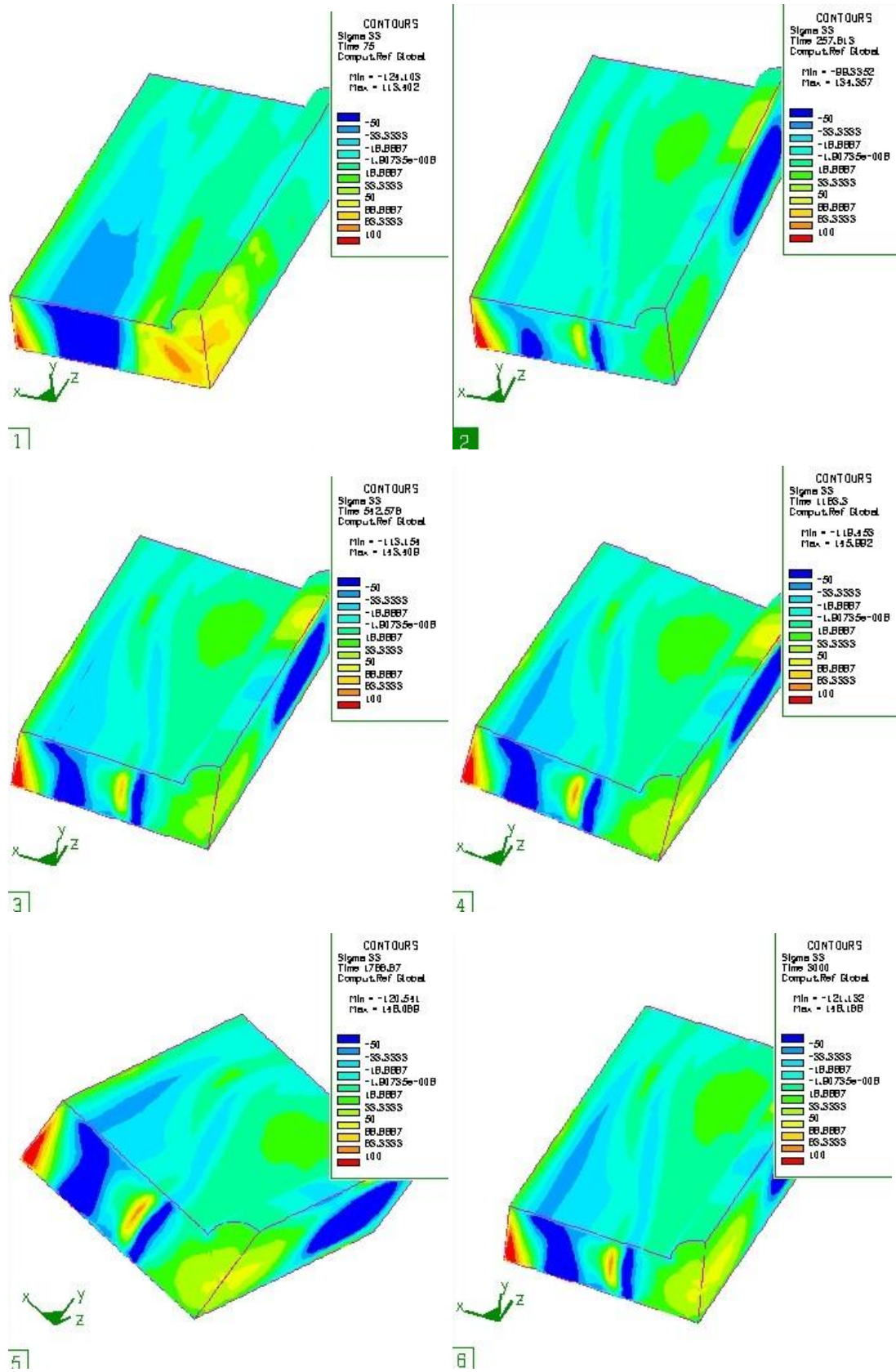


**Figure 5.20** Residual stress  $\sigma_{33}$  distributions during cooling process. (1)  $t=75$ ; (2)  $t=257$ ; (3)  $t=542$ ; (4)  $t=1183$ ; (5)  $t=1788$ ; (6)  $t=3000$ .

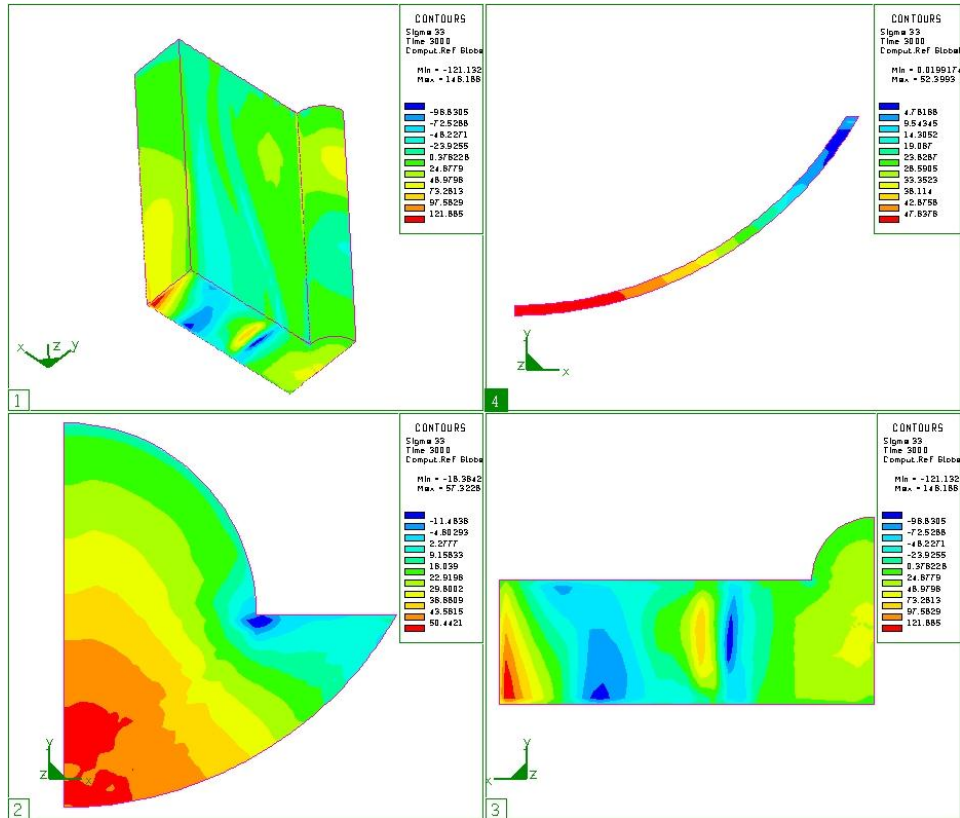


**Figure 5.21**  $\sigma_{33}$  configuration for finer mesh case. (1)  $\sigma_{33}$  of the whole welding plate. (2) Residual stress  $\sigma_{33}$  in crack surface after fusion welding (3) Cross view of  $\sigma_{33}$  in plane of crack surface. (4)  $\sigma_{33}$  along the crack front.

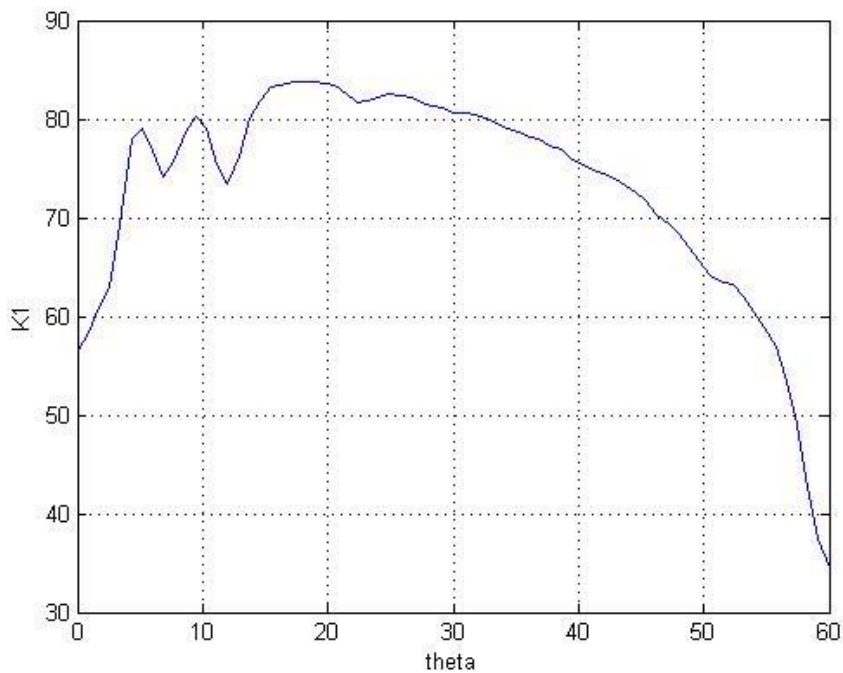


**Figure 5.22** Stress intensity factor  $k_1$  ( $\text{Mpa}/\sqrt{\text{m}}$ )

### 3 coarser mesh case

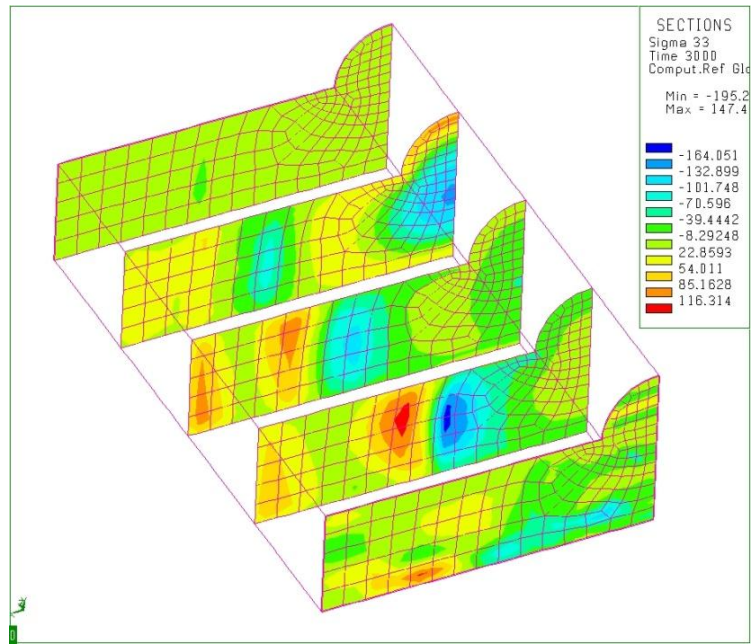


**Figure 5.23** Residual stresses distribution after fusion welding for coarser mesh case

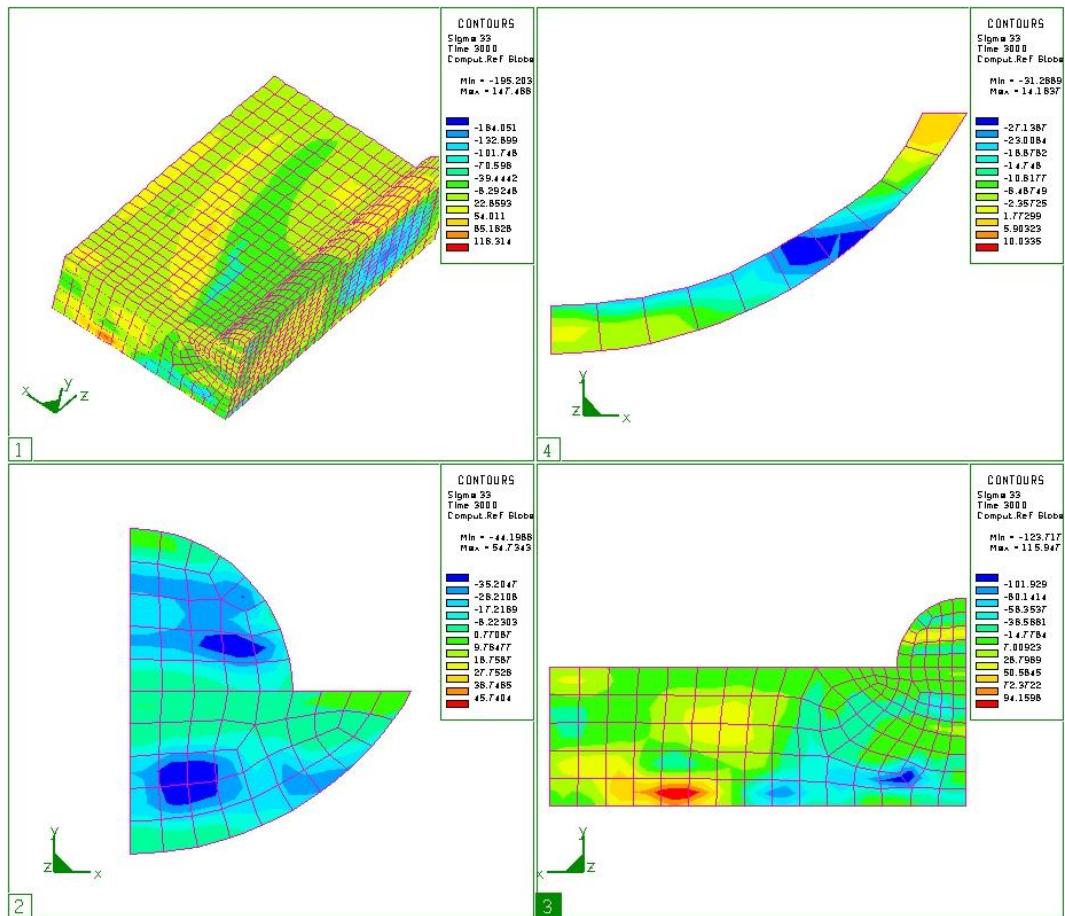


**Figure 5.24**  $\sigma_{33}$  configuration for coarser mesh case. (1)  $\sigma_{33}$  of the whole welding plate. (2) Residual stress  $\sigma_{33}$  in crack surface after fusion welding. (3) Cross view of  $\sigma_{33}$  in plane of crack surface. (4)  $\sigma_{33}$  along the crack front.



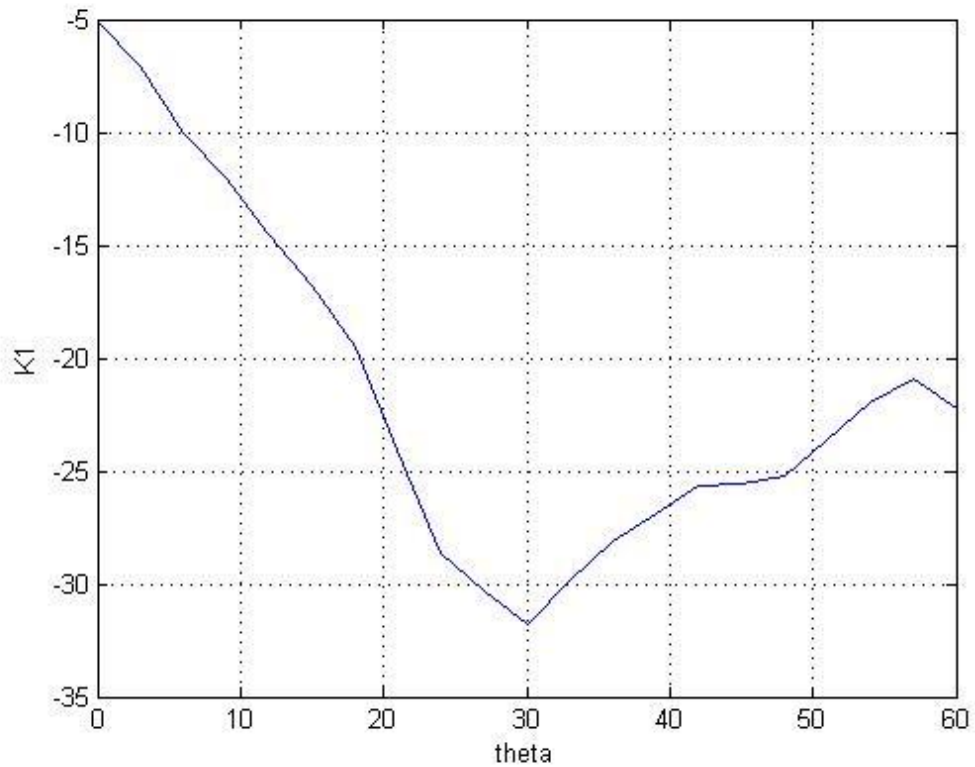


**Figure 5.25** Stress intensity factor  $k_1$  (Mpa/√m).

Section two and section one use the same geometry which is described in Chapter2, section2. Compare figure 5.24 and 5.23, the residual stress exported from fusion welding simulation is sensitive to mesh density. Figure 5.22 uses finer mesh along the crack front and the heat source path, thus the residual stress is positive which means the crack will be extravagant. The reason why Figure 5.25 is negative is probably that the element density and welding run time is not high enough. Negative SIF is a compressive state of stress that is a result of prevent the material from expanding.



#### 4 refined small front mesh case

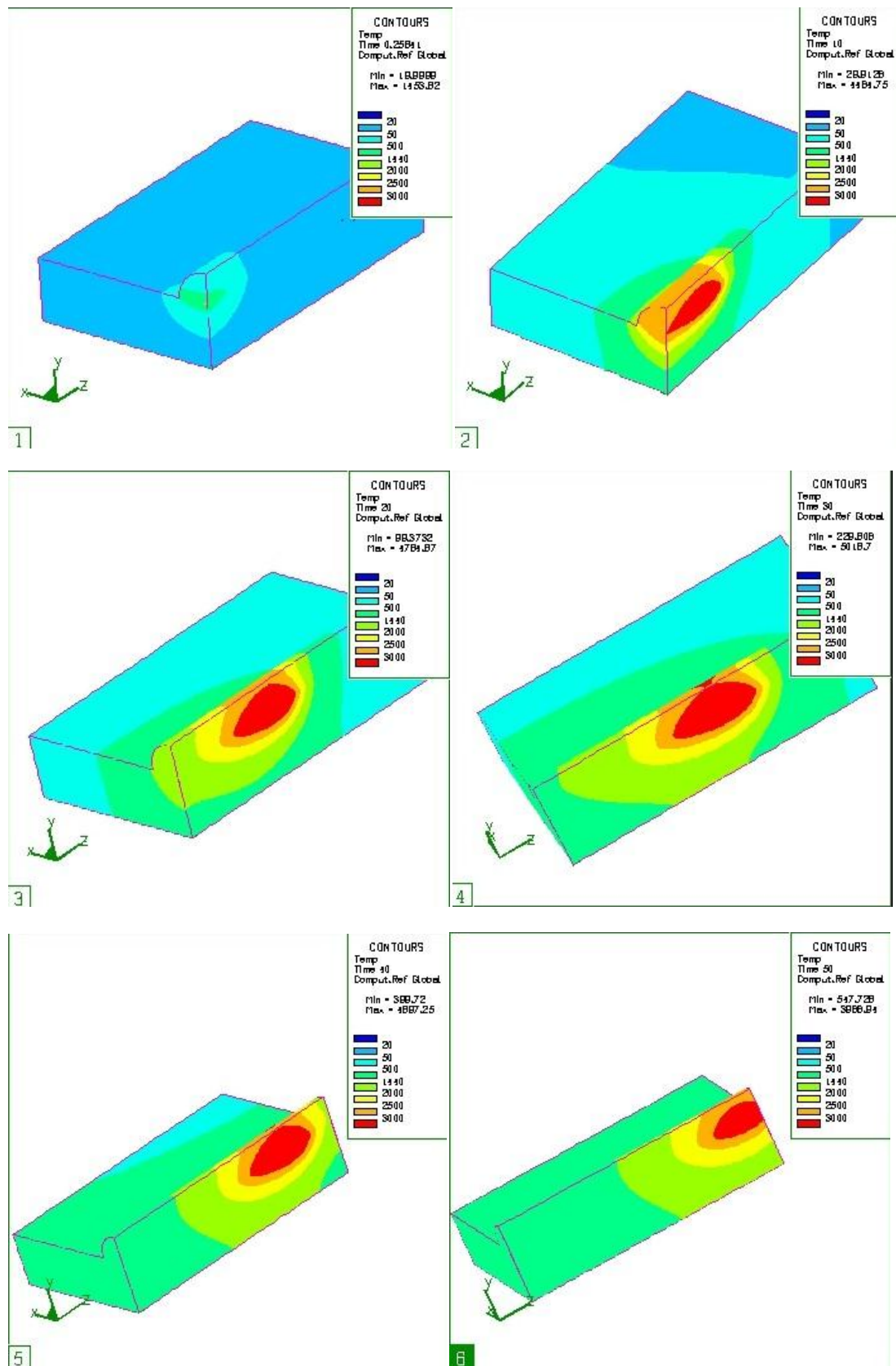


**Figure 5. 26** Temperature distributions during welding process. (1)  $t=5$ ; (2)  $t=10$ ; (3)  $t=20$ ; (4)  $t=30$ ; (5)  $t=40$ ; (6)  $t=50$ .

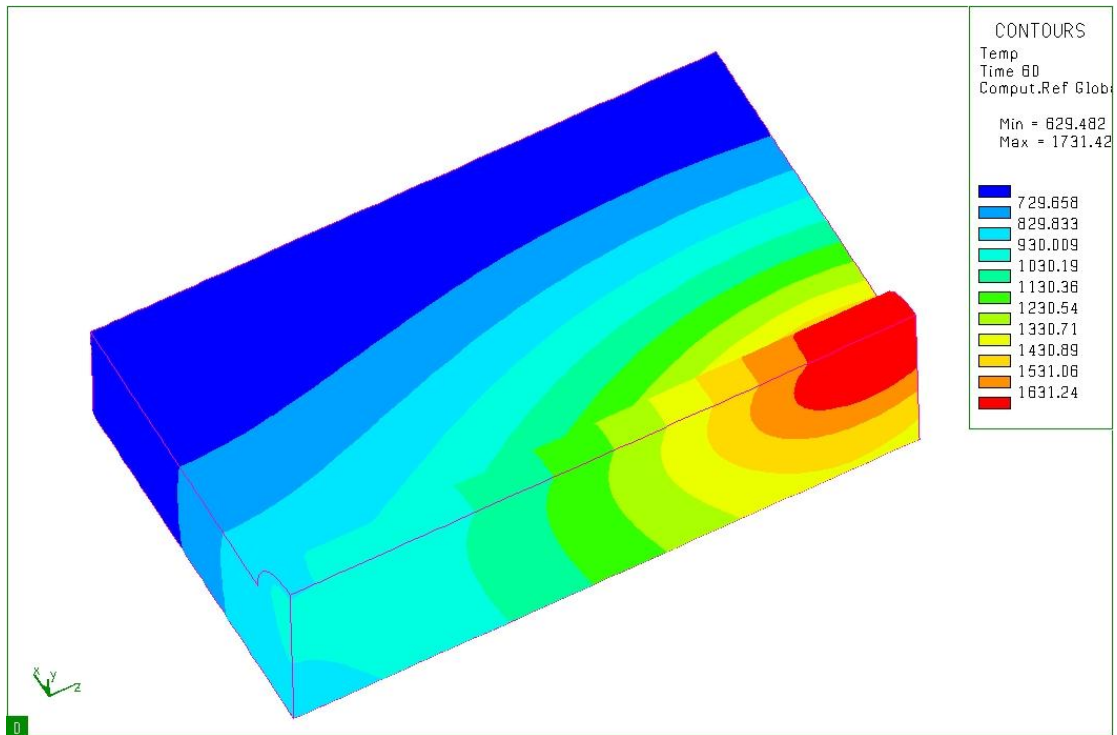


**Figure 5.27** Temperature distributions after welding(time=50s)

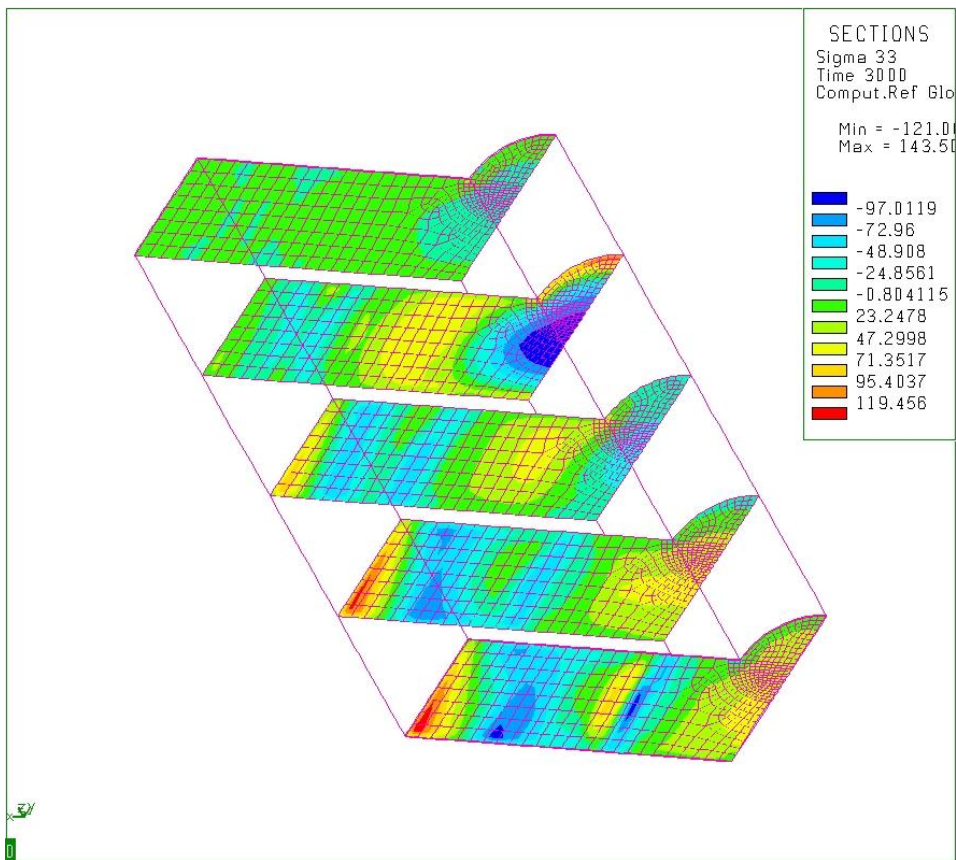


**Figure 5.28** Residual stresses distribution after cooling for smaller front (t=3000s)

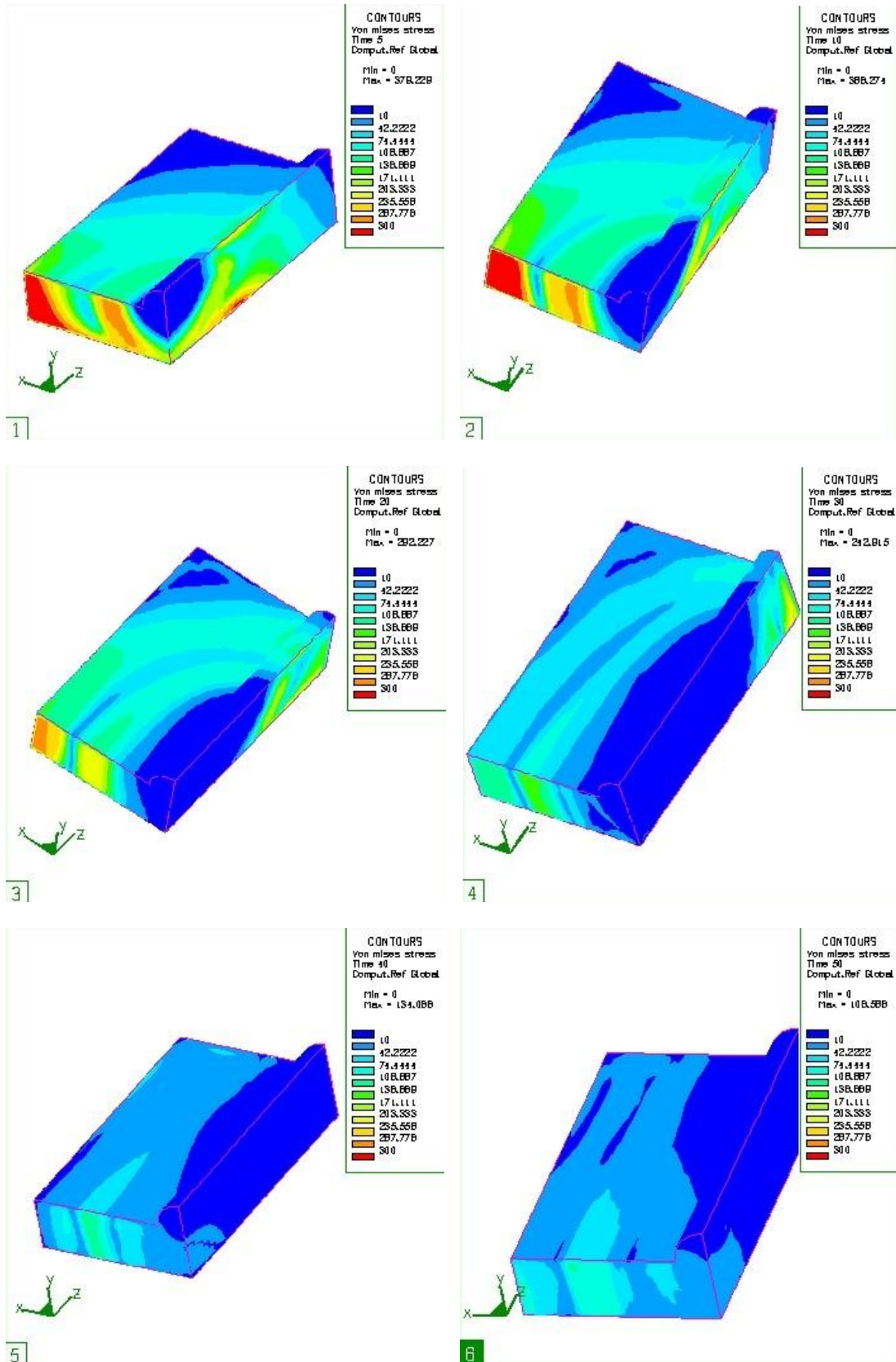


**Figure 5.29** Von Mises stress distributions during welding process. (1)  $t=5$ ; (2)  $t=10$ ;

(3)  $t=20$ ; (4)  $t=30$ ; (5)  $t=40$ ; (6)  $t=50$ .

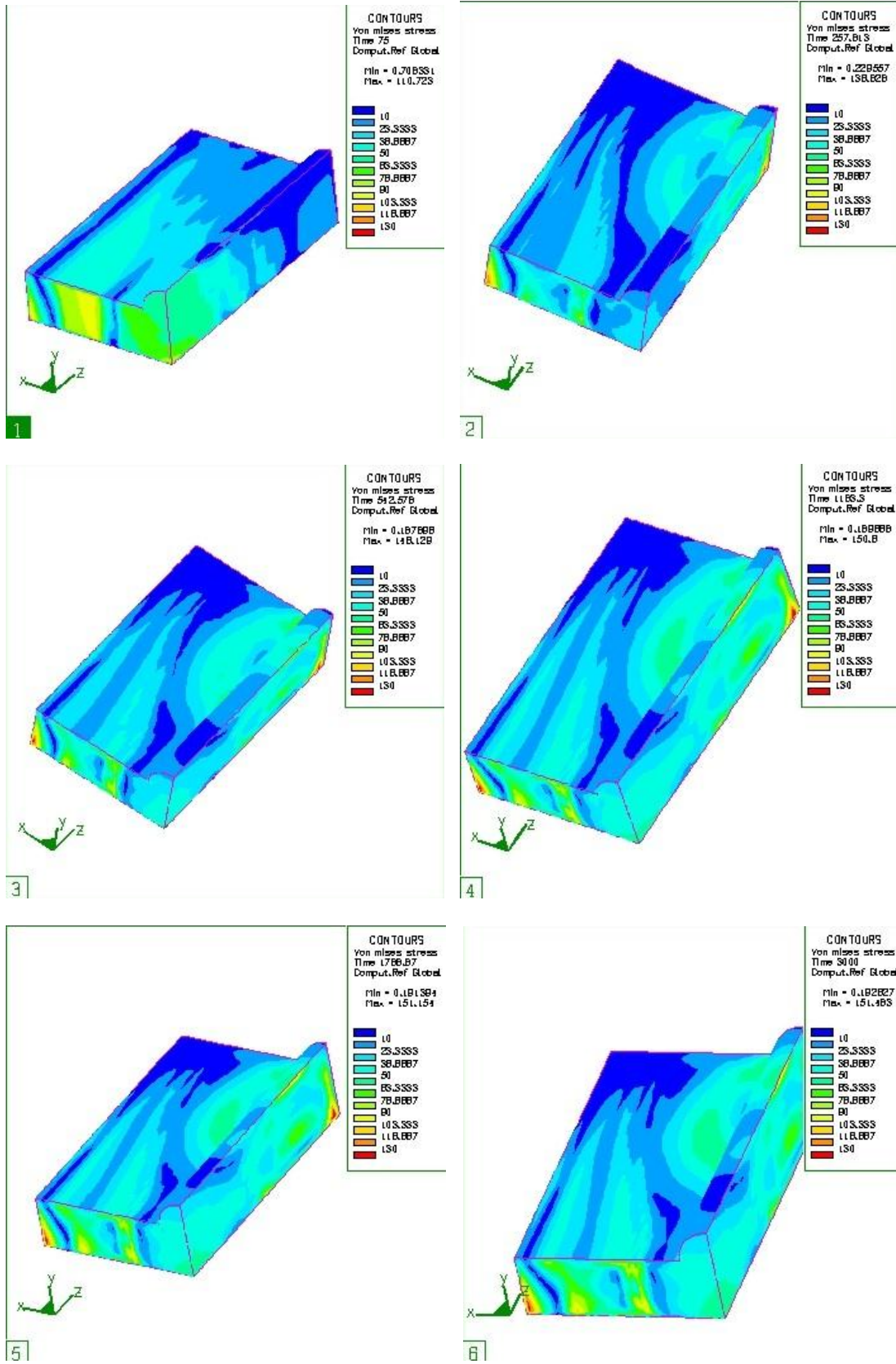


**Figure 5.30** Von Mises stress distributions during cooling process. (1)  $t=75$ ; (2)  $t=257$ ;  
 (3)  $t=542$ ; (4)  $t=1183$ ; (5)  $t=1788$ ; (6)  $t=3000$ .



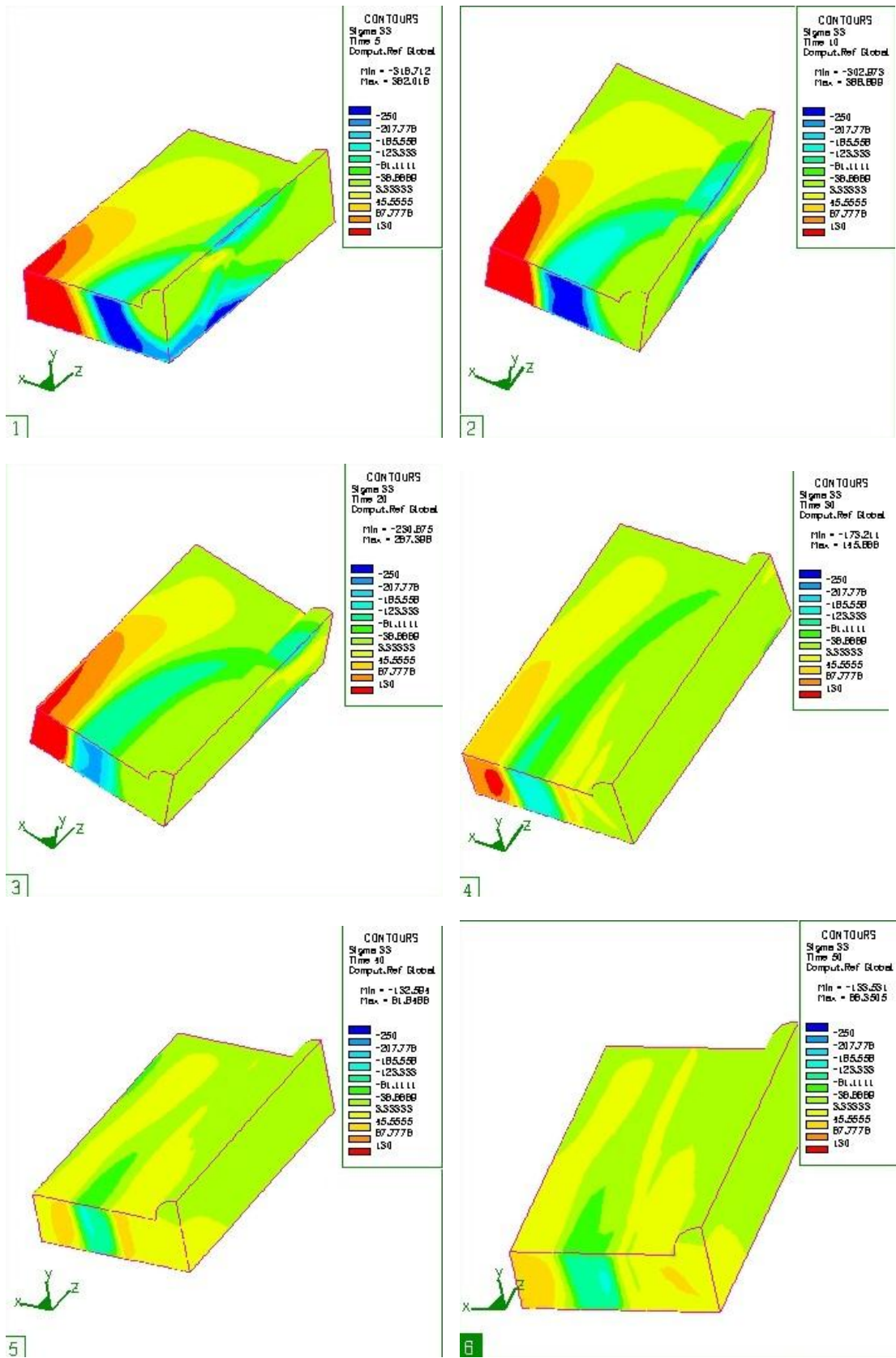


**Figure 5.31** Residual stress  $\sigma_{33}$  distributions during welding process. (1)  $t=5$ ; (2)  $t=10$ ; (3)  $t=20$ ; (4)  $t=30$ ; (5)  $t=40$ ; (6)  $t=50$ .

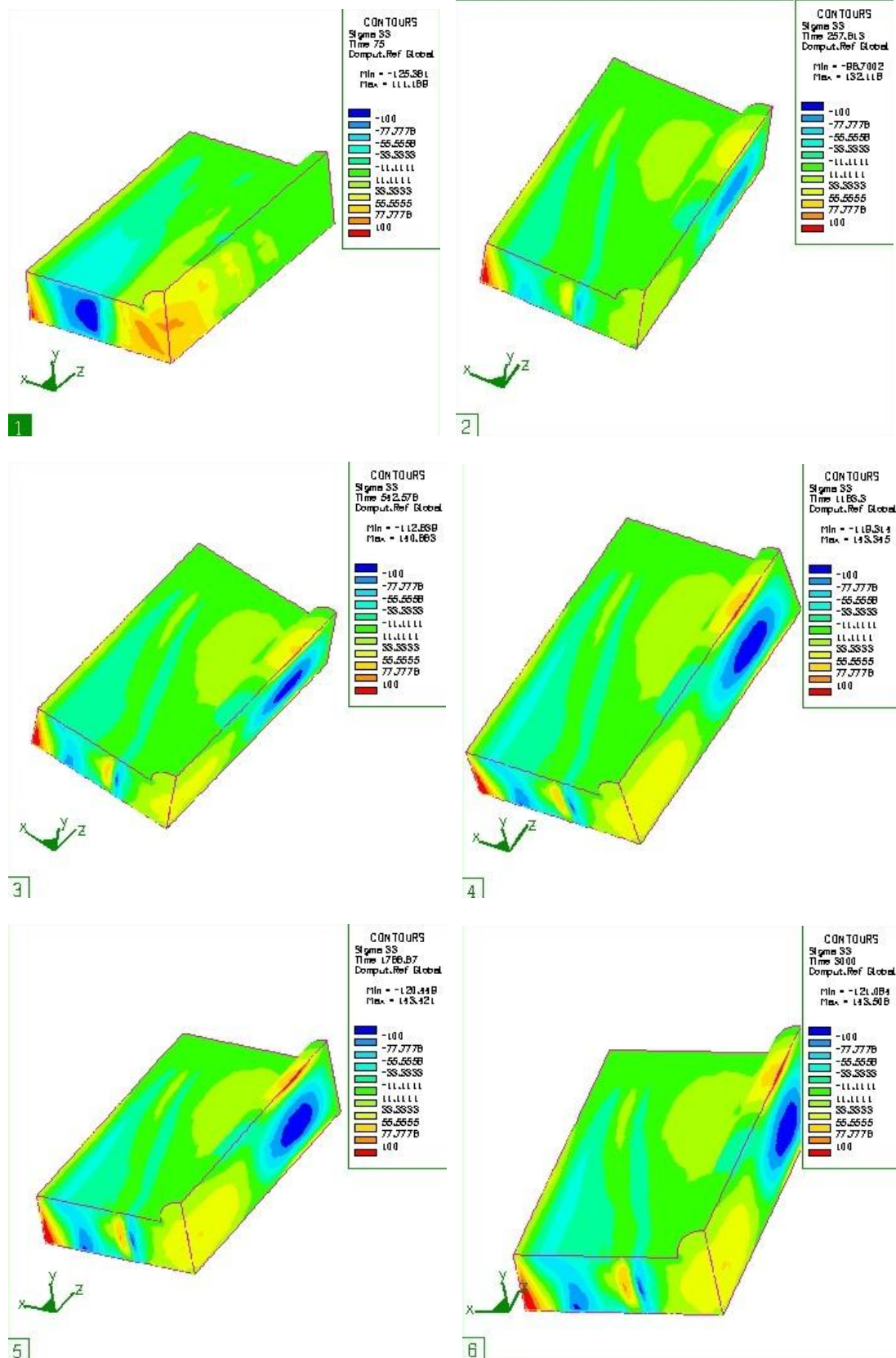


**Figure 5.32** Residual stress  $\sigma_{33}$  distributions during cooling process. (1)  $t=75$ ; (2)  $t=257$ ; (3)  $t=542$ ; (4)  $t=1183$ ; (5)  $t=1788$ ; (6)  $t=3000$ .

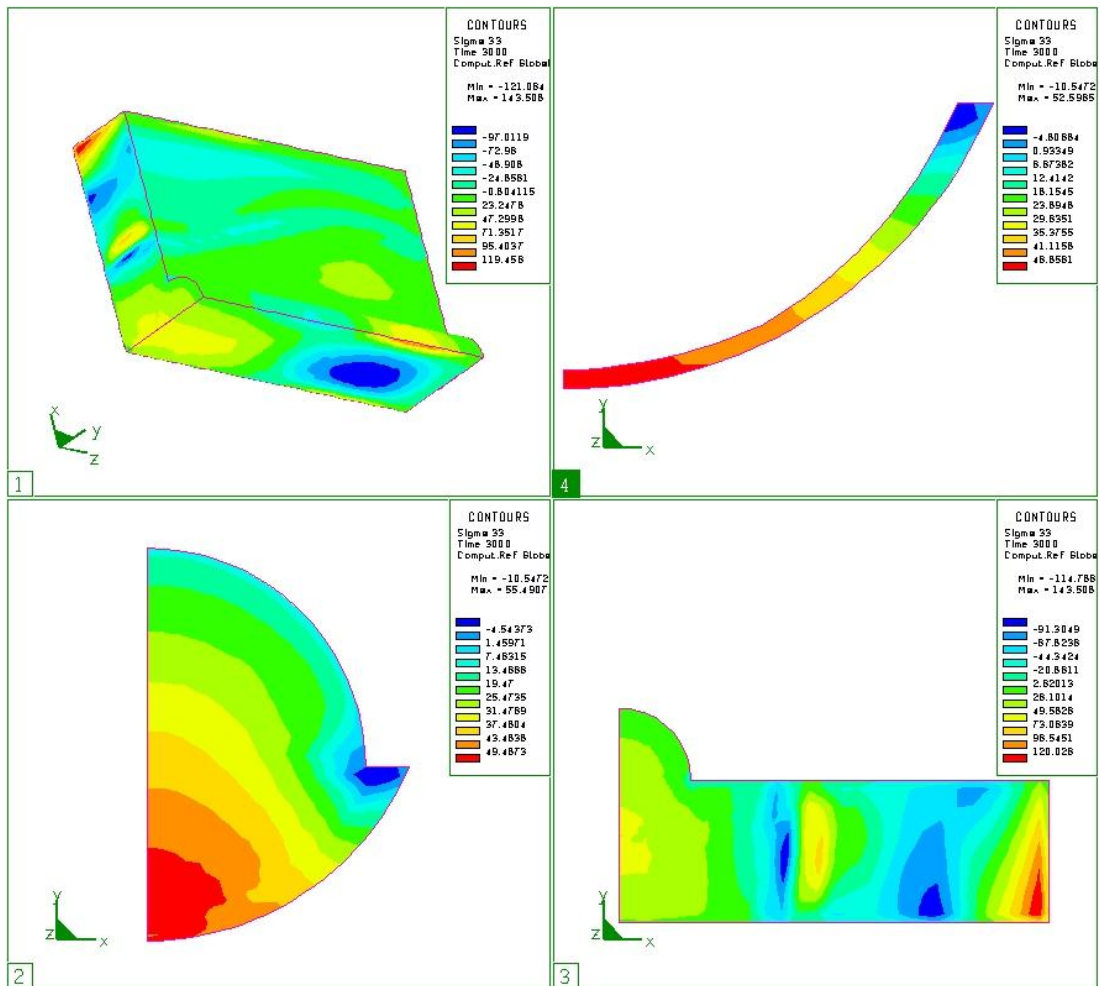


**Figure 5.33**  $\sigma_{33}$  configuration after cooling for smaller front case. (1)  $\sigma_{33}$  of the whole welding plate after cooling. (2) Residual stress  $\sigma_{33}$  in crack surface after cooling. (3) Cross view of  $\sigma_{33}$  in plane of crack surface after cooling. (4)  $\sigma_{33}$  along the crack front after cooling.

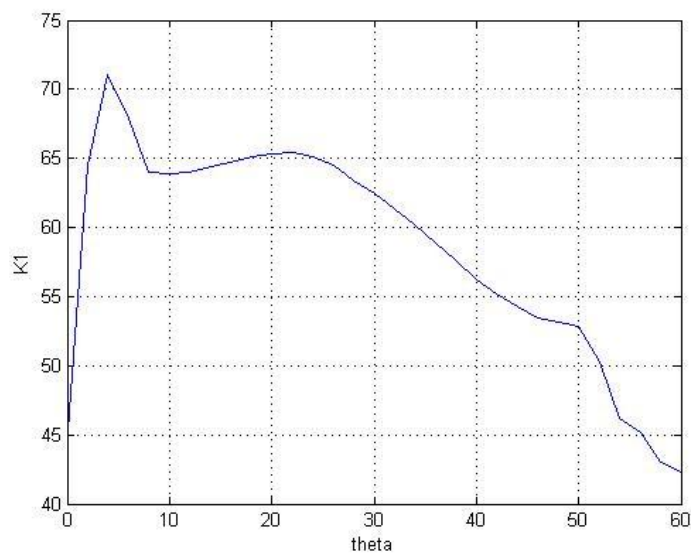


**Figure 5.34** Stress intensity factor  $k_1$  (Mpa/ $\sqrt{m}$ ).

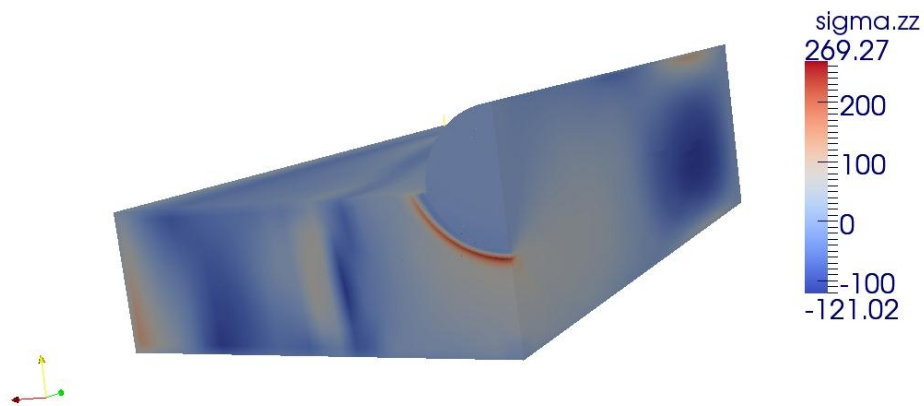


**Figure 5.35** Total stress  $\sigma_{33}$  configurations in direction of zz axial

The total superposed stress component (Figure 5.17) is in the zz axial direction.

In this picture, there are very low stresses everywhere, but along the crack front. Thus, in this simulation, welding process will increase the tendency of crack.

## 5 Conclusion

The results of stress intensity factor is mesh density sensitive and crack size sensitive, thus finer mesh will provide better understand of the whole process.

In conclusion, fusion welding introduces residual stress along the longitudinal welding direction. The residual stresses will affect stress intensity factor, especially at the symmetry center of the crack front. And the influence of the residual stresses tend to result in a susceptibility to crack growth, which is existed before fusion welding.



## 5.2 Future Works

The model which is currently used in this study uses two identical heat sources moving from the two ends of the substrate block and reaches the center point at the same time. A modified model will be a heat source moving from one end to the other end. To modify the model, these steps should be followed:

1. Build a 1/2 model in HYPERMESH.
2. The mesh will be tested in both ANSYS/ FRAC3d and SYSWELD to make sure the shape of the element is accepted in both of the software (sometimes ANSYS will not accept the mesh the).
3. Renumber the finite elements and nodes. In this step, control the number of the mesh, for example, keep the nodes and elements start from 1 and continuously to 10000 or 5000. See the picture below:

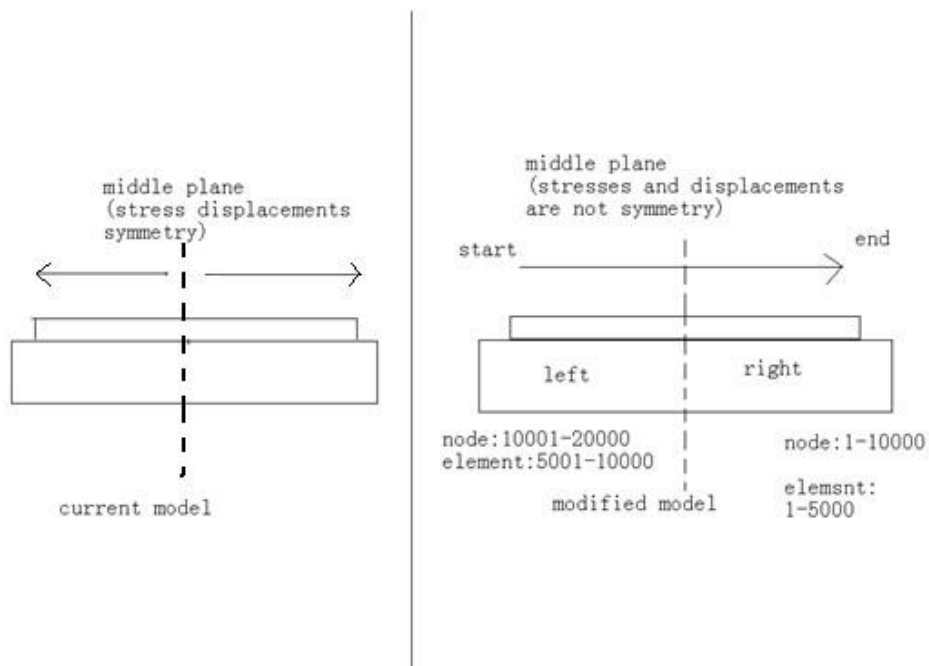


**Figure 5.36** Current model and model for future work.

In the same time elements and nodes in left part will continuously start from 5001, and from 10001, respectively.

4. Create 20°C room temperature model and weld line model. Renumber them
5. Create groups which are needed in SYSWELD simulation.
6. Save the model in another file. Delete the whole left part. Create groups which will be used to generate files for FRAC3D.( I am not quite sure if this step can be done)
7. Perform welding simulation for 1/2 model.(this need 48 hours if I run it on our work station)
8. Export residual stress.
9. Perform FRAC3D computation.
10. Superposition SYSWELD result and Frac3D result.

In future work, the method of this study can be used to study the effect that different welding parameters have on the fracture parameters.

# References

- [1] A. O. Ayhan, H. F. Nied, Frac3D-Finite Element Based Software for 3-D and Generalized Plane Strain Fracture Analysis(second version), Mechanical Engineering and Mechanics, Lehigh University.
- [2] A. O. Ayhan, H. F. Nied, “Stress intensity factors for three-dimensional surface cracks using enriched finite elements”, *International Journal for Numerical Methods in Engineering*, 54:899-921, 2002.
- [3] A. O. Ayhan, A. C. Kaya, H. F. Nied, “Analysis of three-dimensional interface cracks using enriched finite elements”, *International Journal of Fracture*, 142,:255-276, 2006.
- [4] ANSYS®, User’s manual, 2010.
- [5] SYSWELD®, User’s manual, ESI Group, 2010.
- [6] Suraj Joshi, Cumali Semetay, John WH Price and Herman F. Nied. Weld-induced residual stresses in a prototype dragline cluster and comparison with design codes. *Thin-Walled Structures*. Volume 48, Issue 2, February 2010, Pages 89-102
- [7] Cumali Senetay, Hussam Mahmoud, Herman F. Nied. Stress and fracture analysis for welded plate Girders in Bridge structures. In: Department of Mechanical Engineering and Mechanics, Lehigh University.
- [8] HYPERMESH®, User’s manual, 2010.
- [9] Herman F. Nied. and S. Marugan, Murat Ozturk, Ergun Nart, Aaron Mengel,

- Erman Citirik. Finite element modeling of residual stress and distortion from welding stainless steel structures. ATLSS report ; no. 04-06.
- [10] Michaleris P, Kirk M, Mohr W, McGaughy T. Incorporation of residual stress effects into fracture assessment via the finite element method. Fatigue and fracture mechanics. In: Underwood JH, Macdonald BD, Mitchell MR, editors. American society for testing and materials, vol. 28. ASTM STP 1321; 1997.
- [11] V. Robin, T. Pyttfl, J. Christlein, A. Strating. fracture analysis of welded components. In: ESI France, Lyon, France. ESI Gmbh, Eschborn , Germany. AUDI AG, Neckarsulm, Germany,
- [12] Z. Barsoum. Residual stress analysis and fatigue of multi-pass welded tubular structures. Royal Institute of Technology, department of Aeronautical and Vehicle Engineering, Teknikringen 8, 100 44 Stockholm, Sweden. Engineering Failure Analysis 15 (2008) 863–874
- [13] E. Citirik, U. Ozkan, H. F. Nied. Three dimensional fracture analysis of I –beams with fillet welds. Journal of Terraspace Science and Engineering 1(2009)89-97
- [14] G. Labeas<sup>1</sup>, S. Tsirkas<sup>2</sup>, J. Diamantakos<sup>2</sup> and A. Kermanidis<sup>1</sup>. Effect of residual stresses due to laser welding on the Stress Intensity Factors of adjacent crack. 1: LTSM, Laboratory of Technology and Strength of Materials, Department of Mechanical Engineering & Aeronautics, University of Patras, Patras 26500, GREECE. 2: ISTRAM, Institute of Structures and Advanced Materials, Patron-Athinon 57, Patras 26441, GREECE

- [15] John W.H. Pricea, Anna Ziara-Paradowskaa, Suraj Joshia, Trevor Finlaysonb, Cumali Semetaya, Herman Nied. Comparison of experimental and theoretical residual stresses in welds: The issue of gauge volume. *International Journal of Mechanical Sciences* 50 (2008) 513–521
- [16] SYSWELED 2008, SYSWELD 2008 Example Manual, ESI Group, 2008.
- [17] Bon Seung Koo, Multi-pass Welding Behavior of Austenitic and Martensitic Stainless steels Using SYSWELD, Department of Mechanical Engineering and Mechanics, Lehigh University, 2009
- [18] P. Sathiya, G. R. Jinu, N. Singh, “Simulation of Weld Bead Geometry in GTA Welded Duplex Stainless Steel,” Scholarly Research Exchange, Volume 2009,
- [19] E. Armentani, R. Esposito, R. Sepe, “The Effect of Thermal properties and weld Efficiency on Residual Stresses in Welding,” *Journal of Achievements in Materials and Manufacturing Engineering*, Volume 20, Issues 1-2, January-February 2007.
- [20] Ali O.Ayhan,H.F.Nied. Issues in finite element analysis of fracture problems using enriched elements. In: Department of Mechanical Engineering and Mechanics, Lehigh University.
- [21] Bill Wright ,Case Study of the Hoan Bridge. Turner-Fairbank Highway Research Center McLean, VA. Third Annual Bridge Workshop: Fatigue and Fracture. University of DelawareMarch 5, 2004
- [22]Ali O. Ayhan, Ergun Nart, FCPAS Fracture and Crack Propagation Analysis

system version 1.0 Software and Tutorial document. May, 2010

# Appendix

## Element details in HYPERMESH and SYSWELD

Class of elements	Source element type in HYPERMESH	Target element type in SYSWELD
1D linear	PLOTEL, BAR2, ROD, GAP	1002
1D quadratic	BAR3	1003
2D linear	TRIA3	2003
	QUAD4	2004
2D quadratic	TRIA6	2006
	QUAD8	2008
3D linear	TETRA4	3004
	PYRAMID5	degenerated 3008
	PENTA6	3006
	HEXA8	3008

3D quadratic	TETRA10	3010
	PYRAMID13	degenerated 3020
	PENTA15	3015
	HEXA20	3020



# SAMPLE63\_HT.DAT

NAME SAMPLE63\_MESH\_  
SEARCH DATA 2222 ASCII

## DEFINITION

SAMPLE63

OPTION THERMAL METALLURGY SPATIAL

RESTART GEOMETRY

MATERIAL PROPERTIES

ELEMENTS / INTE 2

ELEMENTS GROUPS \$V1\$ / MATE 1 INTE 2

ELEMENTS GROUPS \$PART\$ / MATE 1 INTE 2

MEDIUM

WELDLINE / GROUPS \$TRLINES\$ REFERENCE \$REFLINES\$ ELEMENTS \$LES\$ START \$LNS\$--

ARRIVAL \$FN\$ VELOCITY 1 TINF 0 MODEL 1

\$GROUP CREATE NAME GROUPNODEONLYTRAJ

NODES 39078 39079 39080 39081 39082 39083 39084 39085 39086 39087 39088

39089 39090 39091 39092 39093 39094 39095 39096 39097 39098 39099 39100

39101 39102 39103 39104 39105 39106 39107 39108 39109 39110 39111 39112

39113 39114 39115 39116 39117 39118 39119 39120 39121 39122 39123 39124

39125 39126 39127 39128 39129 39130 39131 39132 39133 39134 39135 39136

39137 39138 39139 39140 39141 39142 39143 39144 39145 39146 39147 39148

39149 39150 39151 39152 39153 39154 39155 39156 39157 39158 39159 39160

39161 39162 39163 39164 39165 39166 39167 39168 39169 39170 39171 39172

39173 39174 39175 39176 39177 39178 39179

\$RETURN

CONSTRAINTS

ELEMENTS GROUPS \$SKIN\$ / KT 1 VARIABLE 1

LOAD

1

ELEMENTS GROUPS \$SKIN\$ / TT 20.

ELEMENTS GROUPS \$V1\$ / QR 1 VARIABLE -10000 TRAJECTORY 1

TABLE

1 / FORTRAN

function f(t)

c

c radiative losses :  $f = \text{sig} * e * (t + \text{to})(t^{**2} + \text{to}^{**2})$

c

e = 0.8

sig = 5.67\*-8

to = 20.

```

to = 20. + 273.15
t1 = t + 273.15
a = t1 * t1
b = to * to
c = a + b
d = t1 + to
d = d * c
d = d * e
d = d * sig
c
c convective losses = 25 W/m2
  f = d + 25.
c change to W/mm2
  d = 1*-6
  f = f * d
c
  return
  END
10000 /  FORTRAN
  FUNCTION F(X)
C
C  F = QC * V1 * V2 * V3 with
C  V1 = exp( -( YY-Y0-VY*TT )^2/AC^2 )
C  V2 = exp( -( XX-X0 )^2/B^2 )
C  V3 = exp( -( ZZ-Z0 )^2/C^2 )
C  if ( -YY + Y0 +VY*TT ) greater than 0
C    QC = QF et AC = AF
C  else
C    QC = QR et AC = AR
C
  DIMENSION X(4)
C
C Input
C
  XX = X(1)  ; X Coordinate
  YY = X(2)  ; Y Coordinate
  ZZ = X(3)  ; Z Coordinate
  TT = X(4)  ; Time
C
C Variables
C
  QF = 129.996002197  ; Maximal front source intensity

```

QR = 66.93800354 ; Maximal rear source intensity

AF = 4 ; Gaussian parameter

AR = 8 ; Gaussian parameter

B = 7 ; Gaussian parameter

C = 0.80000001192 ; Gaussian parameter

X0 = 0 ; X initial location of source center

Y0 = 0 ; Y initial location of source center

Z0 = 0 ; Z initial location of source center

VY = 0 ; Source displacement velocity

AY = 0 ; Angle of torch [deg.]

C

C Constant

C

MI = -1

PIDEG = ATAN(1.)

PIDEG = PIDEG / 45.

AY = AY \* PIDEG

C

C Transformation of global to local coordinates

C

XD = XX - X0

YD = VY \* TT

YD = YD + Y0

ZD = ZZ - Z0

C

C Source rotation about Y axis

C

SA = SIN(AY)

SA = - SA

CA = COS(AY)

A1 = XD \* CA

A2 = ZD \* SA

XL = A1 + A2

YL = YY - YD

A1 = ZD \* CA

A2 = XD \* SA

ZL = A1 - A2

C

C Condition computation, QC and AC initialisation

C

COND = VY \* YL

IF (VY .EQ. 0.) COND = YL

```

QC   = QR
AC   = AR
IF( COND .GT. 0. ) QC = QF
IF( COND .GT. 0. ) AC = AF
C
C V1 computation
C
A1   = YL * YL
A2   = AC * AC
A2   = A1 / A2
A2   = M1 * A2
V1   = EXP( A2 )
C
C V2 computation
C
A1   = XL * XL
A2   = B * B
A2   = A1 / A2
A2   = M1 * A2
V2   = EXP( A2 )
C
C V3 computation
C
A1   = ZL * ZL
A2   = C * C
A2   = A1 / A2
A2   = M1 * A2
V3   = EXP( A2 )
C
C F computation
C
F    = QC * V1
F    = F * V2
F    = F * V3
C
RETURN
END
RETURN

```

```

NAME SAMPLE63_
SAVE DATA 2222

```

MEDIUM  
EXTRACT MEDIUM

# SAMPLE63\_MECH.DAT

NAME SAMPLE63\_MESH\_

SEARCH DATA 2222 ASCII

DEFINITION

SAMPLE63

OPTION THREEDIMENSIONAL THERMOELASTICITY

RESTART GEOMETRY

MATERIAL PROPERTIES

ELEMENTS / INTE 2

ELEMENTS GROUPS \$V1\$ / E -10000 NU -10001 YIELD -10002 LX -10003 LY -10003 --

LZ -10003 SLOPE -10004 MODEL 3 PHAS 6 AUST 6 TF 1300 KY 0 INTE 2

ELEMENTS GROUPS \$PART\$ / E -10000 NU -10001 YIELD -10002 LX -10003 LY -10003 --

LZ -10003 SLOPE -10004 MODEL 3 PHAS 6 AUST 6 TF 1300 KY 0 INTE 2

MEDIUM

WELDLINE / GROUPS \$TRLINES\$ REFERENCE \$REFLINES\$ ELEMENTS \$LES\$ START \$LNS\$--

ARRIVAL \$FN\$ VELOCITY 1 TINF 0 MODEL 1

\$GROUP CREATE NAME GROUPNODEONLYTRAJ

NODES 39078 39079 39080 39081 39082 39083 39084 39085 39086 39087 39088

39089 39090 39091 39092 39093 39094 39095 39096 39097 39098 39099 39100

39101 39102 39103 39104 39105 39106 39107 39108 39109 39110 39111 39112

39113 39114 39115 39116 39117 39118 39119 39120 39121 39122 39123 39124

39125 39126 39127 39128 39129 39130 39131 39132 39133 39134 39135 39136

39137 39138 39139 39140 39141 39142 39143 39144 39145 39146 39147 39148

39149 39150 39151 39152 39153 39154 39155 39156 39157 39158 39159 39160

39161 39162 39163 39164 39165 39166 39167 39168 39169 39170 39171 39172

39173 39174 39175 39176 39177 39178 39179

\$RETURN

CONSTRAINTS

PLANE PSI 90.0000 THETA -74.4904 PHI 90.0000 XX -0.0000 YY 7.5000 ZZ--

22.9735 / SYMMETRY

PLANE PSI -18.9114 THETA 0.0000 PHI 180.0000 XX 13.6235 YY 5.6106 ZZ 0.0000--

/ SYMMETRY

NODES GROUPS \$UXUYUZ\$ / UX UY UZ

LOAD

1 NOTHING

TABLE

10000 / -10005 -10006 -10005 -10005 -10005 -10005

10001 / 1 20 0.33 1505 0.33

10002 / -10007 -10008 -10009 -10010 -10011 -10012

10003 / -10013 -10014 -10013 -10013 -10013 -10015

10004 / -10016 -10017  
 10005 / 1 20 210000 200 200000 400 175000 600 135000 800 78000 1000  
 15000 1100 7000 1200 3000 1300 1000 1500 1000  
 10006 / 1 20 1000 1505 1000  
 10007 / 1 20 390 200 258 300 232 400 200 500 187 600 137 700  
 78 800 75 900 45 1000 30 1100 18 1200 10 1300 5 1505 5  
 10008 / 1 20 245 200 200 350 160 650 70 900 45 1000 30 1100  
 18 1200 10 1300 5 1505 5  
 10009 / 1 20 710 200 620 300 592 400 563 500 505 600 395 700  
 200 800 90 900 45 1000 30 1100 18 1200 10 1300 5 1505 5  
 10010 / 1 20 500 200 490 300 472 400 438 500 384 600 280 700  
 140 800 80 900 45 1000 30 1100 18 1200 10 1300 5 1505 5  
 10011 / 1 20 390 200 258 300 232 400 200 500 187 600 137 700  
 78 800 75 900 45 1000 30 1100 18 1200 10 1300 5 1505 5  
 10012 / 1 20 245 200 200 350 160 650 70 900 45 1000 30 1100  
 18 1200 10 1300 5 1505 5  
 10013 / 1 25 0.0 1200 0.0192 1300 0.0208  
 10014 / 1 0 0.0 1505 0.0  
 10015 / 1 25 -0.0095 1200 0.0180 1300 0.020305  
 10016 / -10018 -10018 -10019 -10020 -10018  
 10017 / 7 20 10021 200 10022 300 10023 400 10024 500 10025 600  
 10026 700 10027 800 10028 900 10029 1000 10030 1100 10031 1200  
 10032 1300 10033  
 10018 / 7 20 10034 200 10035 300 10036 400 10037 500 10038 600  
 10039 700 10040 800 10041 900 10042 1000 10043 1100 10044 1200  
 10045 1300 10046  
 10019 / 7 20 10047 200 10048 300 10049 400 10050 500 10051 600  
 10052 700 10053 800 10054 900 10055 1000 10056 1100 10057 1200  
 10058 1300 10059  
 10020 / 7 20 10060 200 10061 300 10062 400 10063 500 10064 600  
 10065 700 10066 800 10067 900 10068 1000 10069 1100 10070 1200  
 10071 1300 10072  
 10021 / 1 0 0 0.003 32.4 0.0035 46.2 0.0054 59.2 0.01 69.3 0.03  
 104.0 0.04 120.2 0.05 129.4 0.07 143.3 0.085 145.6 0.10 147.9  
 0.13 152.5 0.17 159.5 0.24 168.7 0.30 173.3 0.40 180.3 0.50 187.2  
 0.80 198.8 1 206  
 10022 / 1 0 0 0.003 29.1 0.0035 41.5 0.0054 53.1 0.01 62.3 0.03  
 93.4 0.04 107.9 0.05 116.2 0.07 128.7 0.085 130.8 0.10 132.8  
 0.13 137.0 0.17 143.2 0.24 151.5 0.30 155.7 0.40 161.9 0.50 168.1  
 0.80 178.5 1 185  
 10023 / 1 0 0 0.003 26.4 0.0035 37.7 0.0054 48.3 0.01 56.6 0.03  
 84.9 0.04 98.1 0.05 105.7 0.07 117.0 0.085 118.9 0.10 120.8

0.13 124.5 0.17 130.2 0.24 137.7 0.30 141.5 0.40 147.2 0.50 152.8  
 0.80 162.3 1 167.9  
 10024 / 1 0 0 0.003 23.8 0.0035 34.0 0.0054 43.5 0.01 50.9 0.03  
 76.4 0.04 88.3 0.05 95.1 0.07 105.3 0.085 107.0 0.10 108.7  
 0.13 112.1 0.17 117.2 0.24 124.0 0.30 127.4 0.40 132.5 0.50 137.5  
 0.80 146.0 1 151.1  
 10025 / 1 0 0 0.003 19.2 0.0035 27.4 0.0054 35.0 0.01 41.0 0.03  
 61.6 0.04 71.1 0.05 76.6 0.07 84.8 0.085 86.2 0.10 87.5  
 0.13 90.3 0.17 94.4 0.24 99.9 0.30 102.6 0.40 106.7 0.50 110.8  
 0.80 117.6 1 121.7  
 10026 / 1 0 0 0.003 15.8 0.0035 22.6 0.0054 29.0 0.01 34.0 0.03  
 50.9 0.04 58.9 0.05 63.4 0.07 70.2 0.085 71.3 0.10 72.5  
 0.13 74.7 0.17 78.1 0.24 82.6 0.30 84.9 0.40 88.3 0.50 91.7  
 0.80 97.4 1 100.8  
 10027 / 1 0 0 0.003 12.5 0.0035 17.9 0.0054 22.9 0.01 26.9 0.03  
 40.3 0.04 46.6 0.05 50.2 0.07 55.6 0.085 56.5 0.10 57.4  
 0.13 59.2 0.17 61.8 0.24 65.4 0.30 67.2 0.40 69.9 0.50 72.6  
 0.80 77.1 1 79.8  
 10028 / 1 0 0 0.003 9.2 0.0035 13.2 0.0054 16.9 0.01 19.8 0.03  
 29.7 0.04 34.3 0.05 37.0 0.07 40.9 0.085 41.6 0.10 42.3  
 0.13 43.6 0.17 45.6 0.24 48.2 0.30 49.5 0.40 51.5 0.50 53.5  
 0.80 56.8 1 58.8  
 10029 / 1 0 0 0.003 6.6 0.0035 9.4 0.0054 12.1 0.01 14.2 0.03  
 21.2 0.04 24.5 0.05 26.4 0.07 29.2 0.085 29.7 0.10 30.2  
 0.13 31.1 0.17 32.5 0.24 34.4 0.30 35.4 0.40 36.8 0.50 38.2  
 0.80 40.6 1 42.0  
 10030 / 1 0 0 0.003 4.2 0.0035 6.0 0.0054 7.7 0.01 9.1 0.03  
 13.6 0.04 15.7 0.05 16.9 0.07 18.7 0.085 19.0 0.10 19.3  
 0.13 19.9 0.17 20.8 0.24 22.0 0.30 22.6 0.40 23.5 0.50 24.5  
 0.80 26.0 1 26.9  
 10031 / 1 0 0 0.003 0.0 0.0035 0.0 0.0054 0.0 0.01 0.0 0.03  
 0.0 0.04 0.0 0.05 0.0 0.07 0.0 0.085 0.0 0.10 0.0  
 0.13 0.0 0.17 0.0 0.24 0.0 0.30 0.0 0.40 0.0 0.50 0.0  
 0.80 0.0 1 0.0  
 10032 / 1 0 0 0.003 0.0 0.0035 0.0 0.0054 0.0 0.01 0.0 0.03  
 0.0 0.04 0.0 0.05 0.0 0.07 0.0 0.085 0.0 0.10 0.0  
 0.13 0.0 0.17 0.0 0.24 0.0 0.30 0.0 0.40 0.0 0.50 0.0  
 0.80 0.0 1 0.0  
 10033 / 1 0 0 0.003 0.0 0.0035 0.0 0.0054 0.0 0.01 0.0 0.03  
 0.0 0.04 0.0 0.05 0.0 0.07 0.0 0.085 0.0 0.10 0.0  
 0.13 0.0 0.17 0.0 0.24 0.0 0.30 0.0 0.40 0.0 0.50 0.0  
 0.80 0.0 1 0.0



10034 / 1 0 0 0.003 51.5 0.0035 73.6 0.0054 94.2 0.01 110.4 0.03  
 165.6 0.04 191.3 0.05 206.0 0.07 228.1 0.085 231.8 0.10 235.5  
 0.13 242.8 0.17 253.9 0.24 268.6 0.30 275.9 0.40 287.0 0.50 298.0  
 0.80 316.4 1 327  
 10035 / 1 0 0 0.003 50.7 0.0035 72.5 0.0054 92.7 0.01 108.7 0.03  
 163.0 0.04 188.4 0.05 202.9 0.07 224.6 0.085 228.2 0.10 231.8  
 0.13 239.1 0.17 250.0 0.24 264.5 0.30 271.7 0.40 282.6 0.50 293.4  
 0.80 311.5 1 322  
 10036 / 1 0 0 0.003 49.7 0.0035 70.9 0.0054 90.8 0.01 106.4 0.03  
 159.6 0.04 184.5 0.05 198.6 0.07 219.9 0.085 223.5 0.10 227.0  
 0.13 234.1 0.17 244.8 0.24 258.9 0.30 266.0 0.40 276.7 0.50 287.3  
 0.80 305.1 1 315.7  
 10037 / 1 0 0 0.003 46.0 0.0035 65.7 0.0054 84.0 0.01 98.5 0.03  
 147.7 0.04 170.7 0.05 183.8 0.07 203.5 0.085 206.8 0.10 210.1  
 0.13 216.7 0.17 226.5 0.24 239.7 0.30 246.2 0.40 256.1 0.50 265.9  
 0.80 282.3 1 292.2  
 10038 / 1 0 0 0.003 40.0 0.0035 57.2 0.0054 73.2 0.01 85.8 0.03  
 128.6 0.04 148.6 0.05 160.1 0.07 177.2 0.085 180.1 0.10 182.9  
 0.13 188.7 0.17 197.2 0.24 208.7 0.30 214.4 0.40 223.0 0.50 231.5  
 0.80 245.8 1 254.4  
 10039 / 1 0 0 0.003 29.1 0.0035 41.5 0.0054 53.1 0.01 62.3 0.03  
 93.4 0.04 107.9 0.05 116.2 0.07 128.7 0.085 130.8 0.10 132.8  
 0.13 137.0 0.17 143.2 0.24 151.5 0.30 155.7 0.40 161.9 0.50 168.1  
 0.80 178.5 1 184.7  
 10040 / 1 0 0 0.003 14.5 0.0035 20.8 0.0054 26.6 0.01 31.1 0.03  
 46.7 0.04 54.0 0.05 58.1 0.07 64.3 0.085 65.4 0.10 66.4  
 0.13 68.5 0.17 71.6 0.24 75.8 0.30 77.8 0.40 80.9 0.50 84.1  
 0.80 89.2 1 92.4  
 10041 / 1 0 0 0.003 9.9 0.0035 14.2 0.0054 18.1 0.01 21.2 0.03  
 31.8 0.04 36.8 0.05 39.6 0.07 43.9 0.085 44.6 0.10 45.3  
 0.13 46.7 0.17 48.8 0.24 51.7 0.30 53.1 0.40 55.2 0.50 57.3  
 0.80 60.8 1 63.0  
 10042 / 1 0 0 0.003 6.9 0.0035 9.8 0.0054 12.6 0.01 14.7 0.03  
 22.1 0.04 25.5 0.05 27.5 0.07 30.4 0.085 30.9 0.10 31.4  
 0.13 32.4 0.17 33.8 0.24 35.8 0.30 36.8 0.40 38.3 0.50 39.7  
 0.80 42.2 1 43.7  
 10043 / 1 0 0 0.003 4.4 0.0035 6.2 0.0054 8.0 0.01 9.3 0.03  
 14.0 0.04 16.2 0.05 17.4 0.07 19.3 0.085 19.6 0.10 19.9  
 0.13 20.5 0.17 21.5 0.24 22.7 0.30 23.3 0.40 24.3 0.50 25.2  
 0.80 26.8 1 27.7  
 10044 / 1 0 0 0.003 0.0 0.0035 0.0 0.0054 0.0 0.01 0.0 0.03  
 0.0 0.04 0.0 0.05 0.0 0.07 0.0 0.085 0.0 0.10 0.0

0.13 0.0 0.17 0.0 0.24 0.0 0.30 0.0 0.40 0.0 0.50 0.0  
 0.80 0.0 1 0.0  
 10045 / 1 0.0 0.003 0.0 0.0035 0.0 0.0054 0.0 0.01 0.0 0.03  
 0.0 0.04 0.0 0.05 0.0 0.07 0.0 0.085 0.0 0.10 0.0  
 0.13 0.0 0.17 0.0 0.24 0.0 0.30 0.0 0.40 0.0 0.50 0.0  
 0.80 0.0 1 0.0  
 10046 / 1 0.0 0.003 0.0 0.0035 0.0 0.0054 0.0 0.01 0.0 0.03  
 0.0 0.04 0.0 0.05 0.0 0.07 0.0 0.085 0.0 0.10 0.0  
 0.13 0.0 0.17 0.0 0.24 0.0 0.30 0.0 0.40 0.0 0.50 0.0  
 0.80 0.0 1 0.0  
 10047 / 1 0.0 0.003 93.8 0.0035 134.0 0.0054 171.5 0.01 200.9  
 0.03 301.4 0.04 348.3 0.05 375.1 0.07 415.3 0.085 422.0 0.10 428.7  
 0.13 442.1 0.17 462.2 0.24 489.0 0.30 502.4 0.40 522.5 0.50 542.5  
 0.80 576.0 1 596  
 10048 / 1 0.0 0.003 81.9 0.0035 117.0 0.0054 149.7 0.01 175.5  
 0.03 263.2 0.04 304.2 0.05 327.5 0.07 362.6 0.085 368.5 0.10 374.3  
 0.13 386.0 0.17 403.6 0.24 427.0 0.30 438.7 0.40 456.2 0.50 473.8  
 0.80 503.0 1 521  
 10049 / 1 0.0 0.003 78.2 0.0035 111.7 0.0054 143.0 0.01 167.5  
 0.03 251.3 0.04 290.4 0.05 312.8 0.07 346.3 0.085 351.8 0.10 357.4  
 0.13 368.6 0.17 385.4 0.24 407.7 0.30 418.9 0.40 435.6 0.50 452.4  
 0.80 480.3 1 497.1  
 10050 / 1 0.0 0.003 74.4 0.0035 106.2 0.0054 136.0 0.01 159.3  
 0.03 239.0 0.04 276.2 0.05 297.4 0.07 329.3 0.085 334.6 0.10 339.9  
 0.13 350.5 0.17 366.5 0.24 387.7 0.30 398.3 0.40 414.3 0.50 430.2  
 0.80 456.8 1 472.7  
 10051 / 1 0.0 0.003 66.7 0.0035 95.3 0.0054 122.0 0.01 142.9  
 0.03 214.4 0.04 247.7 0.05 266.8 0.07 295.4 0.085 300.1 0.10 304.9  
 0.13 314.4 0.17 328.7 0.24 347.8 0.30 357.3 0.40 371.6 0.50 385.9  
 0.80 409.7 1 424.0  
 10052 / 1 0.0 0.003 52.2 0.0035 74.5 0.0054 95.4 0.01 111.8  
 0.03 167.7 0.04 193.8 0.05 208.7 0.07 231.0 0.085 234.8 0.10 238.5  
 0.13 245.9 0.17 257.1 0.24 272.0 0.30 279.5 0.40 290.7 0.50 301.8  
 0.80 320.5 1 331.7  
 10053 / 1 0.0 0.003 26.4 0.0035 37.7 0.0054 48.3 0.01 56.6  
 0.03 84.9 0.04 98.1 0.05 105.7 0.07 117.0 0.085 118.9 0.10 120.8  
 0.13 124.5 0.17 130.2 0.24 137.7 0.30 141.5 0.40 147.2 0.50 152.8  
 0.80 162.3 1 167.9  
 10054 / 1 0.0 0.003 11.9 0.0035 17.0 0.0054 21.7 0.01 25.5  
 0.03 38.2 0.04 44.2 0.05 47.5 0.07 52.6 0.085 53.5 0.10 54.3  
 0.13 56.0 0.17 58.6 0.24 62.0 0.30 63.7 0.40 66.2 0.50  
 68.8 0.80 73.0 1 75.6

10055 / 1 0 0 0.003 7.5 0.0035 10.8 0.0054 13.8 0.01 16.1  
 0.03 24.2 0.04 28.0 0.05 30.1 0.07 33.3 0.085 33.9 0.10 34.4  
 0.13 35.5 0.17 37.1 0.24 39.3 0.30 40.3 0.40 41.9 0.50  
 43.6 0.80 46.2 1 47.9  
 10056 / 1 0 0 0.003 4.6 0.0035 6.6 0.0054 8.5 0.01 9.9  
 0.03 14.9 0.04 17.2 0.05 18.5 0.07 20.5 0.085 20.8 0.10 21.1  
 0.13 21.8 0.17 22.8 0.24 24.1 0.30 24.8 0.40 25.8 0.50  
 26.7 0.80 28.4 1 29.4  
 10057 / 1 0 0 0.003 0.0 0.0035 0.0 0.0054 0.0 0.01 0.0  
 0.03 0.0 0.04 0.0 0.05 0.0 0.07 0.0 0.085 0.0 0.10 0.0  
 0.13 0.0 0.17 0.0 0.24 0.0 0.30 0.0 0.40 0.0 0.50  
 0.0 0.80 0.0 1 0.0  
 10058 / 1 0 0 0.003 0.0 0.0035 0.0 0.0054 0.0 0.01 0.0  
 0.03 0.0 0.04 0.0 0.05 0.0 0.07 0.0 0.085 0.0 0.10 0.0  
 0.13 0.0 0.17 0.0 0.24 0.0 0.30 0.0 0.40 0.0 0.50  
 0.0 0.80 0.0 1 0.0  
 10059 / 1 0 0 0.003 0.0 0.0035 0.0 0.0054 0.0 0.01 0.0  
 0.03 0.0 0.04 0.0 0.05 0.0 0.07 0.0 0.085 0.0 0.10 0.0  
 0.13 0.0 0.17 0.0 0.24 0.0 0.30 0.0 0.40 0.0 0.50  
 0.0 0.80 0.0 1 0.0  
 10060 / 1 0 0 0.003 66.0 0.0035 94.3 0.0054 120.8 0.01 141.5  
 0.03 212.3 0.04 245.3 0.05 264.2 0.07 292.5 0.085 297.2 0.10 301.9  
 0.13 311.3 0.17 325.5 0.24 344.3 0.30 353.8 0.40 367.9 0.50 382.1  
 0.80 405.7 1 420  
 10061 / 1 0 0 0.003 64.7 0.0035 92.5 0.0054 118.3 0.01 138.7  
 0.03 208.0 0.04 240.4 0.05 258.9 0.07 286.6 0.085 291.2 0.10 295.8  
 0.13 305.1 0.17 319.0 0.24 337.5 0.30 346.7 0.40 360.6 0.50 374.4  
 0.80 397.5 1 411  
 10062 / 1 0 0 0.003 62.3 0.0035 89.1 0.0054 114.0 0.01 133.6  
 0.03 200.4 0.04 231.5 0.05 249.4 0.07 276.1 0.085 280.5 0.10 285.0  
 0.13 293.9 0.17 307.2 0.24 325.1 0.30 334.0 0.40 347.3 0.50 360.7  
 0.80 382.9 1 396.3  
 10063 / 1 0 0 0.003 57.8 0.0035 82.6 0.0054 105.8 0.01 124.0  
 0.03 185.9 0.04 214.9 0.05 231.4 0.07 256.2 0.085 260.3 0.10 264.5  
 0.13 272.7 0.17 285.1 0.24 301.6 0.30 309.9 0.40 322.3 0.50 334.7  
 0.80 355.4 1 367.8  
 10064 / 1 0 0 0.003 50.7 0.0035 72.5 0.0054 92.7 0.01 108.7  
 0.03 163.0 0.04 188.4 0.05 202.9 0.07 224.6 0.085 228.2 0.10 231.8  
 0.13 239.1 0.17 250.0 0.24 264.5 0.30 271.7 0.40 282.6 0.50 293.4  
 0.80 311.5 1 322.4  
 10065 / 1 0 0 0.003 37.0 0.0035 52.8 0.0054 67.6 0.01 79.2  
 0.03 118.9 0.04 137.4 0.05 147.9 0.07 163.8 0.085 166.4 0.10 169.1

0.13 174.3 0.17 182.3 0.24 192.8 0.30 198.1 0.40 206.0 0.50 214.0  
 0.80 227.2 1 235.1  
 10066 / 1 0 0 0.003 18.5 0.0035 26.4 0.0054 33.8 0.01 39.6  
 0.03 59.4 0.04 68.7 0.05 74.0 0.07 81.9 0.085 83.2 0.10 84.5  
 0.13 87.2 0.17 91.1 0.24 96.4 0.30 99.1 0.40 103.0 0.50 107.0  
 0.80 113.6 1 117.5  
 10067 / 1 0 0 0.003 10.6 0.0035 15.1 0.0054 19.3 0.01 22.6  
 0.03 34.0 0.04 39.2 0.05 42.3 0.07 46.8 0.085 47.5 0.10 48.3  
 0.13 49.8 0.17 52.1 0.24 55.1 0.30 56.6 0.40 58.9 0.50 61.1  
 0.80 64.9 1 67.2  
 10068 / 1 0 0 0.003 7.3 0.0035 10.4 0.0054 13.3 0.01 15.6  
 0.03 23.3 0.04 27.0 0.05 29.1 0.07 32.2 0.085 32.7 0.10 33.2  
 0.13 34.2 0.17 35.8 0.24 37.9 0.30 38.9 0.40 40.5 0.50 42.0  
 0.80 44.6 1 46.2  
 10069 / 1 0 0 0.003 4.5 0.0035 6.4 0.0054 8.2 0.01 9.6  
 0.03 14.4 0.04 16.7 0.05 18.0 0.07 19.9 0.085 20.2 0.10 20.5  
 0.13 21.2 0.17 22.1 0.24 23.4 0.30 24.1 0.40 25.0 0.50 26.0  
 0.80 27.6 1 28.5  
 10070 / 1 0 0 0.003 0.0 0.0035 0.0 0.0054 0.0 0.01 0.0  
 0.03 0.0 0.04 0.0 0.05 0.0 0.07 0.0 0.085 0.0 0.10 0.0  
 0.13 0.0 0.17 0.0 0.24 0.0 0.30 0.0 0.40 0.0 0.50  
 0.0 0.80 0.0 1 0.0  
 10071 / 1 0 0 0.003 0.0 0.0035 0.0 0.0054 0.0 0.01 0.0  
 0.03 0.0 0.04 0.0 0.05 0.0 0.07 0.0 0.085 0.0 0.10 0.0  
 0.13 0.0 0.17 0.0 0.24 0.0 0.30 0.0 0.40 0.0 0.50  
 0.0 0.80 0.0 1 0.0  
 10072 / 1 0 0 0.003 0.0 0.0035 0.0 0.0054 0.0 0.01 0.0  
 0.03 0.0 0.04 0.0 0.05 0.0 0.07 0.0 0.085 0.0 0.10 0.0  
 0.13 0.0 0.17 0.0 0.24 0.0 0.30 0.0 0.40 0.0 0.50  
 0.0 0.80 0.0 1 0.0

RETURN

NAME SAMPLE63\_

SAVE DATA 3333

MEDIUM

EXTRACT MEDIUM

# NEWREFRONT2\_HT.DAT

NAME NEWREFORNT2\_MESH\_

SEARCH DATA 2222 ASCII

DEFINITION

NEWREFORNT2

OPTION THERMAL METALLURGY SPATIAL

RESTART GEOMETRY

MATERIAL PROPERTIES

ELEMENTS / INTE 2

ELEMENTS GROUPS \$V1\$ / MATE 1 INTE 2

ELEMENTS GROUPS \$PART\$ / MATE 1 INTE 2

MEDIUM

WELDLINE / GROUPS \$TRLINES\$ REFERENCE \$REFLINES\$ ELEMENTS

\$WELDFIRSTELM\$--

START \$WELDFIRSTNODE\$ ARRIVAL \$WELDENDNODE\$ VELOCITY 1 TINF 0

MODEL 1

\$GROUP CREATE NAME GROUPNODEONLYTRAJ

NODES 51153 51158 51154 51159 51155 51160 51156 51161 51157 51162 51163

51164 51165 51166 51167 51168 51169 51170 51171 51172 51173 51174 51175

51176 51177 51178 51179 51180 51181 51182 51183 51184 51185 51186 51187

51188 51189 51190 51191 51192 51193 51194 51195 51196 51197 51198 51199

51200 51201 51202 51203 51204 51205 51206 51207 51208 51209 51210 51211

51212 51213 51214 51215 51216 51217 51218 51219 51220 51221 51222 51223

51224 51225 51226 51227 51228 51229 51230 51231 51232 51233 51234 51235

51236 51237 51238 51239 51240 51241 51242 51243 51244 51245 51246 51247

51248 51249 51250 51251 51252 51253 51254

\$RETURN

CONSTRAINTS

ELEMENTS GROUPS \$SKIN\$ / KT 1 VARIABLE 1

LOAD

1

ELEMENTS GROUPS \$SKIN\$ / TT 20.

ELEMENTS GROUPS \$V1\$ / QR 1 VARIABLE -10000 TRAJECTORY 1

TABLE

1 / FORTRAN

function f(t)

c

c radiative losses :  $f = \text{sig} * e * (t + \text{to})(t^{**2} + \text{to}^{**2})$

c

e = 0.8

```

sig = 5.67*-8
to = 20.
to = 20. + 273.15
t1 = t + 273.15
a = t1 * t1
b = to * to
c = a + b
d = t1 + to
d = d * c
d = d * e
d = d * sig
c
c convective losses = 25 W/m2
  f = d + 25.
c change to W/mm2
  d = 1*-6
  f = f * d
c
  return
  END
10000 /  FORTRAN
  FUNCTION F(X)
C
C  F = QC * V1 * V2 * V3 with
C  V1 = exp( -( YY-Y0-VY*TT )^2/AC^2 )
C  V2 = exp( -( XX-X0 )^2/B^2 )
C  V3 = exp( -( ZZ-Z0 )^2/C^2 )
C  if ( -YY + Y0 +VY*TT ) greater than 0
C    QC = QF et AC = AF
C  else
C    QC = QR et AC = AR
C
C    DIMENSION X(4)
C
C Input
C
C    XX = X(1)  ; X Coordinate
C    YY = X(2)  ; Y Coordinate
C    ZZ = X(3)  ; Z Coordinate
C    TT = X(4)  ; Time
C
C Variables

```

C

QF = 129.996002197 ; Maximal front source intensity

QR = 66.93800354 ; Maximal rear source intensity

AF = 4 ; Gaussian parameter

AR = 8 ; Gaussian parameter

B = 7 ; Gaussian parameter

C = 0.80000001192 ; Gaussian parameter

X0 = 0 ; X initial location of source center

Y0 = 0 ; Y initial location of source center

Z0 = 0 ; Z initial location of source center

VY = 0 ; Source displacement velocity

AY = 0 ; Angle of torch [deg.]

C

C Constant

C

M1 = -1

PIDEG = ATAN(1.)

PIDEG = PIDEG / 45.

AY = AY \* PIDEG

C

C Transformation of global to local coordinates

C

XD = XX - X0

YD = VY \* TT

YD = YD + Y0

ZD = ZZ - Z0

C

C Source rotation about Y axis

C

SA = SIN( AY )

SA = - SA

CA = COS( AY )

A1 = XD \* CA

A2 = ZD \* SA

XL = A1 + A2

YL = YY - YD

A1 = ZD \* CA

A2 = XD \* SA

ZL = A1 - A2

C

C Condition computation, QC and AC initialisation

C

```

COND = VY * YL
IF (VY .EQ. 0.) COND = YL
QC   = QR
AC   = AR
IF( COND .GT. 0. ) QC = QF
IF( COND .GT. 0. ) AC = AF
C
C V1 computation
C
  A1   = YL * YL
  A2   = AC * AC
  A2   = A1 / A2
  A2   = M1 * A2
  V1   = EXP( A2 )
C
C V2 computation
C
  A1   = XL * XL
  A2   = B * B
  A2   = A1 / A2
  A2   = M1 * A2
  V2   = EXP( A2 )
C
C V3 computation
C
  A1   = ZL * ZL
  A2   = C * C
  A2   = A1 / A2
  A2   = M1 * A2
  V3   = EXP( A2 )
C
C F computation
C
  F    = QC * V1
  F    = F * V2
  F    = F * V3
C
  RETURN
  END
RETURN

```



NAME NEWREFORNT2\_  
SAVE DATA 2222

MEDIUM  
EXTRACT MEDIUM

# NEWREFORNT2\_MECH.DAT

NAME NEWREFORNT2\_MESH\_

SEARCH DATA 2222 ASCII

DEFINITION

NEWREFORNT2

OPTION THREEDIMENSIONAL THERMOELASTICITY

RESTART GEOMETRY

MATERIAL PROPERTIES

ELEMENTS / INTE 2

ELEMENTS GROUPS \$V1\$ / E -10000 NU -10001 YIELD -10002 LX -10003 LY -10003 --

LZ -10003 SLOPE -10004 MODEL 3 PHAS 6 AUST 6 TF 1300 KY 0 INTE 2

ELEMENTS GROUPS \$PART\$ / E -10000 NU -10001 YIELD -10002 LX -10003 LY -10003

--

LZ -10003 SLOPE -10004 MODEL 3 PHAS 6 AUST 6 TF 1300 KY 0 INTE 2

MEDIUM

WELDLINE / GROUPS \$TRLIN\$ REFERENCE \$REFLINE\$ ELEMENTS

\$WELDFIRSTELM\$--

START \$WELDFIRSTNODE\$ ARRIVAL \$WELDENDNODE\$ VELOCITY 1 TINF 0

MODEL 1

\$GROUP CREATE NAME GROUPNODEONLYTRAJ

NODES 51153 51158 51154 51159 51155 51160 51156 51161 51157 51162 51163

51164 51165 51166 51167 51168 51169 51170 51171 51172 51173 51174 51175

51176 51177 51178 51179 51180 51181 51182 51183 51184 51185 51186 51187

51188 51189 51190 51191 51192 51193 51194 51195 51196 51197 51198 51199

51200 51201 51202 51203 51204 51205 51206 51207 51208 51209 51210 51211

51212 51213 51214 51215 51216 51217 51218 51219 51220 51221 51222 51223

51224 51225 51226 51227 51228 51229 51230 51231 51232 51233 51234 51235

51236 51237 51238 51239 51240 51241 51242 51243 51244 51245 51246 51247

51248 51249 51250 51251 51252 51253 51254

\$RETURN

CONSTRAINTS

PLANE PSI -90.0000 THETA -74.2023 PHI 90.0000 XX -0.0000 YY 7.9904 ZZ--

21.7580 / SYMMETRY

PLANE PSI -17.9160 THETA 0.0000 PHI 0.0000 XX 8.1628 YY 7.0599 ZZ 0.0000 /--

SYMMETRY

NODES GROUPS \$UXUYUZ\$ / UX UY UZ

LOAD

1 NOTHING

TABLE

10000 / -10005 -10006 -10005 -10005 -10005 -10005

10001 / 1 20 0.33 1505 0.33  
10002 / -10007 -10008 -10009 -10010 -10011 -10012  
10003 / -10013 -10014 -10013 -10013 -10013 -10015  
10004 / -10016 -10017  
10005 / 1 20 210000 200 200000 400 175000 600 135000 800 78000 1000  
15000 1100 7000 1200 3000 1300 1000 1500 1000  
10006 / 1 20 1000 1505 1000  
10007 / 1 20 390 200 258 300 232 400 200 500 187 600 137 700  
78 800 75 900 45 1000 30 1100 18 1200 10 1300 5 1505 5  
10008 / 1 20 245 200 200 350 160 650 70 900 45 1000 30 1100  
18 1200 10 1300 5 1505 5  
10009 / 1 20 710 200 620 300 592 400 563 500 505 600 395 700  
200 800 90 900 45 1000 30 1100 18 1200 10 1300 5 1505 5  
10010 / 1 20 500 200 490 300 472 400 438 500 384 600 280 700  
140 800 80 900 45 1000 30 1100 18 1200 10 1300 5 1505 5  
10011 / 1 20 390 200 258 300 232 400 200 500 187 600 137 700  
78 800 75 900 45 1000 30 1100 18 1200 10 1300 5 1505 5  
10012 / 1 20 245 200 200 350 160 650 70 900 45 1000 30 1100  
18 1200 10 1300 5 1505 5  
10013 / 1 25 0.0 1200 0.0192 1300 0.0208  
10014 / 1 0 0.0 1505 0.0  
10015 / 1 25 -0.0095 1200 0.0180 1300 0.020305  
10016 / -10018 -10018 -10019 -10020 -10018  
10017 / 7 20 10021 200 10022 300 10023 400 10024 500 10025 600  
10026 700 10027 800 10028 900 10029 1000 10030 1100 10031 1200  
10032 1300 10033  
10018 / 7 20 10034 200 10035 300 10036 400 10037 500 10038 600  
10039 700 10040 800 10041 900 10042 1000 10043 1100 10044 1200  
10045 1300 10046  
10019 / 7 20 10047 200 10048 300 10049 400 10050 500 10051 600  
10052 700 10053 800 10054 900 10055 1000 10056 1100 10057 1200  
10058 1300 10059  
10020 / 7 20 10060 200 10061 300 10062 400 10063 500 10064 600  
10065 700 10066 800 10067 900 10068 1000 10069 1100 10070 1200  
10071 1300 10072  
10021 / 1 0 0 0.003 32.4 0.0035 46.2 0.0054 59.2 0.01 69.3 0.03  
104.0 0.04 120.2 0.05 129.4 0.07 143.3 0.085 145.6 0.10 147.9  
0.13 152.5 0.17 159.5 0.24 168.7 0.30 173.3 0.40 180.3 0.50 187.2  
0.80 198.8 1 206  
10022 / 1 0 0 0.003 29.1 0.0035 41.5 0.0054 53.1 0.01 62.3 0.03  
93.4 0.04 107.9 0.05 116.2 0.07 128.7 0.085 130.8 0.10 132.8  
0.13 137.0 0.17 143.2 0.24 151.5 0.30 155.7 0.40 161.9 0.50 168.1

0.80 178.5 1 185  
 10023 / 1 0 0 0.003 26.4 0.0035 37.7 0.0054 48.3 0.01 56.6 0.03  
 84.9 0.04 98.1 0.05 105.7 0.07 117.0 0.085 118.9 0.10 120.8  
 0.13 124.5 0.17 130.2 0.24 137.7 0.30 141.5 0.40 147.2 0.50 152.8  
 0.80 162.3 1 167.9  
 10024 / 1 0 0 0.003 23.8 0.0035 34.0 0.0054 43.5 0.01 50.9 0.03  
 76.4 0.04 88.3 0.05 95.1 0.07 105.3 0.085 107.0 0.10 108.7  
 0.13 112.1 0.17 117.2 0.24 124.0 0.30 127.4 0.40 132.5 0.50 137.5  
 0.80 146.0 1 151.1  
 10025 / 1 0 0 0.003 19.2 0.0035 27.4 0.0054 35.0 0.01 41.0 0.03  
 61.6 0.04 71.1 0.05 76.6 0.07 84.8 0.085 86.2 0.10 87.5  
 0.13 90.3 0.17 94.4 0.24 99.9 0.30 102.6 0.40 106.7 0.50 110.8  
 0.80 117.6 1 121.7  
 10026 / 1 0 0 0.003 15.8 0.0035 22.6 0.0054 29.0 0.01 34.0 0.03  
 50.9 0.04 58.9 0.05 63.4 0.07 70.2 0.085 71.3 0.10 72.5  
 0.13 74.7 0.17 78.1 0.24 82.6 0.30 84.9 0.40 88.3 0.50 91.7  
 0.80 97.4 1 100.8  
 10027 / 1 0 0 0.003 12.5 0.0035 17.9 0.0054 22.9 0.01 26.9 0.03  
 40.3 0.04 46.6 0.05 50.2 0.07 55.6 0.085 56.5 0.10 57.4  
 0.13 59.2 0.17 61.8 0.24 65.4 0.30 67.2 0.40 69.9 0.50 72.6  
 0.80 77.1 1 79.8  
 10028 / 1 0 0 0.003 9.2 0.0035 13.2 0.0054 16.9 0.01 19.8 0.03  
 29.7 0.04 34.3 0.05 37.0 0.07 40.9 0.085 41.6 0.10 42.3  
 0.13 43.6 0.17 45.6 0.24 48.2 0.30 49.5 0.40 51.5 0.50 53.5  
 0.80 56.8 1 58.8  
 10029 / 1 0 0 0.003 6.6 0.0035 9.4 0.0054 12.1 0.01 14.2 0.03  
 21.2 0.04 24.5 0.05 26.4 0.07 29.2 0.085 29.7 0.10 30.2  
 0.13 31.1 0.17 32.5 0.24 34.4 0.30 35.4 0.40 36.8 0.50 38.2  
 0.80 40.6 1 42.0  
 10030 / 1 0 0 0.003 4.2 0.0035 6.0 0.0054 7.7 0.01 9.1 0.03  
 13.6 0.04 15.7 0.05 16.9 0.07 18.7 0.085 19.0 0.10 19.3  
 0.13 19.9 0.17 20.8 0.24 22.0 0.30 22.6 0.40 23.5 0.50 24.5  
 0.80 26.0 1 26.9  
 10031 / 1 0 0 0.003 0.0 0.0035 0.0 0.0054 0.0 0.01 0.0 0.03  
 0.0 0.04 0.0 0.05 0.0 0.07 0.0 0.085 0.0 0.10 0.0  
 0.13 0.0 0.17 0.0 0.24 0.0 0.30 0.0 0.40 0.0 0.50 0.0  
 0.80 0.0 1 0.0  
 10032 / 1 0 0 0.003 0.0 0.0035 0.0 0.0054 0.0 0.01 0.0 0.03  
 0.0 0.04 0.0 0.05 0.0 0.07 0.0 0.085 0.0 0.10 0.0  
 0.13 0.0 0.17 0.0 0.24 0.0 0.30 0.0 0.40 0.0 0.50 0.0  
 0.80 0.0 1 0.0  
 10033 / 1 0 0 0.003 0.0 0.0035 0.0 0.0054 0.0 0.01 0.0 0.03

0.0 0.04 0.0 0.05 0.0 0.07 0.0 0.085 0.0 0.10 0.0  
 0.13 0.0 0.17 0.0 0.24 0.0 0.30 0.0 0.40 0.0 0.50 0.0  
 0.80 0.0 1 0.0  
 10034 / 1 0 0 0.003 51.5 0.0035 73.6 0.0054 94.2 0.01 110.4 0.03  
 165.6 0.04 191.3 0.05 206.0 0.07 228.1 0.085 231.8 0.10 235.5  
 0.13 242.8 0.17 253.9 0.24 268.6 0.30 275.9 0.40 287.0 0.50 298.0  
 0.80 316.4 1 327  
 10035 / 1 0 0 0.003 50.7 0.0035 72.5 0.0054 92.7 0.01 108.7 0.03  
 163.0 0.04 188.4 0.05 202.9 0.07 224.6 0.085 228.2 0.10 231.8  
 0.13 239.1 0.17 250.0 0.24 264.5 0.30 271.7 0.40 282.6 0.50 293.4  
 0.80 311.5 1 322  
 10036 / 1 0 0 0.003 49.7 0.0035 70.9 0.0054 90.8 0.01 106.4 0.03  
 159.6 0.04 184.5 0.05 198.6 0.07 219.9 0.085 223.5 0.10 227.0  
 0.13 234.1 0.17 244.8 0.24 258.9 0.30 266.0 0.40 276.7 0.50 287.3  
 0.80 305.1 1 315.7  
 10037 / 1 0 0 0.003 46.0 0.0035 65.7 0.0054 84.0 0.01 98.5 0.03  
 147.7 0.04 170.7 0.05 183.8 0.07 203.5 0.085 206.8 0.10 210.1  
 0.13 216.7 0.17 226.5 0.24 239.7 0.30 246.2 0.40 256.1 0.50 265.9  
 0.80 282.3 1 292.2  
 10038 / 1 0 0 0.003 40.0 0.0035 57.2 0.0054 73.2 0.01 85.8 0.03  
 128.6 0.04 148.6 0.05 160.1 0.07 177.2 0.085 180.1 0.10 182.9  
 0.13 188.7 0.17 197.2 0.24 208.7 0.30 214.4 0.40 223.0 0.50 231.5  
 0.80 245.8 1 254.4  
 10039 / 1 0 0 0.003 29.1 0.0035 41.5 0.0054 53.1 0.01 62.3 0.03  
 93.4 0.04 107.9 0.05 116.2 0.07 128.7 0.085 130.8 0.10 132.8  
 0.13 137.0 0.17 143.2 0.24 151.5 0.30 155.7 0.40 161.9 0.50 168.1  
 0.80 178.5 1 184.7  
 10040 / 1 0 0 0.003 14.5 0.0035 20.8 0.0054 26.6 0.01 31.1 0.03  
 46.7 0.04 54.0 0.05 58.1 0.07 64.3 0.085 65.4 0.10 66.4  
 0.13 68.5 0.17 71.6 0.24 75.8 0.30 77.8 0.40 80.9 0.50 84.1  
 0.80 89.2 1 92.4  
 10041 / 1 0 0 0.003 9.9 0.0035 14.2 0.0054 18.1 0.01 21.2 0.03  
 31.8 0.04 36.8 0.05 39.6 0.07 43.9 0.085 44.6 0.10 45.3  
 0.13 46.7 0.17 48.8 0.24 51.7 0.30 53.1 0.40 55.2 0.50 57.3  
 0.80 60.8 1 63.0  
 10042 / 1 0 0 0.003 6.9 0.0035 9.8 0.0054 12.6 0.01 14.7 0.03  
 22.1 0.04 25.5 0.05 27.5 0.07 30.4 0.085 30.9 0.10 31.4  
 0.13 32.4 0.17 33.8 0.24 35.8 0.30 36.8 0.40 38.3 0.50 39.7  
 0.80 42.2 1 43.7  
 10043 / 1 0 0 0.003 4.4 0.0035 6.2 0.0054 8.0 0.01 9.3 0.03  
 14.0 0.04 16.2 0.05 17.4 0.07 19.3 0.085 19.6 0.10 19.9  
 0.13 20.5 0.17 21.5 0.24 22.7 0.30 23.3 0.40 24.3 0.50 25.2

0.80 26.8 1 27.7  
 10044 / 1 0 0 0.003 0.0 0.0035 0.0 0.0054 0.0 0.01 0.0 0.03  
 0.0 0.04 0.0 0.05 0.0 0.07 0.0 0.085 0.0 0.10 0.0  
 0.13 0.0 0.17 0.0 0.24 0.0 0.30 0.0 0.40 0.0 0.50 0.0  
 0.80 0.0 1 0.0  
 10045 / 1 0 0 0.003 0.0 0.0035 0.0 0.0054 0.0 0.01 0.0 0.03  
 0.0 0.04 0.0 0.05 0.0 0.07 0.0 0.085 0.0 0.10 0.0  
 0.13 0.0 0.17 0.0 0.24 0.0 0.30 0.0 0.40 0.0 0.50 0.0  
 0.80 0.0 1 0.0  
 10046 / 1 0 0 0.003 0.0 0.0035 0.0 0.0054 0.0 0.01 0.0 0.03  
 0.0 0.04 0.0 0.05 0.0 0.07 0.0 0.085 0.0 0.10 0.0  
 0.13 0.0 0.17 0.0 0.24 0.0 0.30 0.0 0.40 0.0 0.50 0.0  
 0.80 0.0 1 0.0  
 10047 / 1 0 0 0.003 93.8 0.0035 134.0 0.0054 171.5 0.01 200.9  
 0.03 301.4 0.04 348.3 0.05 375.1 0.07 415.3 0.085 422.0 0.10 428.7  
 0.13 442.1 0.17 462.2 0.24 489.0 0.30 502.4 0.40 522.5 0.50 542.5  
 0.80 576.0 1 596  
 10048 / 1 0 0 0.003 81.9 0.0035 117.0 0.0054 149.7 0.01 175.5  
 0.03 263.2 0.04 304.2 0.05 327.5 0.07 362.6 0.085 368.5 0.10 374.3  
 0.13 386.0 0.17 403.6 0.24 427.0 0.30 438.7 0.40 456.2 0.50 473.8  
 0.80 503.0 1 521  
 10049 / 1 0 0 0.003 78.2 0.0035 111.7 0.0054 143.0 0.01 167.5  
 0.03 251.3 0.04 290.4 0.05 312.8 0.07 346.3 0.085 351.8 0.10 357.4  
 0.13 368.6 0.17 385.4 0.24 407.7 0.30 418.9 0.40 435.6 0.50 452.4  
 0.80 480.3 1 497.1  
 10050 / 1 0 0 0.003 74.4 0.0035 106.2 0.0054 136.0 0.01 159.3  
 0.03 239.0 0.04 276.2 0.05 297.4 0.07 329.3 0.085 334.6 0.10 339.9  
 0.13 350.5 0.17 366.5 0.24 387.7 0.30 398.3 0.40 414.3 0.50 430.2  
 0.80 456.8 1 472.7  
 10051 / 1 0 0 0.003 66.7 0.0035 95.3 0.0054 122.0 0.01 142.9  
 0.03 214.4 0.04 247.7 0.05 266.8 0.07 295.4 0.085 300.1 0.10 304.9  
 0.13 314.4 0.17 328.7 0.24 347.8 0.30 357.3 0.40 371.6 0.50 385.9  
 0.80 409.7 1 424.0  
 10052 / 1 0 0 0.003 52.2 0.0035 74.5 0.0054 95.4 0.01 111.8  
 0.03 167.7 0.04 193.8 0.05 208.7 0.07 231.0 0.085 234.8 0.10 238.5  
 0.13 245.9 0.17 257.1 0.24 272.0 0.30 279.5 0.40 290.7 0.50 301.8  
 0.80 320.5 1 331.7  
 10053 / 1 0 0 0.003 26.4 0.0035 37.7 0.0054 48.3 0.01 56.6  
 0.03 84.9 0.04 98.1 0.05 105.7 0.07 117.0 0.085 118.9 0.10 120.8  
 0.13 124.5 0.17 130.2 0.24 137.7 0.30 141.5 0.40 147.2 0.50 152.8  
 0.80 162.3 1 167.9  
 10054 / 1 0 0 0.003 11.9 0.0035 17.0 0.0054 21.7 0.01 25.5

0.03 38.2 0.04 44.2 0.05 47.5 0.07 52.6 0.085 53.5 0.10 54.3  
 0.13 56.0 0.17 58.6 0.24 62.0 0.30 63.7 0.40 66.2 0.50  
 68.8 0.80 73.0 1 75.6  
 10055 / 1 0 0 0.003 7.5 0.0035 10.8 0.0054 13.8 0.01 16.1  
 0.03 24.2 0.04 28.0 0.05 30.1 0.07 33.3 0.085 33.9 0.10 34.4  
 0.13 35.5 0.17 37.1 0.24 39.3 0.30 40.3 0.40 41.9 0.50  
 43.6 0.80 46.2 1 47.9  
 10056 / 1 0 0 0.003 4.6 0.0035 6.6 0.0054 8.5 0.01 9.9  
 0.03 14.9 0.04 17.2 0.05 18.5 0.07 20.5 0.085 20.8 0.10 21.1  
 0.13 21.8 0.17 22.8 0.24 24.1 0.30 24.8 0.40 25.8 0.50  
 26.7 0.80 28.4 1 29.4  
 10057 / 1 0 0 0.003 0.0 0.0035 0.0 0.0054 0.0 0.01 0.0  
 0.03 0.0 0.04 0.0 0.05 0.0 0.07 0.0 0.085 0.0 0.10 0.0  
 0.13 0.0 0.17 0.0 0.24 0.0 0.30 0.0 0.40 0.0 0.50  
 0.0 0.80 0.0 1 0.0  
 10058 / 1 0 0 0.003 0.0 0.0035 0.0 0.0054 0.0 0.01 0.0  
 0.03 0.0 0.04 0.0 0.05 0.0 0.07 0.0 0.085 0.0 0.10 0.0  
 0.13 0.0 0.17 0.0 0.24 0.0 0.30 0.0 0.40 0.0 0.50  
 0.0 0.80 0.0 1 0.0  
 10059 / 1 0 0 0.003 0.0 0.0035 0.0 0.0054 0.0 0.01 0.0  
 0.03 0.0 0.04 0.0 0.05 0.0 0.07 0.0 0.085 0.0 0.10 0.0  
 0.13 0.0 0.17 0.0 0.24 0.0 0.30 0.0 0.40 0.0 0.50  
 0.0 0.80 0.0 1 0.0  
 10060 / 1 0 0 0.003 66.0 0.0035 94.3 0.0054 120.8 0.01 141.5  
 0.03 212.3 0.04 245.3 0.05 264.2 0.07 292.5 0.085 297.2 0.10 301.9  
 0.13 311.3 0.17 325.5 0.24 344.3 0.30 353.8 0.40 367.9 0.50 382.1  
 0.80 405.7 1 420  
 10061 / 1 0 0 0.003 64.7 0.0035 92.5 0.0054 118.3 0.01 138.7  
 0.03 208.0 0.04 240.4 0.05 258.9 0.07 286.6 0.085 291.2 0.10 295.8  
 0.13 305.1 0.17 319.0 0.24 337.5 0.30 346.7 0.40 360.6 0.50 374.4  
 0.80 397.5 1 411  
 10062 / 1 0 0 0.003 62.3 0.0035 89.1 0.0054 114.0 0.01 133.6  
 0.03 200.4 0.04 231.5 0.05 249.4 0.07 276.1 0.085 280.5 0.10 285.0  
 0.13 293.9 0.17 307.2 0.24 325.1 0.30 334.0 0.40 347.3 0.50 360.7  
 0.80 382.9 1 396.3  
 10063 / 1 0 0 0.003 57.8 0.0035 82.6 0.0054 105.8 0.01 124.0  
 0.03 185.9 0.04 214.9 0.05 231.4 0.07 256.2 0.085 260.3 0.10 264.5  
 0.13 272.7 0.17 285.1 0.24 301.6 0.30 309.9 0.40 322.3 0.50 334.7  
 0.80 355.4 1 367.8  
 10064 / 1 0 0 0.003 50.7 0.0035 72.5 0.0054 92.7 0.01 108.7  
 0.03 163.0 0.04 188.4 0.05 202.9 0.07 224.6 0.085 228.2 0.10 231.8  
 0.13 239.1 0.17 250.0 0.24 264.5 0.30 271.7 0.40 282.6 0.50 293.4

0.80 311.5 1 322.4  
 10065 / 1 0 0 0.003 37.0 0.0035 52.8 0.0054 67.6 0.01 79.2  
 0.03 118.9 0.04 137.4 0.05 147.9 0.07 163.8 0.085 166.4 0.10 169.1  
 0.13 174.3 0.17 182.3 0.24 192.8 0.30 198.1 0.40 206.0 0.50 214.0  
 0.80 227.2 1 235.1  
 10066 / 1 0 0 0.003 18.5 0.0035 26.4 0.0054 33.8 0.01 39.6  
 0.03 59.4 0.04 68.7 0.05 74.0 0.07 81.9 0.085 83.2 0.10 84.5  
 0.13 87.2 0.17 91.1 0.24 96.4 0.30 99.1 0.40 103.0 0.50 107.0  
 0.80 113.6 1 117.5  
 10067 / 1 0 0 0.003 10.6 0.0035 15.1 0.0054 19.3 0.01 22.6  
 0.03 34.0 0.04 39.2 0.05 42.3 0.07 46.8 0.085 47.5 0.10 48.3  
 0.13 49.8 0.17 52.1 0.24 55.1 0.30 56.6 0.40 58.9 0.50 61.1  
 0.80 64.9 1 67.2  
 10068 / 1 0 0 0.003 7.3 0.0035 10.4 0.0054 13.3 0.01 15.6  
 0.03 23.3 0.04 27.0 0.05 29.1 0.07 32.2 0.085 32.7 0.10 33.2  
 0.13 34.2 0.17 35.8 0.24 37.9 0.30 38.9 0.40 40.5 0.50 42.0  
 0.80 44.6 1 46.2  
 10069 / 1 0 0 0.003 4.5 0.0035 6.4 0.0054 8.2 0.01 9.6  
 0.03 14.4 0.04 16.7 0.05 18.0 0.07 19.9 0.085 20.2 0.10 20.5  
 0.13 21.2 0.17 22.1 0.24 23.4 0.30 24.1 0.40 25.0 0.50 26.0  
 0.80 27.6 1 28.5  
 10070 / 1 0 0 0.003 0.0 0.0035 0.0 0.0054 0.0 0.01 0.0  
 0.03 0.0 0.04 0.0 0.05 0.0 0.07 0.0 0.085 0.0 0.10 0.0  
 0.13 0.0 0.17 0.0 0.24 0.0 0.30 0.0 0.40 0.0 0.50  
 0.0 0.80 0.0 1 0.0  
 10071 / 1 0 0 0.003 0.0 0.0035 0.0 0.0054 0.0 0.01 0.0  
 0.03 0.0 0.04 0.0 0.05 0.0 0.07 0.0 0.085 0.0 0.10 0.0  
 0.13 0.0 0.17 0.0 0.24 0.0 0.30 0.0 0.40 0.0 0.50  
 0.0 0.80 0.0 1 0.0  
 10072 / 1 0 0 0.003 0.0 0.0035 0.0 0.0054 0.0 0.01 0.0  
 0.03 0.0 0.04 0.0 0.05 0.0 0.07 0.0 0.085 0.0 0.10 0.0  
 0.13 0.0 0.17 0.0 0.24 0.0 0.30 0.0 0.40 0.0 0.50  
 0.0 0.80 0.0 1 0.0

RETURN

NAME NEWREFORNT2\_

SAVE DATA 3333

MEDIUM

EXTRACT MEDIUM



# VITA

Zhiye Li was born on December 18, 1986 in DaQing, Heilongjiang Province in P. R. China. She has been at Lehigh University since 2009 as a graduate student in Department of Mechanical Engineering and Mechanics.